

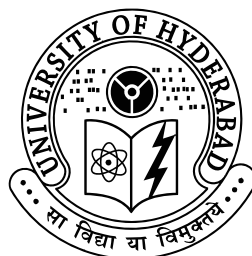
Rheological Studies on Nematic and Smectic-A Thermotropic Liquid Crystals

A Thesis submitted for the award of the degree of
Doctor of Philosophy in Physics

by

Ananthaiah J

09PHPH03



School of Physics
University of Hyderabad
Telangana, India 500 046

December, 2014

TO

My Parents

Declaration

I, **Ananthaiah J**, hereby declare that this thesis entitled “**Rheological Studies on Nematic and Smectic-A Thermotropic Liquid Crystals**” submitted by me under the supervision of **Dr. Surajit Dhara** is a bonafide research work. I also declare that it has not been submitted previously in part or in full to this University or any other University or Institution for the award of any degree or diploma. I hereby agree that my thesis can be deposited in Shodhganga/INFLIBNET.

Ananthaiah J

Reg. No: 09PHPH03

Date:

Place: Hyderabad.

Certificate

This is to certify that the thesis entitled “**Rheological Studies on Nematic and Smectic-A Thermotropic Liquid Crystals**” submitted by **Ananthaiah J** bearing Reg. No. 09PHPH03 in fulfillment of the requirements for the award of Doctor of Philosophy in Physics is a bonafide work carried out by him under my supervision and is free of plagiarism.

The matter embodied in this report has not been submitted previously in part or in full to this University or any other University or Institution for the award of any degree or diploma.

Dr. Surajit Dhara
Thesis Supervisor,
School Of Physics,
University of Hyderabad.

Dean,
School Of Physics,
University of Hyderabad.

Acknowledgement

I would like to express my sincere gratitude to my supervisor, Dr. Surajit Dhara for his continuous guidance, instigation and encouragement throughout my Ph.D programme. His direction and knowledge paved a splendid path to enlighten me and my thoughts which is an invaluable part of my life.

I would like to thank my Doctoral Committee member, Prof. V. S. S. Sastry, for his teaching, insightful comments, immense support and guidance throughout the integral part of this work. I am also grateful to Prof. K. P. N Murthy for fruitful discussions.

I would like to express my heartfelt thanks to Prof. N. V. Madhusudana (RRI, Bangalore) for his enlightening suggestions.

I would like to extend my warm thanks to Prof. R. Dabrowski (Military University of Technology, Warsaw, Poland) for providing many samples for my research work.

I cherish the invaluable support from former Deans, Prof. C. Bansal, Prof. S. P. Tewari and the present Dean, Prof. S. Chaturvedi, for providing needful facilities. I would also like to thank the faculty of School of Physics for their impetus suggestions.

Earnest gratitude to my seniors Dr. T. Arun kumar and Dr. P. Sathyanarayana, who had been of great assistance. I learned many scientific aspects as well as about various other techniques from them.

I would like to thank Dr. Rajeswari and M. Suman Kalyan for their friendly support.

I wish all the best to my lab mates Venkata Sai, Rasmitha Sahoo, M. V. Rasna, K. P. Zuhail, Krishna Kanth and Junaid Ahmad Sofi in their future endeavors.

I will remember my amicable and cordial friends R. Manda, Joshua, Varul, Srinu, Ramesh, Raju, Ravi, Ashok, Pasha, Yadaiah, Naga, Musavir, Sathyanarayana, Pavan Naik, Rajesh, Narsimhappa, Manikanta, Dhanunjaya, Shilpa, Madhuri, Anji, Sampath, Pundarikam, Punna, Sathish, Eshwar, Naresh, Vengal Rao, Bhaskar, Mahipal, Niman, Prakash and Raghu for their motivation and relentless support.

My sincere gratitude to Dr. Sudha Nirmala, Kamala Lata, Regina Jose, Dr. Shankaraiah, Dr. Yugandhar, Dr. Devaraju, Dr. Ramudu, Dr. Cholleti Srinivas, Dr. P. Shankar, Siva N. Chari, Alu, Sanjeev and I. V. Shankar for their continuous support throughout the research.

I extend my warm regards to my batch-mates Azeem Baig Mirza, M. Geo Philip, Ch. Narasimha Raju, Vijay Kumar, G. Thirupathi, K. Lakshun Naidu, Abhishek Prakash, Syed Hamad, G. Srinu, C. Bhagyaraj, K. Rama Obulesu, M. M. Lakshmi, K. Hasna, T. Satya Krishna, R. Kuladeep for their cheerful company.

I cherish the Teachers I had in my Schooling, College and my dearest childhood friends Sidhu, Bhanu, Harikrishna, Saireddy, Ganesh, Venkatramulu, Yellaiah, Narsimulu, Ravi, Vandana, Vinoda, Swapna, Radhika and Vijaya Lakshmi.

My Sincere gratitude to Mr. Surender Rao and his family for being kind and extending their unconditional support throughout my stay in the university.

I thank T. Abraham, N. Shailaja, Prasad, P. Krishna, K. Srinivas and

other non-teaching staff for their help and support.

I would like to thank Promod and Srinivas (Anton Paar) for their technical support.

Assistance from the University of Hyderabad (through BBL scholarship), UGC (BSR) and Council of Scientific Industrial Research (CSIR-SRF) are also gratefully acknowledged.

I feel blessed and fortunate to have such grand parents, Mamas, aunts, uncles, sisters, brothers, sister-in-laws and brother-in-laws for their trust in my abilities and doing their part in moulding my career.

I would not be able to walk out of the soft matter laboratory today without the love and constant support of my parents. This thesis is dedicated to my parents, whose character reflected in me, the person you are witnessing today. From an early age, they instilled in me the importance of education and provided a stable home without which I would not have had the courage to pursue this challenging path. Being a single parent, my mother never made me feel like one and let it have its influence on me. I give all the credit to her for being the force behind me for attaining this great achievement and made me who I am.

I feel such a deep love, support and encouragement from my wife Alavelu towards the completion of my Doctoral degree.

Preface

Liquid Crystals (LCs) are intermediate state of matter observed between crystalline solids and amorphous liquids. They exhibit both the liquid-like and the solid-like properties. The molecules in this state exhibit long-range orientational order in addition a few of them also exhibit 1 or 2-dimensional translational order. Liquid crystals (LCs) are mostly of two categories namely, thermotropic and lyotropic. In thermotropic LCs, the mesophases arise due to temperature whereas in lyotropic LCs, mesophases arise due to the concentration as well as the temperature.

Generally, the liquid crystalline materials exhibit a variety of phase transitions owing to their molecular structure and shape. The common liquid crystal phases exhibited by low molecular weight liquid crystals (LCs) are nematic (N), smectic-A (SmA) and cholesteric (N^*) etc. Phase transitions, physical properties and electrooptic properties of thermotropic liquid crystals have always been the major area of interest to the researchers with a goal to achieve improved liquid crystal display properties. Rheology is a multidisciplinary science that concerns with the study of deformation and flow of matter. The flow behavior of ideal viscous liquids and the deformation of ideal elastic solids are well explained by using Newton's and Hooke's law respectively. Usually soft materials are neither ideal solids nor ideal liquids but exhibit both properties and are therefore referred as viscoelastic materials. The rheology of thermotropic liquid crystals has not been explored much as they are not directly related to the device properties. The rheology of anisotropic fluids are very interesting and they are important from the fundamental point of view. There are a few reports on the measurement of rheological properties such as Miesowicz viscosities or

Leslie coefficients of thermotropic nematic liquid crystals. However, the effect of molecular structure, phase transitions on the rheological properties of various LCs are not fully explored. In this thesis we studied the rheological properties of a few thermotropic liquid crystals showing nematic (N), smectic-A (SmA) and cholesteric (N^*) phases. We used various rheological techniques such as electro-rheology and rheo-small angle light scattering to study and understand the temperature dependent rheological properties.

The thesis is organized into six chapters.

The first chapter is the introductory part that focuses on the liquid crystals and their basic rheological properties.

The second chapter discusses the experimental techniques used in this thesis. For non-rheological study, we used some techniques to measure birefringence (Δn) and dielectric anisotropy ($\Delta\epsilon$). For rheological characterisation, we used rheological techniques such as rheo-dielectric and rheo-SALS (Small Angle Light Scattering).

The third chapter focuses on the rheological properties of three nematic liquid crystals with highly polar molecules namely trans,trans-4-n-heptyl-4'-cyanobicyclohexane (CCH-7), trans-4-(4-heptyl-cyclohexyl)-benzonitrile (PCH-7) and 4-(n-heptyl)-4'-cyanobiphenyl (CB-7), which are having a systematic variation in the molecular structure. The two Miesowicz viscosities η_2 (director parallel to the shear direction) and η_1 (director perpendicular to the shear direction) were measured as a function of temperature and the orientation of the director was studied using small angle light scattering (SALS) technique. η_2 was measured in presheared sample whereas η_1 is measured by electrorheological technique.

We observed that nematic compounds with more number of aromatic rings and lower Kirkwood correlation factor have the larger viscosities. The temperature dependent viscosities (η_2 and η_1) were understood based on the intramolecular π -electron conjugation of neighboring molecules and the antiparallel correlation of molecular dipoles.

The fourth chapter deals with the simultaneous measurement of shear viscosity (η) and effective dielectric constant (ϵ) of octyloxy cyanobiphenyl (8OCB) in the nematic (N) and smectic-A (SmA) phases as a function of temperature and electric field. The flow curves at various applied fields show that competing orientation effect of the flow field and electric field. As electric field increases, effective viscosity increases in the N phase whereas in the SmA phase it decreases and saturates beyond a particular electric field in both the phases. The temperature-dependent effective viscosity and effective dielectric constant at zero or at small electric field suggests the occurrence of several structures that results from the precessional motion of the director along the neutral direction. We show that the precessional motion is gradually suppressed with increasing electric field and the effective viscosity resembles with the Miesowicz viscosity η_1 at high enough electric field. In the intermediate field range the temperature-dependent effective viscosity exhibit anomalous behavior across the N -SmA phase transition which is attributed to the large contribution of Leslie coefficient α_1 .

The fifth chapter presents the experimental studies of small angle light scattering (SALS), rheodielectric and electrorheological properties of a binary mixture made of octyloxy cyanobiphenyl (8OCB) and hexyloxy cyanobiphenyl (6OCB). This mixture exhibits nematic (N) to smectic-A (SmA) phase transition, and then again to a reentrant nematic (N_R) phase transition. Shear thinning in the quenched sample in the low shear

rate region in the N and SmA phases is observed from SALS experiments and attributed to the realignment of the director within the domain. The domain elongation starts beyond a threshold shear rate in both the phases. In case of SmA, the threshold shear rate is about five times higher than that of the N phase. At a steady shear rate the effective viscosity increases with the electric field in all the phases and saturates at much higher fields. It also exhibits two anomalous peaks across N -SmA- N_R phase transitions beyond a particular field. The shear modulus of the SmA phase in an intermediate field is significantly larger than that measured at both low and high fields. The enhanced viscoelasticity of the SmA phase is aided by the presence of dislocations, which disappear on application of strong external electric field.

The shear and micro-rheological viscosities of bent-core nematic (BCN) liquid crystal are presented in the sixth chapter. The shear viscosity is measured using a rheometer and the micro-rheological viscosities are measured by measuring the self-diffusion coefficient of a microsphere in the aligned sample. The effective (shear) viscosity is larger and the effect of presmectic fluctuations are observed much higher than the N -SmC transition temperature than commonly seen in calamitic liquid crystals. The temperature dependent micro-rheological viscosities are stronger than that of shear viscosity. The study of Brownian fluctuation is useful to understand the smectic fluctuations in bent-core nematic liquid crystals. This, however, needs to be substantiated by more experiments as well as simulations.

Contents

Preface	xii
Contents	xvi
List of Symbols	xx
List of Figures	xxii
List of Tables	xxix
1 Introduction	1
1.1 Rheology	1
1.1.1 Rheology of liquid crystals	2
1.2 Liquid crystals	3
1.3 Types of liquid crystals	3
1.3.1 Nematic phase	4
1.3.2 Cholesteric phase	5
1.3.3 Smectic phases	6
1.3.4 Smectic-A phase	6
1.3.5 Smectic-C phase	7
1.3.6 Smectic-C* phase	7
1.3.7 Bent-core liquid crystals	8
1.4 Physical properties of nematic liquid crystals	9
1.4.1 Birefringence	9
1.4.2 Dielectric constant	10
1.4.3 Order parameter	10

1.4.4 Alignment of liquid crystals	11
1.5 Rheological properties of nematic liquid crystals	12
1.5.1 Oscillation test	12
1.5.2 Rotational test	14
1.6 Leslie-Ericksen theory	14
1.6.1 Curvature elastic constants of nematic liquid crystals	15
1.6.2 Viscosities of nematic liquid crystals	15
References	19
2 Instrumentation	23
2.1 Introduction	23
2.2 Rheometer (MCR 501 Anton Paar)	23
2.3 Measuring geometries	25
2.3.1 Cone-plate (CP) geometry	25
2.3.2 Parallel-plate (PP) geometry	27
2.4 Electro-Rheology	28
2.5 Small Angle Light Scattering (SALS)	29
2.6 Non-rheological techniques	32
2.6.1 Liquid crystal cell	32
2.6.2 Measurement of dielectric constant	33
2.6.3 Measurement of birefringence	34
3 Rheology of nematic liquid crystals with highly polar molecules	37
3.1 Introduction	37
3.2 Experimental	38
3.3 Results and discussion	40
3.3.1 Birefringence and dielectric anisotropy measurements	40
3.3.2 Shear dependent viscosity measurement	41
3.3.3 Miesowicz viscosity η_2	43

3.3.4 Miesowicz viscosity η_1	48
3.4 Conclusions	51
References	53
4 Rheo-dielectric and electro-rheological properties of 8OCB liquid crystal	57
4.1 Introduction	57
4.2 Experimental	60
4.3 Results and discussion	62
4.3.1 Shear dependent effective viscosity (η) and dielectric constant (ϵ) measurements	62
4.3.2 Field dependent effective viscosity (η) and dielectric constant (ϵ) measurements	64
4.3.3 Temperature dependent viscosity (η) and dielectric constant (ϵ) measurements	66
4.4 Conclusions	71
References	73
5 Rheology of a reentrant nematic liquid crystal	79
5.1 Introduction	79
5.2 Experimental	80
5.3 Results and discussion	81
5.3.1 Shear dependent SALS and viscosity (η)	81
5.3.2 Temperature dependent SALS and viscosity (η)	84
5.3.3 Rheodielectric and electrorheological measurements	86
5.3.4 Field-dependent complex shear modulus measurements	89
5.4 Conclusions	92
References	93

6 Rheology of a Bent-Core Nematic Liquid Crystal.	97
6.1 Introduction	97
6.2 Experimental	98
6.3 Results and discussion	100
6.3.1 Measurement of shear viscosity	100
6.3.2 Measurement of viscosity by using a micro- rheological technique	104
6.4 Conclusions	108
References	109
List of Publications	113
Curriculum Vitae	115

List of Abbreviations and Symbols

MCR	: Modular compact rheometer
CSD (CD)	: Controlled shear deformation
CSR (CR)	: Controlled shear rate
CSS (CS)	: Controlled shear stress
CP	: Cone-and-plate
PP	: Parallel-plate
CC	: Coaxial or concentric cylinder
τ	: Shear stress
γ	: Strain
$\dot{\gamma}$: Shear rate
G	: Shear modulus
η	: Shear viscosity
G^*	: Complex modulus
G'	: Storage modulus
G''	: Loss modulus
η^*	: Complex viscosity
η'	: Dynamic viscosity
η''	: Imaginary part of complex viscosity
ω	: Angular frequency
D_e	: Deboarch number
E_r	: Ericksen number
q	: Scattering vector
λ	: Wavelength
θ	: Scattering angle
I	: Intensity
N	: Nematic phase

SmA	: Smectic-A phase
SmC	: Smectic-C phase
N^*	: Cholesteric phase
\hat{n}	: Liquid crystal director
S	: Scalar order parameter
ITO	: Indium tin oxide
V	: Voltage
V_{th}	: Freedericksz threshold voltage
$\Delta\phi$: Optical phase difference
θ	: Tilt angle (polar)
ϕ	: Twist angle (azimuthal)
n_o	: Ordinary refractive index
n_e	: Extraordinary refractive index
$n_{ }$: Refractive index parallel to \hat{n}
n_{\perp}	: Refractive index perpendicular to \hat{n}
$\Delta n = n_e - n_o$: Birefringence
$\epsilon_{ }$: Dielectric constant parallel to \hat{n}
ϵ_{\perp}	: Dielectric constant perpendicular to \hat{n}
$\Delta\epsilon = \epsilon_{ } - \epsilon_{\perp}$: Dielectric anisotropy
$\langle\epsilon\rangle = (\epsilon_{ } + 2\epsilon_{\perp})/3$: Average dielectric constant
K_{11}, K_{22}, K_{33}	: Splay, Twist and Bend elastic constants
K	: Average elastic constant
η_1, η_2, η_3	: Miesowicz viscosity coefficients
$\alpha_1, \dots, \alpha_6$: Leslie coefficients
T	: Absolute temperature
T_{NI}	: Nematic-isotropic phase transition temperature
T_{SN}	: Nematic-smectic-A phase transition temperature
NI	: Nematic-isotropic phase transition
NS	: Nematic-smectic-A phase transition
BC	: Bent-core molecules

List of Figures

1.1	Schematic representation of molecular arrangement in the nematic.	4
1.2	Schematic representation of the molecular arrangement in the cholesteric phase. The arrows indicate the orientation of the director \hat{n}	5
1.3	Schematic representation of the molecular arrangement in the Smectic-A phase.	6
1.4	Schematic representation of the molecular arrangement in the SmC phase. The molecules are tilted with respect to the layer normal \hat{k}	7
1.5	Schematic representation of the molecular arrangement in the SmC* phase. The tilt direction rotates between successive layers as represented by arrows.	8
1.6	Schematic representation of homogeneous and homeotropic alignment of the director between two coated ITO substrates. \hat{n} is the director.	11
1.7	A Schematic representation of the splay, twist and bend deformations.	15
1.8	Schematic representation of the three fundamental director orientations of nematic liquid crystals with respect to the shear direction. Miesowicz viscosities corresponding to each orientations are designated by η_1 , η_2 and η_3 respectively. .	16

2.1	Photograph of a MCR 501 Rheometer (Anton Paar). . . .	24
2.2	Schematic diagram of cone-and-plate measuring geometry. Here the symbols represents the following parameters: R— cone radius, H— gap between the two plates at edge, α — cone angle, ω — angular frequency and a — truncated gap between the plates.	26
2.3	Schematic diagram of parallel-plate measuring geometry. Here the symbols represents the following parameters: R— plate radius, H— gap between the two plates and ω — angu- lar frequency.	27
2.4	Schematic diagram of Electro-Rheology setup.	29
2.5	Photograph of a SALS setup.	30
2.6	Schematic diagram of the small angle light scattering setup.	31
2.7	Schematic representation of LC cell made up ITO glass plates.	33
2.8	Experimental diagram for the measurement of birefringence using PEM.	34
3.1	Chemical structures of CB-7, PCH-7 and CCH-7 liquid crystals and their phase transition temperatures.	39
3.2	Variation of birefringence (Δn) with shifted temperature of CB-7 (stars), PCH-7 (circles) and CCH-7 (squares) liquid crystals with cell thickness 5 μm	41
3.3	Variation of dielectric anisotropy ($\Delta\epsilon$) with shifted temper- ature of CB-7 (stars), PCH-7 (circles) and CCH-7 (squares) liquid crystals. The dielectric constants are measured at a frequency of 4.11 kHz. Cell thickness 5 μm	42

3.4	Variation of the effective viscosity as a function of shear rate in the nematic phase of CB-7 in quenched (squares) and presheared (circles) samples at 35°C. P, A are polarizer and analyzer. Red arrow indicates the direction of shear. .	42
3.5	Variation of η_2 as a function of shifted temperature at a fixed shear rate, $\dot{\gamma} = 50 \text{ s}^{-1}$	44
3.6	Variation of logarithm of η_2 with the inverse of temperature in the isotropic phase. The lines are best fit to Arrhenius equation.	44
3.7	Comparison (ratio) of η_2 of CB-7 and PCH-7 with respect to that of CCH-7.	45
3.8	Variation of effective viscosity (η_{eff}) at a fixed shear rate, $\dot{\gamma} = 50 \text{ s}^{-1}$ as a function of applied field at a frequency 3.11 kHz. At high field (beyond about $80 \times 10^4 \text{ V/m}$) $\eta_{eff} = \eta_1$	49
3.9	Variation of η_1 as a function of shifted temperature and fixed electric field $133 \times 10^4 \text{ V/m}$ ($\dot{\gamma} = 50 \text{ s}^{-1}$).	50
4.1	(a) Three fundamental director orientations under shear flow and SmA fluctuation is shown for the c orientation. Adapted from ref [15].	58
4.2	Bottom: The $\dot{\gamma} - T$ phase diagram for 8CB compound. Top: Schematics of the stable orientation of director in the b regime (right), and the distribution of director in three of the a regimes (left). Adapted from ref [15].	60
4.3	Chemical structure of 8OCB liquid crystal with phase transition temperatures.	61

4.4	Schematic representation of the three fundamental director orientations in the N and SmA phase under shear. The director orientations are along the x (neutral), y (velocity) and z (velocity gradient) directions in a , b , c respectively. Layer orientations in the SmA phase that are parallel to the zy , xz , and xy planes in a' , b' , and c' respectively. Miesowicz viscosities corresponding to each orientations in the N phase are designated by η_3 , η_2 and η_1 respectively.	61
4.5	Variation of (a) shear viscosity (η) (which we represent as effective viscosity) and (b) dielectric constant (ϵ) (which we represent as effective dielectric constant) as a function of shear rate ($\dot{\gamma}$) at various applied a.c electric fields. Dotted lines are drawn as a guide to the eye.	63
4.6	(a) Variation of shear viscosity (η) as a function of applied electric field at various shear rates ($\dot{\gamma}$) at 72 °C. (b) Variation of dielectric constant (ϵ) as a function of applied electric field at shear rates $\dot{\gamma} = 0$ and 50 s^{-1} at the same temperature. Dotted lines are drawn as a guide to the eye.	65
4.7	Variation of (a) shear viscosity (η) (which we represent as effective viscosity) and (b) dielectric constant (ϵ) (which we represent as effective dielectric constant) as a function of temperature and various applied electric fields. Vertical dotted lines are drawn considering the similarity of temperature dependent zero field viscosity with that of 8CB [19] and represent the approximate temperature regions with possible director orientations. The vertically down arrow indicates the peak position in the viscosity ($T - T_{NI} = -13.8^\circ\text{C}$). (c) Schematic representation of the precessional motion of the director at $13.3 \times 10^4 \text{ V/m}$ and at various temperatures.	67

5.1	Chemical structures and phase transition temperatures of 6OCB and 8OCB liquid crystals.	81
5.2	Phase diagram of the 6OCB-8OCB binary mixture: I - N - SmA and RN (which we represent as N_R) refer to the isotropic, ordinary nematic, smectic-A and reentrant nematic phase, respectively. The phase diagram was obtained from ref [22].	82
5.3	Shear rate dependent effective shear viscosity (η_{eff}) in the N ($T - T_{NI} = -30^\circ\text{C}$) and SmA phases ($T - T_{NI} = -43^\circ\text{C}$). The depolarized scattering patterns (HV) at some representative shear rates are shown in both the phases. The red arrow indicate the direction of shear. The upper and lower scattering patterns correspond to the SmA and N phases, respectively. The continuous line is a best fit to Eq. (5.1).	83
5.4	Temperature variation of effective shear viscosity (η_{eff}) at a steady shear rate ($\dot{\gamma} = 50 \text{ s}^{-1}$). HV scattering patterns at a few temperatures. The red arrows indicate the direction of shear. The possible director orientations at different temperatures are also indicated considering the similarity of temperature dependent zero-field viscosity of 8CB [18] and 8OCB [19].	85
5.5	(a) Variation of effective shear viscosity (η_{eff}) with temperature at various a.c electric fields. All the data were collected at a steady shear rate ($\dot{\gamma}=50 \text{ s}^{-1}$). Inset: Suppression of peaks under strong electric fields. (b) Static dielectric constant at same shear rates and same electric fields as in (a). The dielectric data represented by star were measured without shear and at a field $0.8 \times 10^4 \text{ V/m}$. The frequency of the applied field is 3.11 kHz.	88

5.6	Variation of (a) storage modulus (G') and (b) loss modulus (G'') across N -SmA and N_R phase transitions at various a.c electric fields at angular frequency $\omega = 10$ rad/s and strain amplitude $\gamma = 0.05$	90
5.7	Variation of effective dielectric constant (ϵ_{eff}) across N -SmA and N_R phase transitions at various a.c electric fields at an angular frequency $\omega = 10$ rad/s and strain amplitude $\gamma = 0.05$. The frequency of the applied field is 3.11 kHz. Orientations of SmA layers with respect to field direction are shown schematically.	91
6.1	Chemical structure and the first two phase transition temperatures of the bent-core compound.	98
6.2	Photomicrographs of nematic phase of bent-core compound (a) $T - T_{NI} = -45^\circ\text{C}$ (b) $T - T_{NI} = -15^\circ\text{C}$ cooling from the isotropic phase.	99
6.3	Variation of shear stress with shear rate at various temperatures. The sample was mounted at 140°C . 1^{st} and 2^{nd} indicates the two consecutive measurements at the same temperature.	101

6.4	Temperature variation of η_{eff} in both 8OCB and BCN compounds at a shear rate $\dot{\gamma} = 50 \text{ s}^{-1}$. Upper and lower x-axes corresponds to the temperature scale of BCN (open squares) and 8OCB (filled circles) samples respectively. Common features indicating various steady state structures as described in the text are indicated in the shaded regions. The notation used in the shaded regions follow the notation that was used in the fourth chapter to describe the different dynamical response regimes of 8CB. (Inset) Arrow indicates a small slope change in the viscosity data of BCN liquid crystal.	102
6.5	Schematic diagram for micro-rheology setup.	104
6.6	(a) Distribution of particle displacements along parallel (circles) and perpendicular (stars) to the director for $\tau = 1 \text{ s}$. The solid lines are Gaussian fits. (b) A micro particle with a dipole defect.	105
6.7	Variation of η_{eff} (stars), $\eta_{ }$ (squares) and η_{\perp} (circles) as a function of shifted temperature. (Inset) Two dimensional projection of trajectories of a microsphere closer to the NI transition ($T - T_{NI} = -7.6^{\circ}\text{C}$) and closer to the $N\text{-SmC}$ transition ($T - T_{NI} = -47.6^{\circ}\text{C}$).	106
6.8	Schematic molecular orientation around the microsphere with dipolar defect configuration. It may be noted that the clusters attached to the microsphere are <i>permanent</i> whereas they are <i>temporal</i> in the bulk. A small dot on the upper side indicates a hyperbolic hedgehod.	107

List of Tables

3.1	Molecular weight (M), birefringence (Δn), dielectric anisotropy ($\Delta\epsilon$), activation energy (E_a), dipole moment (μ) and Kirkwood correlation factor (g) [25] . Both Δn and $\Delta\epsilon$ are taken from Fig. 3.2 and Fig. 3.3 at $T - T_{NI} = -10^\circ\text{C}$.	47
3.2	Viscosity anisotropy $\Delta\eta$ ($= \eta_1 - \eta_2$) obtained from Fig. 3.5 and Fig. 3.9 at $T - T_{NI} = -10^\circ\text{C}$	51

1

Introduction

1.1 Rheology

Rheology is a multidisciplinary science which deals with the study of deformation and flow of matter. The term rheology is originated from a Greek word “rheos” which means “flowing”. In these modern days, rheology constitutes a wider science especially in research with a goal to achieve improved material properties. The flow properties of the ideal viscous liquids and the deformation of ideal elastic solids are well explained using Newton’s and Hooke’s law respectively. Generally, soft materials are neither ideal solids nor ideal liquids but exhibits both properties and are so referred as viscoelastic materials. To analyze which property dominates over the these materials, we need to study rheometry, its a group of experimental technique to investigate the rheological properties of soft materials. Some materials exhibit solid-like property in liquids and liquid-like property in solids, its depends on the scale of the deformation process which is determined by the Deborah number (D_e) is defined as [1].

$$D_e = \frac{\tau}{T}$$

where “ T ” is known as the characteristic time of the deformation process being observed and “ τ ” is known as the material characteristic time. For a Hookean elastic solid, the time τ is infinite whereas for Newtonian viscous liquids the time τ is zero. The flow behavior of liquid crystals depends on the flow orientation and also on the boundary induced orientation. It is determined by a dimensionless number called Ericksen number (E_r), which is defined as the ratio of the flow induced viscous stress to the Frank elastic stress. In the limit of low E_r number the elastic forces will exceed the viscous forces and so the director field will not be strongly affected by the flow field. It can be expressed as

$$E_r = \frac{\eta \dot{\gamma}_{eff}}{K/h^2},$$

where η is the Leslie viscosity coefficient, K is the Frank elastic constant, h is the length scale of the flow geometry and $\dot{\gamma}_{eff}$ is the average effective shear rate. In our study, we emphasized on the viscoelastic properties of some thermotropic liquid crystals.

1.1.1 Rheology of liquid crystals

Rheology of thermotropic liquid crystals have not been studied rigorously as they are not directly related to the device properties. Nevertheless, rheological studies of anisotropic fluids are very interesting in structural point of view. However, some significant progress was made in understanding the flow behavior of low molecular weight thermotropic liquid crystals both theoretically and experimentally. Among these, there are some reports on the measurements of Miesowicz viscosities [2] or Leslie coefficients in the nematic phase as a function of temperature using various experimental techniques. However, the temperature dependent shear viscosity properties are complex in compounds exhibiting N -SmA

phase transition. In this thesis we studied the rheological properties of a few thermotropic liquid crystals exhibiting nematic (N) and smectic-A (SmA) phases.

1.2 Liquid crystals

Liquid crystalline state is a distinct state of matter observed between the crystalline solid and amorphous liquid. Many of the organic compounds having shape anisotropy exhibit this intermediate state. In 1888, an Austrian botanist Fredrich Reinitzer first observed this state of matter and was later named as liquid crystal by Lehmann in 1889. As the name implies liquid crystals have both the liquid-like as well as solid-like properties. In the liquid crystalline phase, molecules exhibit long range orientational order and few of them also exhibit positional order [3–5]. These liquid crystals exhibit liquid-like properties such as highly fluidity, viscosity and surface tension. At the same time they also exhibit solid-like properties such as optical birefringence, anisotropic refractive indices, dielectric and diamagnetic susceptibilities [6, 7]. Liquid crystals are mainly two types namely, thermotropic and lyotropic liquid crystals. In thermotropic liquid crystals, the liquid crystalline phase arises because of temperature, whereas in lyotropic it is by concentration as well as temperature [8, 9].

1.3 Types of liquid crystals

Shape anisotropy is an essential requirement for exhibiting the liquid crystalline phase. Depending on the shape of the molecules, liquid crys-

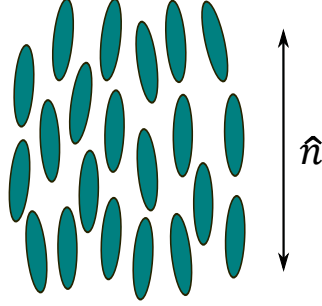


Figure 1.1: Schematic representation of molecular arrangement in the nematic.

tals are classified broadly into three categories [10, 11] namely, calamitic, bent core and discotic liquid crystals.

- (i). Calamitic liquid crystals: consists of rod-like molecules
- (ii). Discotic liquid crystals: consists of disc-like molecules
- (iii). Bent-core liquid crystals: consists of bent-shape molecules

1.3.1 Nematic phase

Nematic(N) phase is the simplest phase among all the known liquid crystalline phases having rotational symmetry. Molecules in this phase exhibit long range orientational order and the center of mass of the molecules are distributed randomly. The average alignment of the molecules with their long axes parallel to each other in a particular direction as shown schematically in Fig. 1.1. The direction is called as **director**, which is a dimensionless unit vector and represented by \hat{n} . The director \hat{n} is apolar in nature *i.e.*, \hat{n} and $-\hat{n}$ and are physically indistinguishable [12]. Some discotic and bent-core liquid crystals also exhibit nematic phase.

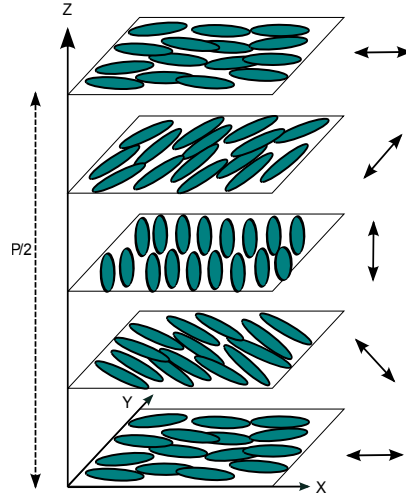


Figure 1.2: Schematic representation of the molecular arrangement in the cholesteric phase. The arrows indicate the orientation of the director \hat{n} .

1.3.2 Cholesteric phase

Cholesteric (N^*) phase is observed when the molecules are either intrinsically chiral or a chiral dopant is added to nematic liquid crystals. In this phase, the molecules exhibit long range orientational order and the director rotates in a helical fashion, whose axis is perpendicular to the director. This helical structure arises from the chiral properties of the constituent molecules, in which the director \hat{n} rotates continuously in space along the z direction. A single rotation of \hat{n} is completed over a distance p , called as pitch. The repetition period is $p/2$, \hat{n} and $-\hat{n}$ are equivalent. The pitch of the cholesteric helix which would be right or left handed and it strongly depends on the temperature. A schematic representation of the director orientation is shown in Fig. 1.2.

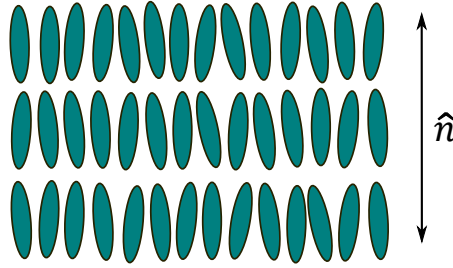


Figure 1.3: Schematic representation of the molecular arrangement in the Smectic-A phase.

1.3.3 Smectic phases

In smectic liquid crystals, the molecules are arranged in layers having a well defined interlayer distance. These phases exhibit an orientational order along with some positional order. There are several types of smectic mesophases based on the molecular arrangement within the layer. The center of mass of the molecules are distributed randomly in the layer.

1.3.4 Smectic-A phase

In Smectic-A (SmA) phase, the molecules are arranged in layers as shown in Fig. 1.3. The director \hat{n} is aligned perpendicular to the layers and is parallel to the layer normal. The center of mass of the molecules in each layers are distributed randomly. In this phase, if the molecules are symmetric and non-polar, the layer spacing is approximately equal to the molecular length.

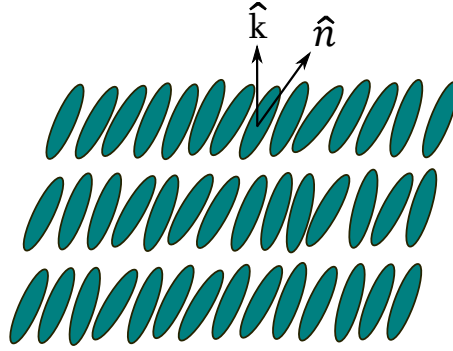


Figure 1.4: Schematic representation of the molecular arrangement in the SmC phase. The molecules are tilted with respect to the layer normal \hat{k} .

1.3.5 Smectic-C phase

In Smectic-C (SmC) phase, the director \hat{n} is tilted at an angle θ to the layer normal as shown in Fig. 1.4, resulting in optical biaxiality of the SmC phase. The tilt angle θ (polar) reduces the thickness of the layer, whereas the azimuthal angle ϕ does not affect the layer thickness. The angle θ is temperature dependent and is called as smectic cone angle. In this phase, the director \hat{n} and $-\hat{n}$ are physically indistinguishable.

1.3.6 Smectic-C* phase

Smectic-C* (SmC^*) phase consists of chiral molecules, where the chiral interactions lead to the formation of a helical structure and the phase is called Smectic-C*. In this phase, the helical axis and the layer normal are in the same direction and it can be right or left handed. The tilt angle θ remains the same whereas the azimuthal angle ϕ varies as we move from layer to layer. The helix of the SmC^* can be unwound either by

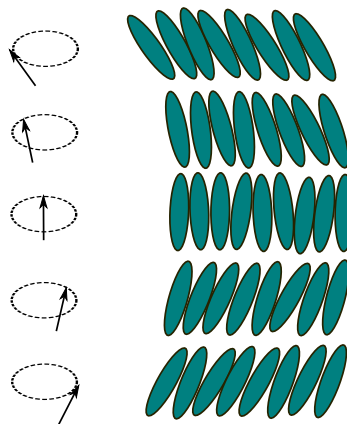


Figure 1.5: Schematic representation of the molecular arrangement in the SmC^* phase. The tilt direction rotates between successive layers as represented by arrows.

surface interactions or by the application of strong magnetic or electric fields. A schematic representation of the molecular arrangement of rod-like molecules in the SmC^* phase is shown in Fig. 1.5.

1.3.7 Bent-core liquid crystals

Liquid crystals consisting of bent core molecules show various mesophases and they are mostly different from those exhibited by rod-like and disk-like molecules [12]. The bent-core molecules are strongly polar and biaxial in shape and thus deviate from the cylindrical symmetry. Bent-core molecules exhibit a new class of liquid crystals, these are known as banana phases B_1, B_2, \dots, B_8 [13]. In addition, these bent-core molecules also show nematic and smectic phases. In the last chapter of this thesis we discuss the rheological properties of a bent-core nematic liquid crystal.

1.4 Physical properties of nematic liquid crystals

1.4.1 Birefringence

Refractive index is a material property which determines the relative speed of light in the material. In liquid crystals, the speed of light for polarization parallel to the director is different from that for the perpendicular direction. Uniaxial nematic phase has two principal refractive indices called n_e and n_o , suffix “e” and “o” stands for extraordinary and ordinary rays respectively. For uniaxial nematic, $n_e = n_{||}$ and $n_o = n_{\perp}$, where the parallel and perpendicular directions are defined in relation to the director. The average value of the refractive indices in the nematic phase is given by

$$\langle n^2 \rangle = \frac{1}{3}(n_{||}^2 + 2n_{\perp}^2)$$

When a plane polarized light enters a birefringent medium, it results in two mutually perpendicular components called the ordinary (o) and extraordinary (e) rays. In uniaxial nematics, the electric field of the o-ray is always perpendicular to the optic axis, so its refractive index n_o is a constant which is independent of propagation direction. In nematic or uniaxial smectic liquid crystal, the optical axis is parallel to the director and $n_e = n_{||}$ and $n_o = n_{\perp}$. The birefringence is given by $\Delta n = n_e - n_o = n_{||} - n_{\perp}$. Generally, the birefringence varies within 0 to 0.5. Δn is used to calculate the approximate order parameter (S) of the nematic liquid crystals by using the relation [12].

$$S \approx \frac{\Delta n}{\Delta n_o}$$

where Δn_o is the birefringence in the fully aligned state.

1.4.2 Dielectric constant

The dielectric constant (ϵ) is a measure of the response of materials in the presence of external electric field. It depends on the intrinsic properties of the materials like distribution of the charges in the molecules as well as the intermolecular interactions. The dielectric constant of the material depends on temperature as well as frequency of applied electric field [14]. In liquid crystals, the dielectric constant $\epsilon_{||}$ and ϵ_{\perp} are measured with electric field parallel and perpendicular to the director (\hat{n}) respectively. The dielectric anisotropy is given by

$$\Delta\epsilon = \epsilon_{||} - \epsilon_{\perp}$$

The dielectric permittivity $\epsilon_{||,\perp}$ of a LC is defined as the ratio of the capacitance $C_{||,\perp}$ of the parallel plate capacitor that contains the material to the empty capacitance C_{emp} of the cell.

$$\epsilon_{||,\perp} = \frac{C_{||,\perp}}{C_{emp}}$$

1.4.3 Order parameter

The order parameter S is a measure of order in the relevant phase. In a nematic liquid crystal, the orientational order parameter defines the average orientation of the long axis of the molecules with respect to the director. The order parameter for uniaxial nematic phase is represented by

$$S_{\alpha\beta}(\vec{r}) = S(n_{\alpha}(\vec{r})n_{\beta}(\vec{r}) - \frac{1}{3}\delta_{\alpha\beta}), \quad (1.1)$$

here, S is a measure of the degree of alignment of the long axis of the molecules along $\hat{n}(\vec{r})$. \hat{n} is independent of \vec{r} in a well aligned nematic

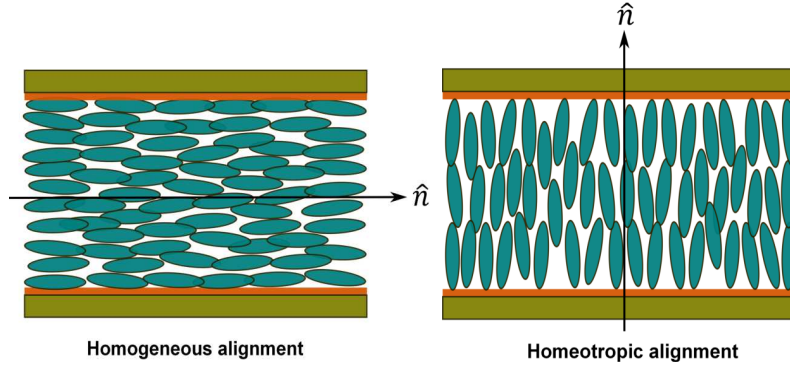


Figure 1.6: Schematic representation of homogeneous and homeotropic alignment of the director between two coated ITO substrates. \hat{n} is the director.

phase. For a cylindrically symmetric molecules the scalar order parameter is defined as [15].

$$S = \frac{\langle 3\cos^2\theta - 1 \rangle}{2} \quad (1.2)$$

In a perfectly aligned sample, the order parameter $S = 1$, whereas in a isotropic phase $S = 0$. Generally, the value of S in a nematic liquid crystal varies from $\simeq 0.3$ to 0.8 with change in temperature. The order parameter S is connected to determination of experimental quantities such as diamagnetic, dielectric anisotropy and birefringence [12].

1.4.4 Alignment of liquid crystals

Alignment of liquid crystals on substrate is very important from technological as well as fundamental research point of view [16, 17]. The uniform orientation of the director is needed to measure several physical properties such as birefringence, dielectric and elastic constants. Here we briefly

discuss about two different alignment of liquid crystals namely, homogeneous and homeotropic. Both homogeneous and homeotropic alignments of liquid crystals can be achieved by coating substrate with appropriate polyimide. In the case of homogeneous alignment, the surface is rubbed in a particular direction and the director is parallel to the rubbing direction, whereas in homeotropic alignment, the alignment layer is oriented perpendicular to the substrate. A schematic representation of the homogeneous and homeotropic alignments of the director is shown in Fig. 1.6.

1.5 Rheological properties of nematic liquid crystals

Two types of measurements are usually made to study the visco-elastic properties of nematic liquid crystals (NLCs) [18–20], we discuss them in the following subsections. We also briefly discuss the Leslie-Ericksen theory that is used to study the viscous properties of NLCs.

1.5.1 Oscillation test

In oscillation test, the amplitude sweep and frequency sweep are the two different measurements which provide the structural behavior of the liquid crystals. In the amplitude sweep, the strain amplitude varies at a constant frequency. This measurement helps in finding the linear viscoelastic (LVE) range of a given material. The viscous and elastic properties are obtained from the amplitude and phase shift of the sinusoidal

functions. For viscoelastic materials the stress is expressed as [19].

$$\tau(t) = \tau_o \sin(\omega t + \delta) \quad (1.3)$$

where $\tau(t)$ is shear stress, τ_o is stress amplitude and δ is phase shift. In general, the sinusoidally varying stress is represented as [19].

$$\tau(t) = \gamma_o [G'(\omega) \sin(\omega t) + G''(\omega) \cos(\omega t)] \quad (1.4)$$

where $G'(\omega)$ is known as the storage modulus which indicates the storage of elastic energy and $G''(\omega)$ is known as the loss modulus which denotes the viscous dissipation energy and γ_o is strain amplitude. In the LVE range at lower amplitudes, storage modulus (G') and loss modulus (G'') are constant. The strain amplitude upto which G' and G'' are constant is represented as γ_L . If $G' > G''$, then the elastic behavior dominates over the viscous behavior which denotes the solid-like behavior. If $G'' > G'$, the viscous behavior dominates over the elastic behavior which indicates the liquid-like behavior of the sample. Using Eq. 1.3 and 1.4, the storage and loss modulus are expressed as,

$$G' = \frac{\tau_o}{\gamma_o} \cos \delta, \quad G'' = \frac{\tau_o}{\gamma_o} \sin \delta.$$

In frequency sweep, the dynamic viscosity, storage and loss moduli are measured by applying a sinusoidal oscillating strain (or stress) to a liquid crystal sample and measuring its stress (or strain) response, as a function of frequency. In liquid-like fluids, the storage modulus is proportional to ω^2 and loss modulus is proportional to ω . In low frequency limit, both G' and G'' obey the power law behavior. In solid-like fluids, the storage modulus is almost independent of frequency. The complex shear modulus can be expressed as [1].

$$G^*(\omega) = G'(\omega) + iG''(\omega) \quad (1.5)$$

where G^* characterizes the overall resistance to deformation of the material (either viscous or elastic). Similarly the complex dynamic viscosity is expressed as [1].

$$\eta^*(\omega) = \eta' - i\eta'' \quad (1.6)$$

Therefore, the relation between the complex shear modulus and complex dynamic viscosity is represented as

$$G^*(\omega) = i\omega\eta^*(\omega) \quad (1.7)$$

By substituting Eqs. 1.5 and 1.6 in Eq. 1.7, we get,

$$G' + iG'' = i\omega[\eta' - i\eta''] \quad (1.8)$$

By comparing real and imaginary parts, we get $\eta' = \frac{G''}{\omega}$ and $\eta'' = \frac{G'}{\omega}$.

1.5.2 Rotational test

Rheological measurements with rotational test reveal the relationship between shear stress versus shear rate and shear viscosity versus shear rate in the form of rheograms (or flow curves) [20]. In these rheograms shear stress and shear viscosities are plotted against shear rate, called as stress and viscous flow curves respectively. Here the shear stress serves as torque and shear rate as speed. In this thesis, we have used rotational test to measure the shear dependent properties of a few thermotropic liquid crystals.

1.6 Leslie-Ericksen theory

The Frank-Oseen theory is used to study elastic properties and Leslie-Ericksen theory used to study the viscous properties of NLCs. These are explained briefly in the following subsections.

1.6.1 Curvature elastic constants of nematic liquid crystals

In nematic liquid crystal the orientation of the director differs from one surface to another. All these deformations that results in elastic distortions which can be considered to be a combination of three basic curvature deformations. They are represented as splay, twist and bend. The deformation free energy density is represented as [3, 4].

$$F_d = \frac{1}{2}K_{11}(\nabla \cdot \hat{n})^2 + \frac{1}{2}K_{22}(\hat{n} \cdot \nabla \times \hat{n})^2 + \frac{1}{2}K_{33}(\hat{n} \times \nabla \times \hat{n})^2 \quad (1.9)$$

where, $\nabla \cdot \hat{n}$ and $\nabla \times \hat{n}$ are the divergence and curl on \hat{n} and K_{11} , K_{22} , K_{33} are splay, twist, bend elastic constants, respectively. Usually, these elastic constants are positive and $K_{33} > K_{11} > K_{22}$ in rod like molecules. The typical magnitude of these constants are $\simeq 10^{-12}$ N. A Schematic representation of splay, twist and bend elastic deformations are shown in Fig. 1.7.

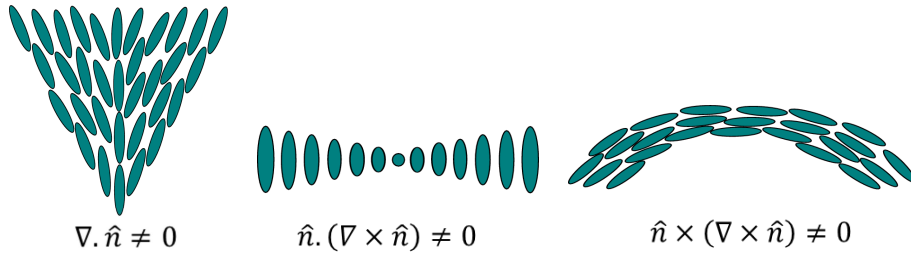


Figure 1.7: A Schematic representation of the splay, twist and bend deformations.

1.6.2 Viscosities of nematic liquid crystals

Viscous effects of nematic liquid crystals are studied by Leslie, called Leslie viscosities. In general, these Leslie viscosities cannot be identified

individually but they are the linear combination of Leslie coefficients and this has been proved experimentally by Miesowicz, referred to as Miesowicz viscosities (η_1, η_2 and η_3). These Miesowicz viscosities are measured

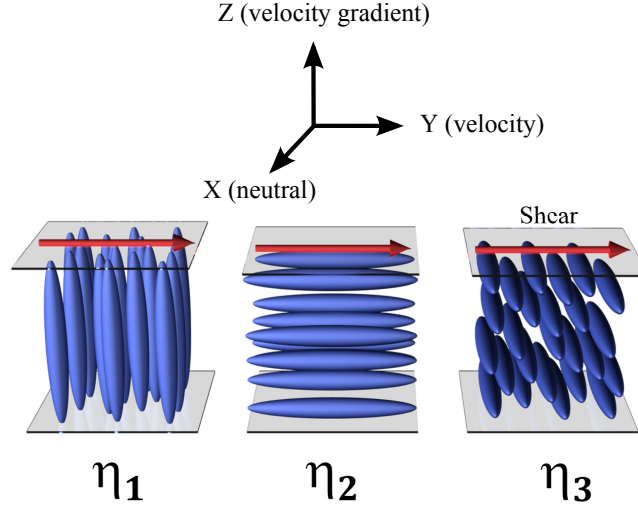


Figure 1.8: Schematic representation of the three fundamental director orientations of nematic liquid crystals with respect to the shear direction. Miesowicz viscosities corresponding to each orientations are designated by η_1 , η_2 and η_3 respectively.

independently by considering the director orientation with respect to velocity (V) and velocity gradient (ΔV). Three basic flow geometries are shown in Fig. 1.8. Miesowicz viscosities η_1 and η_2 are measured when the director is parallel to ΔV and V respectively whereas η_3 measured when the director is perpendicular to both V and ΔV . If the director \hat{n} is aligned in an arbitrary direction with respect to V and ΔV , resulting in the effective viscosity which is a linear combination of the Leslie coefficients. The director \hat{n} can be defined as,

$$\hat{n} = (\cos \theta \cos \phi, \cos \theta \sin \phi, \sin \theta)$$

where θ and ϕ are the angles of the director \hat{n} with respect V and ΔV . From Leslie theory, the viscous stress is expressed as [20].

$$\begin{aligned}\tilde{t}_{i,j} = & \alpha_1 n_k A_{kp} n_p n_i n_j + \alpha_2 N_i n_j + \alpha_3 n_i N_j + \alpha_4 A_{ij} \\ & + \alpha_5 n_j A_{ik} n_k + \alpha_6 n_i A_{jk} n_k\end{aligned}\quad (1.10)$$

where the coefficients $\alpha_1, \alpha_2, \dots, \alpha_6$ are called as Leslie coefficients; n , A and N are represented as the director, stress tensor and the velocity of the director respectively. The apparent viscosity $\eta(\theta, \phi)$ is defined as [20].

$$\begin{aligned}\eta(\theta, \phi) = & \eta_1 \cos^2 \theta \cos^2 \phi + \eta_2 \sin^2 \theta + \eta_3 \sin^2 \phi \cos^2 \theta \\ & + \frac{1}{4} \eta_{12} \sin^2(2\theta) \cos^2 \phi\end{aligned}\quad (1.11)$$

where η_1, η_2, η_3 and η_{12} are the Miesowicz viscosities and η_{12} is a strength type of deformation, which can be neglected. The viscosities η_1, η_2, η_3 are expressed in terms of Leslie coefficients as below

$$\begin{aligned}\eta_1 &= \frac{1}{2}(\alpha_3 + \alpha_4 + \alpha_6) = \frac{1}{2}(\alpha_2 + 2\alpha_3 + \alpha_4 + \alpha_5) \quad \text{when } \theta = 0 \text{ and } \phi = 0 \\ \eta_2 &= \frac{1}{2}(-\alpha_2 + \alpha_4 + \alpha_5) \quad \text{when } \theta = \frac{\pi}{2} \text{ and } \phi = 0 \\ \eta_3 &= \frac{1}{2}\alpha_4 \quad \text{when } \theta = 0 \text{ and } \phi = \frac{\pi}{2}\end{aligned}$$

In terms of Leslie coefficients Eq. 1.11 can be expressed as

$$\begin{aligned}\eta(\theta, 0) = & \alpha_1 \cos^2 \theta \sin^2 \theta + \frac{1}{2}(\alpha_3 + \alpha_6) \sin^2 \theta \\ & + \frac{1}{2}(\alpha_5 - \alpha_2) \cos^2 \theta + \frac{1}{2}\alpha_4\end{aligned}\quad (1.12)$$

This equation is useful to explain some experimental results in chapter fourth and fifth.

References

- [1] H. A. Barnes, J. F. Hutton, and K. Walters. *An Introduction to Rheology*. Annals of Discrete Mathematics. Elsevier, 1989.
- [2] M. Miesowicz. The three coefficients of viscosity of anisotropic liquids. *Nature (London)*, 158:27, 1946.
- [3] Pierre-Gilles De Gennes and Jacques Prost. *The physics of liquid crystals.*, volume 23. Clarendon press Oxford, 1993.
- [4] S. Chandrasekhar. *Liquid Crystals*. Cambridge University Press, 1992.
- [5] V. V. Belyaev. *Viscosity of Nematic Liquid Crystals*. Cambridge International Science Publishing, Cambridge, 2011.
- [6] P. G. de Gennes and J. Prost. *The Physics of Liquid Crystals*. International Series of Monographs on Physics. Clarendon Press, 1995.
- [7] P. J. Collings and M. Hird. *Introduction to Liquid Crystals: Chemistry and Physics*. Liquid Crystals Book Series. Taylor & Francis, 1997.
- [8] Wilhelmus Hendrikus Jeu. *Physical properties of liquid crystalline materials.*, volume 1. CRC Press, 1980.
- [9] W. H. de Jeu. *Physical properties of liquid crystals*. Cambridge University Press, Cambridge, 1992.

-
- [10] G. Friedel. *Ann. Phys. (Paris)*, pages 273–474, 1922.
 - [11] Michael J Stephen and Joseph P. Straley. Physics of liquid crystals. *Reviews of Modern Physics*, 46(4):617, 1974.
 - [12] P. G. de Gennes and J. Prost. *The Physics of Liquid Crystals*. International series of monographs on physics. Clarendon Press, 1993.
 - [13] Hideo Takezoe and Yoichi Takanishi. Bent-core liquid crystals: their mysterious and attractive world. *Japanese journal of applied physics*, 45(2R):597, 2006.
 - [14] L. M. Blinov and V.G. Chigrinov. *Electrooptic Effects in Liquid Crystal Materials*. Partially Ordered Systems. Springer New York, 1996.
 - [15] W. H. Jeu. *Physical Properties of Liquid Crystalline Materials*. Liquid crystal monographs. Gordon and Breach, 1980.
 - [16] A. A. Sonin. *The Surface Physics of Liquid Crystals*. Gordon and Breach Publishers, 1995.
 - [17] K. Takatoh, M. Sakamoto, R. Hasegawa, M. Koden, N. Itoh, and M. Hasegawa. *Alignment Technology and Applications of Liquid Crystal Devices*. Liquid Crystals Book Series. Taylor & Francis, 2005.
 - [18] I. W. Stewart. *The Static and Dynamic Continuum Theory of Liquid Crystals: A Mathematical Introduction*. Liquid Crystals Book Series. Taylor & Francis, 2004.
 - [19] T. G. Mezger. *The Rheology Handbook: For Users of Rotational and Oscillatory Rheometers*. Coatings Compendien. Vincentz Network, 2006.

-
- [20] R. G. Larson. *The Structure and Rheology of Complex Fluids*. Oxford University Press, New York, 1999.

2

Instrumentation

2.1 Introduction

In this chapter, we discuss various experimental techniques used in the thesis. Apart from MCR 501 Rheometer we discuss various geometries and two techniques namely rheo-dielectric and rheo-SALS (Small Angle Light Scattering). We also discuss some non-rheological techniques such as measurement of birefringence (Δn) and dielectric anisotropy ($\Delta\epsilon$).

2.2 Rheometer (MCR 501 Anton Paar)

Anton Paar MCR 501 rheometer is a compact system with air bearings and high performance synchronous motor, having a normal force sensor. The normal force sensor can detect the movement of the bearings. The bottom plate of this rheometer is immovable and is equipped with a Peltier temperature controller unit fitted with a hood to maintain the uniformity of sample temperature. The photograph of MCR 501 rheometer is shown in Fig. 2.1. For air bearing, the oil-free air compressor is used



Figure 2.1: Photograph of a MCR 501 Rheometer (Anton Paar).

which supplies continuous pressure (5-8 bars) to the rheometer. A chiller was used to circulate the water throughout the instrument to maintain the room temperature (25°C). The rheological measurements are controlled and analyzed with the help of RheoPlus software. A wide range of measuring systems are available to measure the rheological properties of variety of samples.

The air bearing supported synchronous motor is one of the prominent component of this rheometer. There are two types of air bearings namely, radial and axial air bearings. The axial air bearing supports weight of all the rotating parts. The optical encoder can measure even very small angular displacements down to $0.1 \mu\text{rad}$. This encoder consists of non-contacting light source and photo cell. The normal force sensor is integrated with the air bearing, it measures the normal force in both positive and negative directions, during the transient and steady state test. The temperature control unit ensures a uniform temperature through out the sample. The Peltier system having an actively controlled

lower plate and hood, which provide a desired level of temperature directly in the plate more rapidly with 0.02°C accuracy. Toolmaster is a fully automated tool, to identify and monitor the MCR 501 rheometer configuration. The TruGap technology is based on induction method which determines the exact gap size between the plates. This technology also aids in suppressing the errors in measurements caused by thermal expansion and normal force. A transponder chip is integrated to the geometry which contains all the relevant geometry data and the same is communicated to the RheoPlus software. The measuring geometries are easily connected to the rheometer rotor using a quick-fitting coupling.

2.3 Measuring geometries

Measuring geometries are mainly divided into three basic categories namely, cone-plate, parallel-plate and cup-bob. Each type of measuring system has its own advantages and disadvantages. In our work we used cone-plate and parallel-plate geometries, and are briefly discussed in the following section.

2.3.1 Cone-plate (CP) geometry

Usually, the measuring geometry consists of a bob with a conical surface and a fixed plate with a flat surface. The geometrical dimensions of this CP are specified by cone radius R and the cone angle α . A schematic setup of the CP geometry is shown in Fig. 2.2. Maintenance of this particular geometry is relatively easy compared to other measuring geometries. It requires relatively small volume of the sample and is well suitable for high viscous materials. The shear rate is maintained uni-

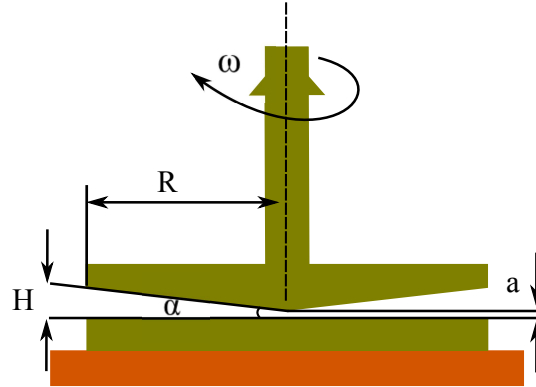


Figure 2.2: Schematic diagram of cone-and-plate measuring geometry. Here the symbols represents the following parameters: R – cone radius, H – gap between the two plates at edge, α – cone angle, ω – angular frequency and a – truncated gap between the plates.

form through out the gap between the plates. Peltier hood is required to reduce any temperature gradients in the sample. To get more accurate rheological measurements in this geometry, the cone tip should be touching the lower plate. For fluids with low viscosity it is preferable to use a large measuring geometry, meaning measuring geometry with large radius that provides a large shear area. Where as for fluids with high viscosity, small measuring geometry would be suitable. The gap between the two plates must be completely filled in order to attain accurate rheological results. Especially in the case of low viscosity liquids, the sample will run out of the gap when the cone rotates and also the turbulent flow behavior may occur at higher shear rates.

2.3.2 Parallel-plate (PP) geometry

Parallel plate (PP) measuring geometry consists of a bob and a fixed plate, both being flat. A schematic setup of this geometry is shown in Fig. 2.3. The geometrical dimensions of this PP geometry, are specified by plate radius R and the gap between the two parallel plates H . Parallel plate geometry alike cone-plate, is easy to clean and also requires only a small sample volume. One major advantage when compared to cone plate geometry is that the distance between two plates is adjustable, so that it is suitable to measure the dispersions containing relatively large particles. The shear rate can be varied between the two plates, and it

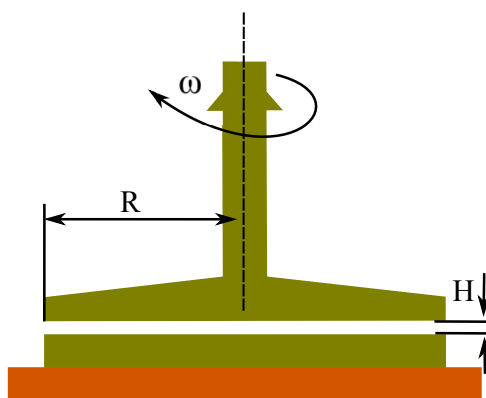


Figure 2.3: Schematic diagram of parallel-plate measuring geometry. Here the symbols represents the following parameters: R — plate radius, H — gap between the two plates and ω — angular frequency.

depends on the distance r from the rotational axis (which increases from zero at the center of the plate to the maximum at the edge). This shear rate has a great influence on the rheological behavior. Peltier hood is used to reduce any temperature gradient in the sample. In this PP geometry, inhomogeneity increases within the sample by increasing H , which leads to the evaporation of solvent. The degree of evaporation can be reduced

using a solvent trap and cover. Therefore, to get accurate rheological data the sample volume must be homogeneous throughout the gap. The large measuring geometry (PP) is preferable to measure the rheological properties of low viscous fluids and some large particle size samples. One major requirement is that the distance between the two plates should be at least 5 times larger than the particle size.

2.4 Electro-Rheology

The Electro-Rheology device is an attachment of Anton Paar MCR 501 rheometer, having Peltier temperature controller unit with a range of -40°C to 200°C . Rheological measurements were performed using a rheometer in the parallel plate geometry with a plate diameter of 50 mm. Parallel plate geometry is a more flexible option to adjust the gap between the plates. The parallel plate configuration was chosen for the simultaneous measurements of the rheological and dielectric properties. Most of the electro-rheological measurements were made with a plate gap of $75\ \mu\text{m}$. The electric field was applied between the plates in upward direction using two electrodes, as shown in Fig. 2.4. The top plate was connected to a low friction spring wire. The **air correction** *i.e.*, contribution due to the small friction in the absence of the sample was subtracted from the measured values when the sample is present.

The dielectric properties can be measured with the help of a LCR meter (Agilent E4980A) upto 20 V. For voltages above 20 V, we have used a signal generator (Tektronix AFG3102) and voltage amplifiers (TEGAM). The frequency of the sinusoidal voltage was 3.11 kHz. Rheometer generates an alternative signal through the M1/M2 port for every measured rheological data and this signal was connected to the LCR meter input.

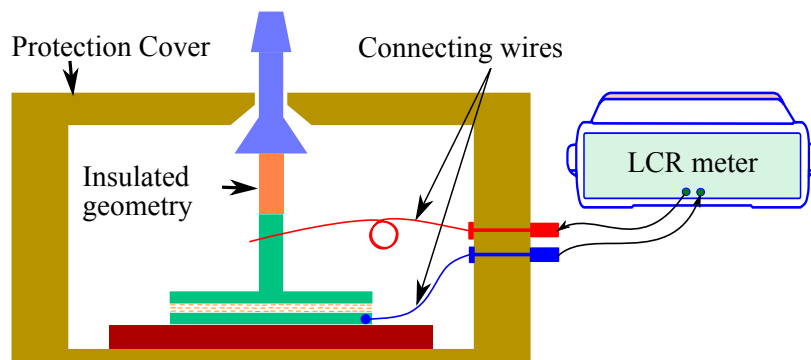


Figure 2.4: Schematic diagram of Electro-Rheology setup.

LCR meter output was connected to the sample with the help of electrodes to measure the capacitance and resistance that can be stored using a storage device. A protecting cover is required to reduce the temperature gradient in the sample and appropriate measuring geometry was connected to the rotor using quick-fitting coupling. Zero-gap was adjusted prior to the sample being mounted between the two plates. The measured rheological data was stored in the computer for further analysis. The temperature of the sample was controlled within an accuracy of 0.1°C by a Peltier temperature controller with an accessory hood for the uniformity of the sample temperature. Calibration of the temperature controller was checked by measuring the phase transition temperature of some standard liquid crystalline materials.

2.5 Small Angle Light Scattering (SALS)

The Small Angle Light Scattering (SALS) is one of the most widely used technique for obtaining the structural information along with the rhe-



Figure 2.5: Photograph of a SALS setup.

ological data simultaneously. Rheological methods exclusively provide the information on the macroscopic behavior of the samples, which are highly dependent on its microscopic structural properties. Study of the micro-structure gave a better insight in understanding the rheological behavior of the samples. SALS working principle involves an incoming beam that is scattered through the sample resulting in the angular distribution, finally analyzing the scattered intensity distribution in the inverse or momentum space. Beam can be scattered because of fluctuations, in concentration or in orientation. Depending upon measurement, the polarizer and the analyzer are kept either parallel (scattering due to fluctuations in concentration) or perpendicular (scattering due to fluctuations in orientation) to each other. Here we studied only scattering due to fluctuations in orientation. The photograph of SALS setup is shown in Fig. 2.5.

A schematic diagram of the setup for SALS is shown in Fig. 2.6.

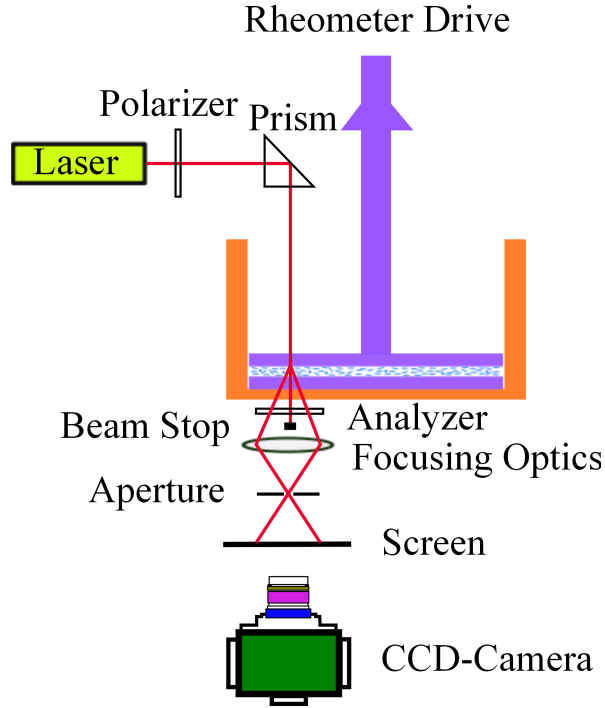


Figure 2.6: Schematic diagram of the small angle light scattering setup.

We used parallel plate geometry (glass plates) with diameter 43 mm, which requires small sample than the concentric cylindrical measuring geometry. Polarized light of a laser diode with a wavelength of 658 nm is deflected into the measuring geometry by a prism. After the sample passes through the analyzer, focusing optics collect the scattered light from a certain point in order to prevent multiple scattering. An analyzer crossed with respect to the polarizer, a beam stopper, and a focusing lens were adjusted to obtain the scattering pattern on the screen. The light scattering patterns are recorded by a CCD camera located below the screen on which the scattered light is directed. The magnitude of scattering vector is defined as,

$$q = \frac{4\pi}{\lambda} \sin\left(\frac{\theta}{2}\right)$$

where λ is the wavelength of light beam and θ represent the scattering angle, respectively. The accessible scattering angle of the SALS system ranges from 2° to 12° , which represent a range for the scattering vector q from $0.3 \mu m^{-1}$ to $2 \mu m^{-1}$. The rate of heating and cooling depends on the circulation bath, used in the setup. The maximum temperature of the liquid bath allowed is 70°C . The appropriate measuring geometry was connected to the rheometer rotor. Zero gap was adjusted prior to the sample being mounted between the two plates. All the measurements were made upon cooling the sample from the isotropic phase. The measured rheological data was stored in computer for further analysis, SALS patterns are analyzed with the help of NewSals software.

2.6 Non-rheological techniques

In this section, we discuss the procedure for cell preparation and the non-rheological experimental techniques that are used for the measurement of birefringence and dielectric constant.

2.6.1 Liquid crystal cell

To prepare liquid crystal cell we used Indium-Tin-Oxide (ITO) coated glass plates with ITO thickness and resistivity of 1500 \AA and $15\text{-}20 \text{ ohm/cm}^2$ respectively. The required pattern of ITO on glass plate is achieved by chemical etching. The ITO patterned glass plates are cleaned thoroughly several times with water, acetone and sonicated in hexane almost 15 min. Nitrogen gas is used to blow off any excess water droplets

before spin coating. Appropriate polyimide is coated at a speed of 6000-8000 rpm. For homogeneous and homeotropic alignments, we used AL-1254 and JALS-204 respectively. The coated glass plates are cured at 180°C and 200°C respectively in an oven for a duration of 1 hr. To obtain the homogeneous alignment, a rubbing machine is used to rub the plates. Two rubbed glass plates are placed one over the other with their active

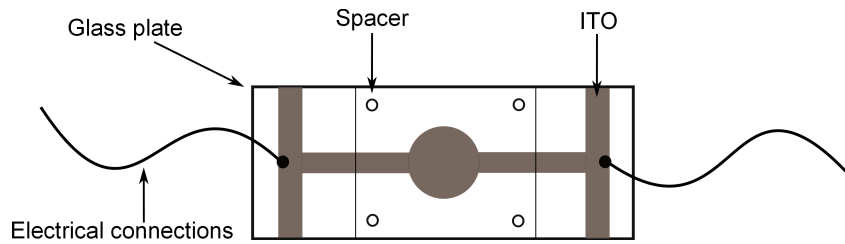


Figure 2.7: Schematic representation of LC cell made up ITO glass plates.

regions facing each other. Making rubbing directions antiparallel. The plates are fixed using a mixture of UV curable adhesive and silica beads. The cell thickness is controlled by the size of silica beads. The schematic diagram of a LC cell is shown in Fig. 2.7.

2.6.2 Measurement of dielectric constant

The LC cell acts as a parallel plate capacitor with an effective area A separated by a distance d . Agilent LCR Meter (E4980A) was used to measure the empty cell capacitance. The LC cell was placed in a heater and heated above T_{NI} of the liquid crystal sample. The sample was filled using the capillary action in the isotropic phase. It is then cooled in the LC phase and observed using a polarizing optical microscope to ensure the desired alignment of the liquid crystal director. The ratio of the capacitances with and without the sample provides the dielectric

constant. In the planer cell, the measured dielectric constant is ϵ_{\perp} , where the applied field is perpendicular to the liquid crystal director. Similarly the dielectric constant measured in a homeotropic cell provides ϵ_{\parallel} as the applied field is parallel to the director. Therefore, the average dielectric constant and dielectric anisotropy can be estimated by using the relations $\langle\epsilon\rangle = (\epsilon_{\parallel} + 2\epsilon_{\perp})/3$ and $\Delta\epsilon = \epsilon_{\parallel} - \epsilon_{\perp}$ respectively.

2.6.3 Measurement of birefringence

We have used phase modulation technique to measure birefringence (Δn) of uniaxial nematic liquid crystals. A schematic optical setup for measurement of Δn using phase modulation technique is shown in Fig 2.8. The setup consists of two crossed Glan-Thompson (GT) polarizers, pho-

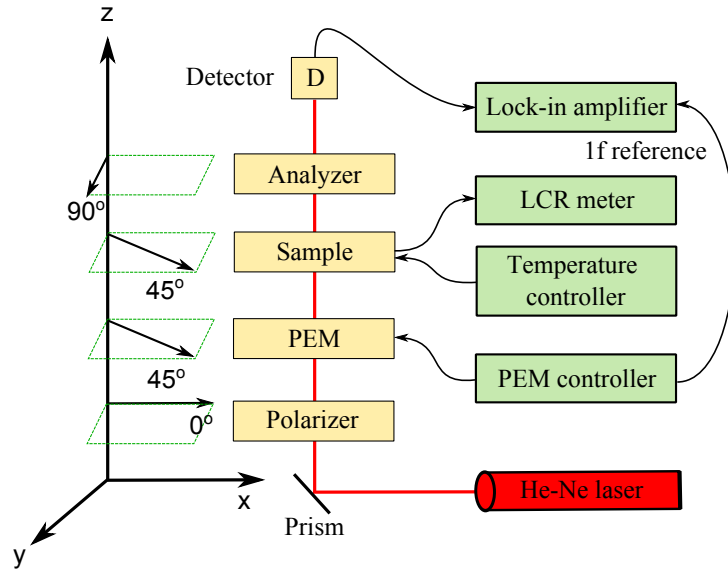


Figure 2.8: Experimental diagram for the measurement of birefringence using PEM.

toelastic modulator (PEM), He-Ne laser and detector. The plane polar-

ized light first passes through a GT polarizer, then through PEM and then through the sample. Here both PEM and sample are kept at an inclination of 45° with respect to polarizer and analyzer. The light transmitted from the sample then passes through analyzer and is detected by the detector. A Lock-in amplifier is connected to the detector to detect the first and second harmonics of the AC signal. Here PEM makes an oscillation with amplitude A_o and an angular frequency ω as a result the retardation (A) can be expressed as $A = A_o \cos(\omega t)$. The intensity at the detector is given by,

$$I = I_o \sin^2(2\theta) \sin^2\left(\frac{\pi(\Delta nd + A)}{\lambda}\right) \quad (2.1)$$

As θ is set to 45° , the above equation reduced to

$$I = I_o \sin^2\left(\frac{\pi(\Delta nd + A)}{\lambda}\right) \quad (2.2)$$

By substituting $A = A_o \cos(\omega t)$ in above equation, we get

$$I = \frac{I_o}{2} \left(1 - \cos\left(\frac{2\pi}{\lambda} \Delta nd + \frac{2\pi}{\lambda} A_o \cos(\omega t)\right)\right) \quad (2.3)$$

$\Delta\Phi$ is the optical phase shift of the liquid crystal sample and defined as $\Delta\Phi = \frac{2\pi d}{\lambda} \Delta n$. By substituting in the above equation, we get

$$I = \frac{I_o}{2} \left[1 - \cos(\Delta\Phi) \cos(A_o \cos(\omega t)) + \sin(\Delta\Phi) \sin(A_o \cos(\omega t))\right] \quad (2.4)$$

The above equation can be written as

$$I = \frac{I_o}{2} \left[1 - \cos(\Delta\Phi) \times \left\{J_0(A_o) + 2(J_2(A_o) \cos(2\omega t)) + \dots\right\} + \sin(\Delta\Phi) \times \left\{2(J_1(A_o) \cos(\omega t)) + \dots\right\}\right] \quad (2.5)$$

where J_0, J_1, J_2 are Bessel functions of various orders, and the intensity can be represented as

$$I = I_o \left[\frac{1 - J_o(A_o) \cos(\Delta\Phi)}{2} + J_1(A_o) \sin(\Delta\Phi) \cos(\omega t) + J_2(A_o) \cos(\Delta\Phi) \cos(2\omega t) + .. \right] \quad (2.6)$$

The intensity measured by the Lock-in amplifier with 1f and 2f frequencies are given by

$$I_{1f} = I_o J_1(A_o) \sin(\Delta\Phi)$$

$$I_{2f} = I_o J_2(A_o) \cos(\Delta\Phi)$$

In this experiments $A_o = 2.405$ and $J_o(A_o) = 0$, $J_1(A_o) = 0.519$ and $J_2(A_o) = 0.4318$. Therefore, the birefringence of the liquid crystal sample is given by

$$\Delta n = \frac{\lambda}{2\pi d} \Delta\Phi = \frac{\lambda}{2\pi d} \arctan \left(\frac{I_{1f} \times J_2(A_o)}{I_{2f} \times J_1(A_o)} \right). \quad (2.7)$$

We have employed this technique to measure the birefringence of highly polar nematic liquid crystals and are discussed in the next chapter.

3

Rheology of nematic liquid crystals with highly polar molecules

3.1 Introduction

In this chapter, we discuss the rheological properties of three nematic liquid crystals with highly polar molecules. Generally, a large number of nematic liquid crystal compounds are used for various applications. Most of the molecules have highly polar cyano or nitro end group. The polar molecules are more stable electrochemically and thermally. The electro-optical response of this liquid crystals depends on their physical properties and they are related to the molecular structures [1–5].

There are several reports on the new electro-optic effects in nematic liquid crystals with highly polar molecules [6]. Apart from those applications, these compounds also exhibit several unusual features such as reentrant phase transitions, smectic-A polymorphism, nematic to nematic transition, strong suppression of director fluctuation by fields etc.

[7–15]. When the nematic liquid crystals are sheared, they exhibit three different viscosities depending on the orientation of the director with respect to the flow and velocity gradient directions and are discussed in the first chapter [see Fig. 1.8]. The Miesowicz viscosities can be expressed in terms of Leslie coefficients (α_1 to α_6) that are used to define the nematic stress tensor as we have already discussed in the first chapter. For a simple shear flow, the dynamic behavior depends on the values of the Leslie coefficients α_2 and α_3 only. If both α_3 and α_2 are negative, then α_2/α_3 is positive indicating that the nematic flow is aligning. The director aligns in the plane of shear at a fixed angle, called Leslie angle, $\theta = \tan^{-1}\sqrt{\alpha_2/\alpha_3}$ [16–20] and in this case the effective viscosity $\eta_{eff} \simeq \eta_2$. The temperature dependent Miesowicz viscosities of nematic liquid crystals depend on the molecular structures and their intermolecular interactions [2, 4, 21]. There are a few studies on the viscosity coefficients of nematic liquid crystals with polar molecules [22–24], but there is no systematic investigation on the structural correlation to the Miesowicz viscosities. In this chapter, we report experimental studies of two Miesowicz viscosities (η_1 and η_2) of three low molecular weight nematic liquid crystals with highly polar molecules. Our results reveal the effect of antiparallel correlation of dipoles and π -electron conjugation of neighboring molecules on the viscosity.

3.2 Experimental

We have chosen the following compounds: 4-(*n*-heptyl)-4'-cyanobiphenyl (CB-7), *trans*-4-(4-heptyl-cyclohexyl)-benzonitrile (PCH-7) and *trans*, *trans*-4-*n*-heptyl-4'-cyanobicyclohexane (CCH-7) having a generic molecular structure. The chemical structures and phase transition tempera-

tures are shown in Fig. 3.1. The lengths and widths of all the molecules

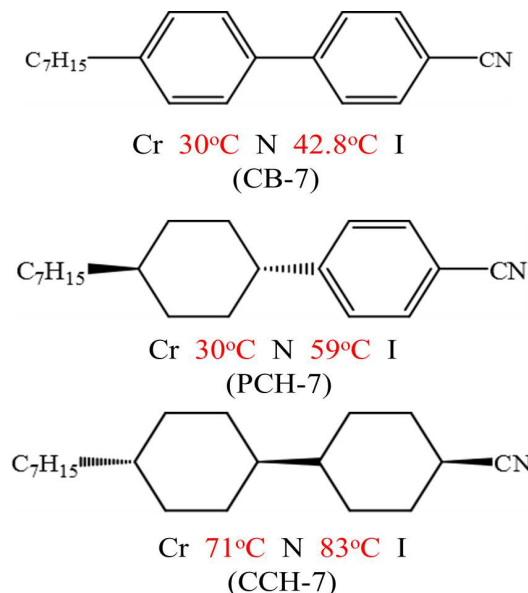


Figure 3.1: Chemical structures of CB-7, PCH-7 and CCH-7 liquid crystals and their phase transition temperatures.

are almost the same [25]. The dielectric anisotropy of all the compounds is positive *i.e.*, $\Delta\epsilon = \epsilon_{\parallel} - \epsilon_{\perp} > 0$, where the subscripts refers to the direction in relation to the director. Some physical properties such as dielectric constants, diamagnetic susceptibility and elastic constants have already been studied [22–25]. Viscosity measurements were made using a Rheometer (Anton Paar MCR 501). Both parallel plate and cone-plate systems induce planar alignment of director [26] and no additional alignment layer was used. We used cone-plate system with diameter 50 mm and cone angle 1° for measuring η_2 and parallel plate geometry with a plate diameter of 50 mm for measuring η_1 . A cell gap of $75 \mu\text{m}$ was used and an electric field was applied between the two plates by using a low friction spring wire [26, 27]. The Freedericksz threshold voltage

for the nematic liquid crystal is given by $V_{th} = \sqrt{K_{11}/\epsilon_o\Delta\epsilon}$, where K_{11} is the splay elastic constant [3]. Since the dielectric anisotropy for the present samples are positive and average molecular orientation is parallel to the direction of shear, the measured viscosity below V_{th} is η_2 . When the applied voltage $V \gg V_{th}$, the director changes orientation and becomes perpendicular to the shear direction and we measure η_1 . The dielectric anisotropy and birefringence were measured by using a photoelastic modulator, He-Ne laser and a LCR meter [28–30]. The small angle light scattering experimental method is already discussed in the previous chapter [27].

3.3 Results and discussion

3.3.1 Birefringence and dielectric anisotropy measurements

First we discuss some non-rheological properties such as the temperature variation of the birefringence (Δn) and dielectric anisotropy ($\Delta\epsilon$). We observe that Δn increases in nematic phase with increasing an aromatic ring from CCH-7 to CB-7 as shown in Fig. 3.2. For example, at a fixed temperature ($T - T_{NI} = -10^\circ\text{C}$) (N phase) $\Delta n_{CCH-7} = 0.046$, $\Delta n_{PCH-7} = 0.086$ and $\Delta n_{CB-7} = 0.16$. Thus merely from the molecular structure point of view (Fig. 3.1), the replacement of a cyclohexane by an aromatic ring increases Δn by an amount of $\simeq 0.04$. Which is expected as the intramolecular conjugation length increases from CCH-7 to CB-7. We observe that $\Delta\epsilon$ also increases in the nematic phase with aromatic ring from CCH-7 to CB-7 as shown in Fig. 3.3. For example, at a fixed temperature ($T - T_{NI} = -10^\circ\text{C}$) $\Delta\epsilon_{CCH-7} = 4$, $\Delta\epsilon_{PCH-7} = 8.7$ and $\Delta\epsilon_{CB-7} = 9.9$. However, the relative difference of dielectric anisotropy between to

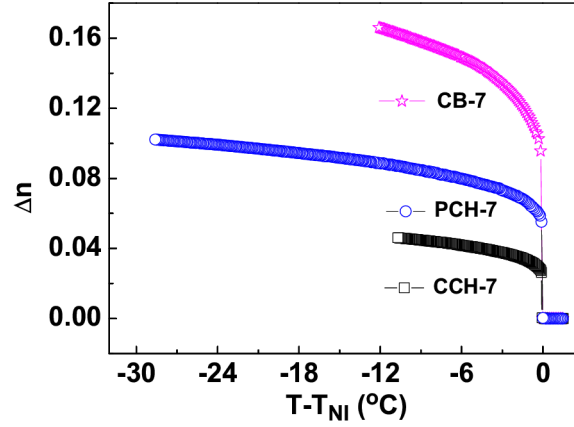


Figure 3.2: Variation of birefringence (Δn) with shifted temperature of CB-7 (stars), PCH-7 (circles) and CCH-7 (squares) liquid crystals with cell thickness $5 \mu\text{m}$.

successive compounds are not regular. For example, at the same temperature, $\Delta\epsilon_{PCH-7} - \Delta\epsilon_{CCH-7} = 4.7$ and $\Delta\epsilon_{CB-7} - \Delta\epsilon_{PCH-7} = 1.2$. Though the dipolar group is the same (-CN), the contribution of the polarizability anisotropy are very different due to the different intramolecular conjugation length.

3.3.2 Shear dependent viscosity measurement

To show the effect of shear on the nematic phase, we show a representative rheo-SALS data of CB-7. We simultaneously measured the effective viscosity as a function of shear rate ($\dot{\gamma}$) in the quenched (isotropic to 35°C) and in presheared samples (Fig. 3.4). It is observed that in the quenched sample, viscosity is high at lower shear rates ($< 10 \text{ s}^{-1}$) and shows strong shear thinning behavior at higher shear rates. When the

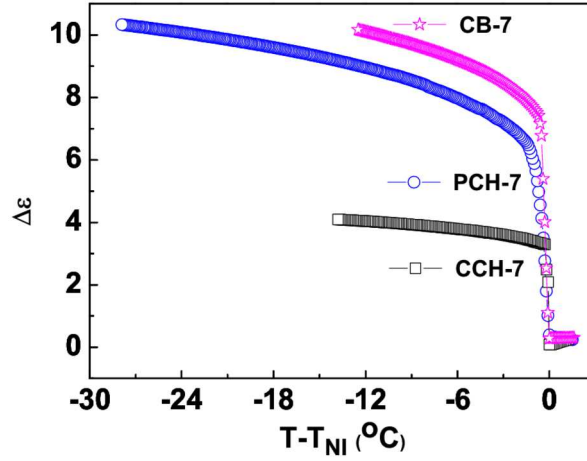


Figure 3.3: Variation of dielectric anisotropy ($\Delta\epsilon$) with shifted temperature of CB-7 (stars), PCH-7 (circles) and CCH-7 (squares) liquid crystals. The dielectric constants are measured at a frequency of 4.11 kHz. Cell thickness 5 μm .

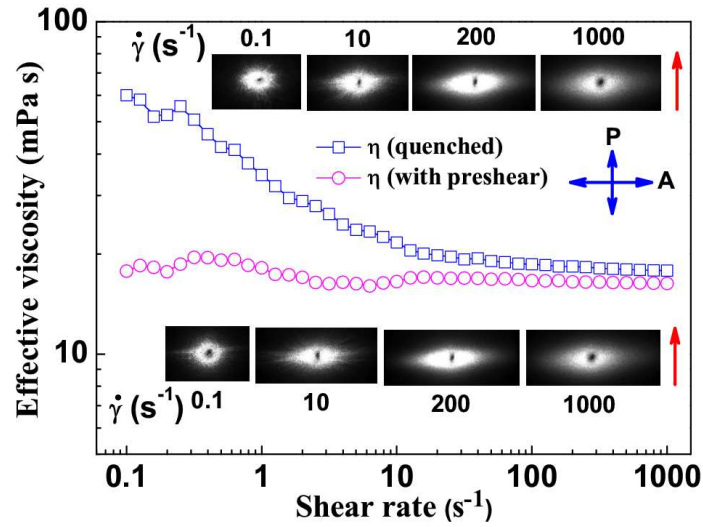


Figure 3.4: Variation of the effective viscosity as a function of shear rate in the nematic phase of CB-7 in quenched (squares) and presheared (circles) samples at 35°C. P, A are polarizer and analyzer. Red arrow indicates the direction of shear.

sample is presheared at 500 s^{-1} for about 10 minutes, the viscosity is almost constant and does not depend on the shear rate. In fact, beyond $\dot{\gamma} = 50 \text{ s}^{-1}$, the effective viscosities are almost comparable. The light scattering patterns in two cases in the low shear-rate range are different. For example, in the quenched sample, at $\dot{\gamma} = 0.1 \text{ s}^{-1}$, the scattering pattern is almost circular. This indicates that in the quenched sample, at the low shear rate, there is a spatial variation of the director which gives polydomain textures. At higher shear rate the circular patterns get elongated perpendicular to the shear direction and the viscosity shows shear thinning behavior. Since SALS measures the image in the \mathbf{q} space, it suggests that the polydomain textures are elongated parallel to the shear direction. This enforces realignment of the director along the shear direction. In the presheared sample the scattering pattern at $\dot{\gamma} = 0.1 \text{ s}^{-1}$ is slightly elongated suggesting that the director is already aligned along the shear direction. The scattering patterns in both the cases are almost similar beyond $\dot{\gamma} = 10 \text{ s}^{-1}$, suggesting that the effective viscosity at higher shear rate is equal to η_2 (*i.e.*, $\eta_{eff} \simeq \eta_2$).

3.3.3 Miesowicz viscosity η_2

In Fig. 3.5, the variation of η_2 of CB-7, PCH-7 and CCH-7 is shown as a function of temperature. The isotropic viscosity (η_{iso}) of CB-7 is much larger than that of PCH-7 and CCH-7 and they vary in the increasing order, $\eta_{iso}^{CB-7} > \eta_{iso}^{PCH-7} > \eta_{iso}^{CCH-7}$. In addition, η_{iso} increases as the temperature is reduced and an abrupt decrease is observed at the nematic-isotropic (NI) transition temperature. The temperature dependent, η_{iso} of all the compounds increase linearly and we fit to Arrhenius equation, $\eta_{iso} = \eta_o \exp(-E_a/kT)$, where η_o is the pre-exponential factor and E_a is the activation energy of the isotropic viscosity.

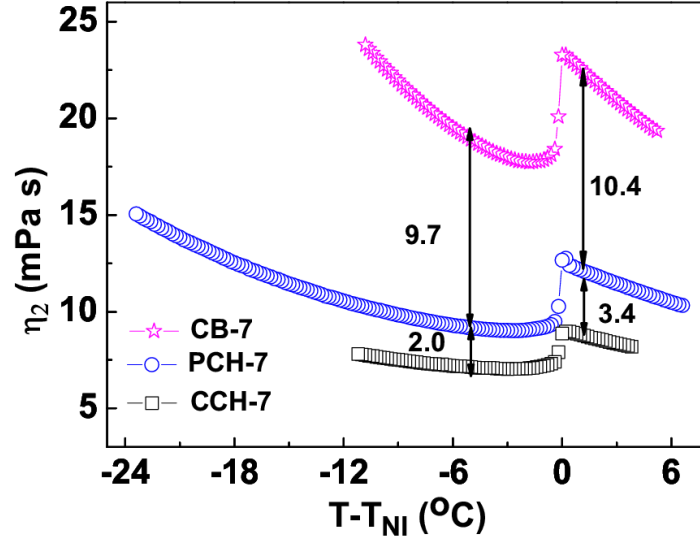


Figure 3.5: Variation of η_2 as a function of shifted temperature at a fixed shear rate, $\dot{\gamma} = 50 \text{ s}^{-1}$.

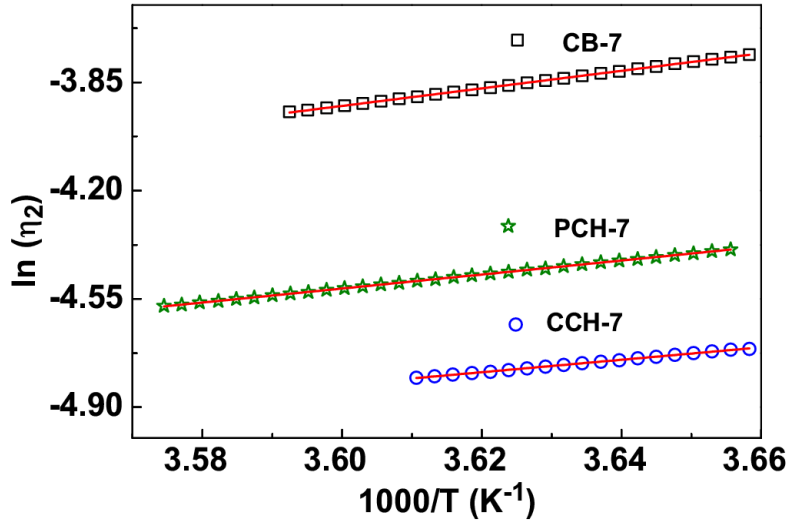


Figure 3.6: Variation of logarithm of η_2 with the inverse of temperature in the isotropic phase. The lines are best fit to Arrhenius equation.

The logarithm of viscosity is plotted against inverse temperature as shown in Fig. 3.6 and the activation energies are listed in the Table 3.1. We notice that they increase in the following order, *i.e.*, $E_a^{CB-7} > E_a^{PCH-7} > E_a^{CCH-7}$. The increase of activation energy is an indicator of increasing intermolecular interaction in the isotropic phase. It may be emphasized that CCH-7 has no aromatic ring, PCH-7 has

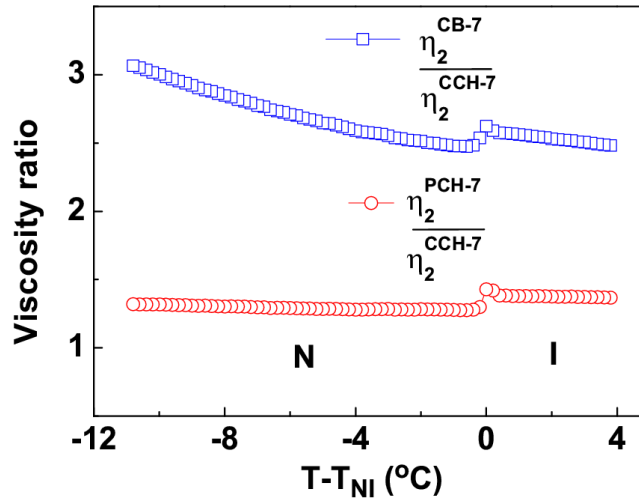


Figure 3.7: Comparison (ratio) of η_2 of CB-7 and PCH-7 with respect to that of CCH-7.

one aromatic ring and CB-7 has two aromatic rings. The increase of number of aromatic rings can enhance the $\pi - \pi$ interaction of aromatic cores (π -electron conjugation) among neighboring molecules and hence the stronger intermolecular interaction is expected. Thus the increase in isotropic viscosity in compounds having phenyl rings can be attributed to the effect of enhanced π -electron conjugation compared to the compounds having cyclohexane because in the later there is no π -electron at the core. In the nematic phase, at a fixed temperature, η_2 also increases in the same order *i.e.*, $\eta_2^{CB-7} > \eta_2^{PCH-7} > \eta_2^{CCH-7}$ (Fig. 3.5).

Further, it is interesting to note that the relative differences among the viscosities of CCH-7, PCH-7 and CB-7 are reduced in the nematic phase than that in the isotropic phase. For example, at $T - T_{NI} = -1^\circ\text{C}$, $\eta_{iso}^{PCH-7} - \eta_{iso}^{CCH-7} = 3.4 \text{ mPa s}$ and $\eta_{iso}^{CB-7} - \eta_{iso}^{PCH-7} = 10.4 \text{ mPa s}$ respectively. In the nematic phase, for example, at $T - T_{NI} = -5^\circ\text{C}$, $\eta_2^{PCH-7} - \eta_2^{CCH-7} = 2 \text{ mPa s}$ and $\eta_2^{CB-7} - \eta_2^{PCH-7} = 9.7 \text{ mPa s}$ respectively. We compare η_2 of CB-7 and PCH-7 with respect to CCH-7 and show their temperature variation in Fig. 3.7. It is noticed that $\eta_2^{CB-7}/\eta_2^{CCH-7}$ is much larger (almost double) than $\eta_2^{PCH-7}/\eta_2^{CCH-7}$ and the former one increases with decreasing temperature. This suggests that the viscosity enhancement is not linear with the number of aromatic rings (replacing cyclohexane rings) keeping the other parts of the molecule same. The molecular weight of the compounds are slightly different (Table 3.1) hence expected not to contribute so much to the viscosity. On the other hand, the nematic to isotropic (NI) phase transition temperatures are very different ($T_{NI}^{CCH-7} > T_{NI}^{PCH-7} > T_{NI}^{CB-7}$) and this will have significant effect on the viscosity in the sense that the viscosity is lower at higher temperature. Nevertheless, the large differences of η_2 among the compounds and their temperature dependence can not be accounted based on this fact alone. To understand this, we present some useful data, in Table 3.1, *i.e.*, the birefringence (Δn), dielectric anisotropy ($\Delta\epsilon$), dipole moment (μ), and Kirkwood correlation factor (g). The Kirkwood correlation factor g is expressed as,

$$g = (\mu_{eff}/\mu)^2 \quad (3.1)$$

where μ_{eff} is the effective dipole moment as calculated from Kirkwood-Froehlich equation [31] using dielectric data and μ is the dipole moment of a single molecule. Both Δn and $\Delta\epsilon$ are positive and increase from CCH-7 to CB-7 as expected because larger contribution of aromatic rings

Table 3.1: Molecular weight (M), birefringence (Δn), dielectric anisotropy ($\Delta\epsilon$), activation energy (E_a), dipole moment (μ) and Kirkwood correlation factor (g) [25]. Both Δn and $\Delta\epsilon$ are taken from Fig. 3.2 and Fig. 3.3 at $T - T_{NI} = -10^\circ\text{C}$.

Compounds:	CCH-7	PCH-7	CB-7
M	289.5	283.45	277.40
Δn	0.046	0.086	0.161
$\Delta\epsilon$	4.0	8.7	9.9
$E_a(\text{eV})$	0.17	0.2	0.24
$\mu(\text{D})$	3.5	4.4	4.7
g	0.70	0.60	0.50

to the birefringence than cyclohexanes as discussed earlier. The dipole moment μ of the molecules obtained from ref. [25] varies in the order $\mu^{CB-7} > \mu^{PCH-7} > \mu^{CCH-7}$. It may be mentioned (Fig. 3.1) that the charge separation of the molecules in the ground state are very different [25]. For example, conjugation between the two aromatic rings in CB-7 is only partial due to the torsional angle between the planes in the ground state is about 35° . The cyano group is conjugated with one aromatic ring in PCH-7 and unconjugated in case of CCH-7, hence no delocalization of the electrons and as a result there is a systematic variation in the dipole moments (see Table 3.1). This gives rise to molecular association that is usually measured in terms of Kirkwood correlation factor.

The Kirkwood correlation factors of these compounds were measured by Schad *et al.* just above the NI transition temperature [25]. It is presented in Table 3.1 for comparative discussion. g lower than 1 for all

the compounds suggest existence of antiparallel correlation of the molecular dipoles even in the isotropic phase. In addition, we notice that, $g^{CB-7} < g^{PCH-7} < g^{CCH-7}$. This suggests that the strength of antiparallel correlation of dipoles is stronger in CB-7 than both PCH-7 and CCH-7. In the nematic phase density increases and the intermolecular distance decreases and antiparallel correlation is even stronger that is reflected in terms of reduction in average dielectric constant ($\bar{\epsilon} = (\epsilon_{||} + 2\epsilon_{\perp})/3$) [25]. In addition to that it causes π -electron conjugation of aromatic rings of neighboring molecules. In case of CB-7, due to the effect of intermolecular π -electron conjugation and dipolar antiparallel correlation it behaves like a dimer because of almost complete overlap of the aromatic rings, whereas CCH-7 behaves like a monomer due to lack of π -electron conjugation [2]. Thus the relative reduction of η_2 in the nematic phase compared to the isotropic viscosity (η_{iso}), can be attributed to the molecular association due to antiparallel correlation of dipole and intermolecular π -electron conjugation.

3.3.4 Miesowicz viscosity η_1

To measure η_1 , first we measured the electric field dependent viscosity at a fixed temperature in the nematic phase (Fig. 3.8). It is observed that the effective viscosity increases with applied electric field for all the samples and saturate beyond about 80×10^4 V/m. Since the dielectric anisotropy is positive (*i.e.*, $\Delta\epsilon > 0$), beyond the Freedericksz threshold field the director tends to orient along the electric field direction. However, the shear field tends to align the director along the shear direction. Thus, there is a competing effect of these two force fields on the director orientation. However, at a steady shear rate if the electric field is strong enough the director is finally orientated along the electric field direction.

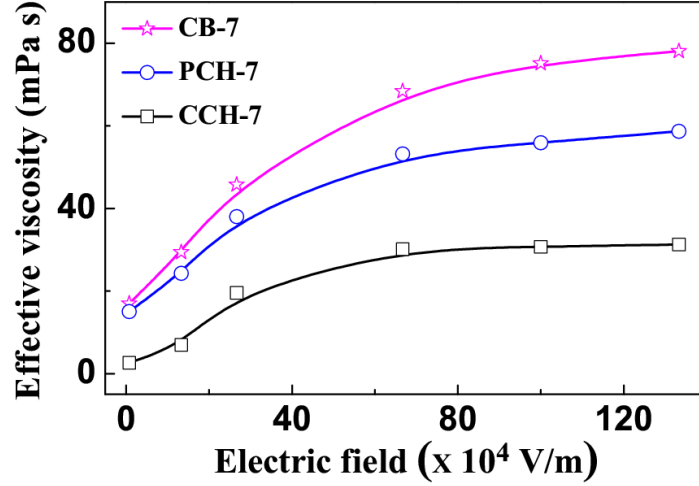


Figure 3.8: Variation of effective viscosity (η_{eff}) at a fixed shear rate, $\dot{\gamma} = 50 \text{ s}^{-1}$ as a function of applied field at a frequency 3.11 kHz. At high field (beyond about $80 \times 10^4 \text{ V/m}$) $\eta_{eff} = \eta_1$.

As a result the equilibrium orientation of the director is perpendicular to the shear direction. Thus essentially we measure η_1 at high electric field ($> 80 \times 10^4 \text{ V/m}$).

In Fig. 3.9, we show the variation of η_1 as a function of temperature for all the compounds. We notice that apart from a sharp increase at the NI transition, η_1 increases almost linearly as the temperature is reduced for all the compounds. At a fixed temperature, in all the compounds, $\eta_1 > \eta_2$ as expected. In the nematic phase, the relative differences of η_1 among the compounds are almost comparable. For example, at $T - T_{NI} = -5^\circ\text{C}$, $\eta_1^{PCH-7} - \eta_1^{CCH-7} = 18.7 \text{ mPa s}$ and $\eta_1^{CB-7} - \eta_1^{PCH-7} = 19.8 \text{ mPa s}$ respectively. The viscosity anisotropy $\Delta\eta$ ($= \eta_1 - \eta_2$) obtained from Fig. 3.5 and Fig. 3.9 are presented in Table 3.2. It is noticed that $\Delta\eta$ increases almost linearly with Δn from CCH-7 to CB-7. As far as

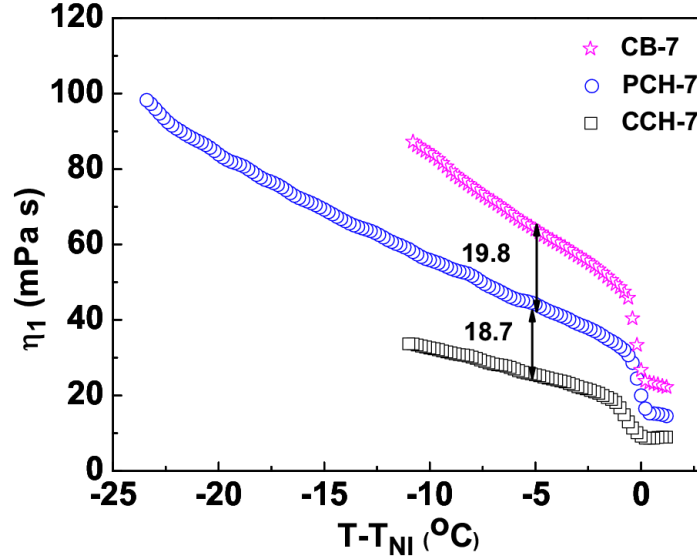


Figure 3.9: Variation of η_1 as a function of shifted temperature and fixed electric field 133×10^4 V/m ($\dot{\gamma} = 50$ s $^{-1}$).

molecular structure is concerned (Fig. 3.1), it seems that the replacement of a cyclohexane by an aromatic ring increases $\Delta\eta$, by 15 to 20 mPa s. In case of η_2 the director is parallel and in case of η_1 , the director is perpendicular to the shear direction. In the rheometer, the bottom plate is fixed and the top plate is rotating hence the velocity gradient decreases from top to bottom. From the microscopic point of view this will cause a net downward flow of momentum per unit time and area which is proportional to the viscous frictional force. The frictional force depends on molecular associations, which is due to intermolecular conjugation length and permanent dipole moment. Thus the molecular associations not only contribute to the dielectric and optical properties but also to the Miesowicz viscosities.

Table 3.2: Viscosity anisotropy $\Delta\eta$ ($= \eta_1 - \eta_2$) obtained from Fig. 3.5 and Fig. 3.9 at $T - T_{NI} = -10^\circ\text{C}$.

Compounds:	CCH-7	PCH-7	CB-7
$\Delta\eta$ (mPa s):	25	45	62

3.4 Conclusions

We have measured temperature dependence of two Miesowicz viscosities (η_1 and η_2) of three highly polar nematic liquid crystals, having a systematic variation in the molecular structure. We showed that nematic compounds with more number of aromatic rings and lower Kirkwood correlation factor have larger viscosities. Low Kirkwood correlation factor is an indication of strong antiparallel correlation of dipoles. The temperature variation of η_2 reveals strong intermolecular associations that results from both the π -electron conjugation of neighboring molecules and antiparallel correlation of molecular dipoles. Compare to molecular associations, intramolecular conjugation length seems to be more significant in determining η_1 . Finally our measurements established that apart from the optical and dielectric properties, molecular associations of highly polar molecules in nematic liquid crystals significantly affect the rheological properties.

References

- [1] P. G. de Gennes. The physics of liquid crystals. *Oxford University Press, Oxford, 2nd ed., 1993.*
- [2] S. Chandrasekhar. Liquid crystals. *Cambridge University Press, 2nd ed., 1992.*
- [3] L. M. Blinov and V. G. Chigrinov. Electrooptic effects in liquid crystal materials. *Springer-Verlag Inc., 1994.*
- [4] W. H. de Jeu. Physical properties of liquid crystals. *Cambridge University Press, 2nd ed., 1992.*
- [5] A. Fukuda D. A. Dunmur and G. R. Luckhurs. Physical properties of liquid crystals:nematics. *Inspect publication, 2001.*
- [6] Geetha Basappa and N. V. Madhusudana. New type of high-field electro-optic response in nematics. *Proc. SPIE*, 4147:116–125, 2000.
- [7] N. V. Madhusudana. liquid crystals made of highly polar compounds. *Brazilian journal of physics*, 28(4), 1998.
- [8] Sobha R. Warriar, D. Vijayaraghavan, and N. V. Madhusudana. Evidence for a nematic-nematic transition in thin cells of a highly polar compound. *EPL (Europhysics Letters)*, 44(3):296, 1998.
- [9] N. V. Madhusudana. S. Chandrasekhar. The role of permanent dipoles in nematic order. 1(3):57–68, 1975.

-
- [10] J. Prost and John. Toner. Dislocation-loop melting theory of phase diagrams with nematic regions surrounded by smectic regions. *Phys. Rev. A*, 36:5008–5014, Nov 1987.
- [11] A. S. Govind and N. V. Madhusudana. A simple molecular theory of a nematic–nematic phase transition in highly polar compounds. *Liquid Crystals*, 14(5):1539–1551, 1993.
- [12] Surajit Dhara and N. V. Madhusudana. Influence of director fluctuations on the electric-field phase diagrams of nematic liquid crystals. *Europhys Lett.*, 67:411, 2004.
- [13] S. Dhara and N. V. Madhusudana. Effect of high electric fields on the nematic to isotropic transition in a material exhibiting large negative dielectric anisotropy. *The European Physical Journal E*, 22(2), 2007.
- [14] M. Miesowicz. Influence of a magnetic field on the viscosity of para-azoxyanisol. *Nature (London)*, 17:261, 1935.
- [15] F. M. Leslie. Some constitutive equations for anisotropic fluids. *The Quarterly Journal of Mechanics and Applied Mathematics*, 19(3):357–370, 1966.
- [16] J. L. Ericksen. Anisotropic fluids. *Arch. Rational Mech. Ana*, 4:231–237, 1960.
- [17] T. Carlsson and K. Skarp. The stabilizing effect of an electric field on the shear flow of nematic liquid crystals when $\alpha_3 > 0$: Flow alignment regained. *Molecular Crystals and Liquid Crystals*, 78(1):157–171, 1981.
- [18] T. Carlsson and K. Skarp. Theoretical investigation of the shear flow of nematic liquid crystals with the leslie viscosity $\alpha_3 > 0$: Hydrody-

- namic analogue of first order phase transitions. *Molecular Crystals and Liquid Crystals*, 104(3-4):307–334, 1984.
- [19] Keishi Negita. Electrorheological effect in the nematic phase of 4-n-pentyl-4'-cyanobiphenyl. *The Journal of Chemical Physics*, 105(17):7837–7841, 1996.
- [20] A. G. Chmielewski. Viscosity coefficients of some nematic liquid crystals. *Molecular Crystals and Liquid Crystals*, 132(3-4):339–352, 1986.
- [21] B. Bahadur. Liquid crystals: Applications and uses. *Vol 1, World Scientific Publishing, 1995*.
- [22] H. H. Graf, H. Knepe, and F. Schneider. Shear and rotational viscosity coefficients of two nematic liquid crystals. *Molecular Physics*, 77(3):521–538, 1992.
- [23] Robert Orr and Richard A. Pethrick. Viscosity coefficients of nematic liquid crystals: Measurements of some nematic liquid crystals. *Liquid Crystals*, 38(9):1183–1191, 2011.
- [24] Hp. Schad, G. Baur, and G. Meier. Investigation of the dielectric constants and the diamagnetic anisotropies of cyanobiphenyls (cb), cyanophenylcyclohexanes (pch), and cyanocyclohexylcyclohexanes (cch) in the nematic phase. *The Journal of Chemical Physics*, 71(8):3174–3181, 1979.
- [25] Hp. Schad and M. A. Osman. Elastic constants and molecular association of cyano-substituted nematic liquid crystals. *The Journal of Chemical Physics*, 75, 1981.
- [26] J. Ananthaiah, M. Rajeswari, V. S. S. Sastry, R. Dabrowski, and S. Dhara. Effect of electric field on the rheological and dielectric

- properties of a liquid crystal exhibiting nematic-to-smectic-a phase transition. *The European Physical Journal E*, 34(8):1–6, 2011.
- [27] J. Ananthaiah, M. Rajeswari, V. S. S. Sastry, R. Dabrowski, and Surajit Dhara. Rheological properties of a reentrant nematic liquid crystal. *Phys. Rev. E*, 86:011710, Jul 2012.
- [28] P. Sathyanarayana, B. K. Sadashiva, and Surajit Dhara. Splay-bend elasticity and rotational viscosity of liquid crystal mixtures of rod-like and bent-core molecules. *Soft Matter*, 7:8556–8560, 2011.
- [29] P. Sathyanarayana, M. Mathew, Q. Li, V. S. S. Sastry, B. Kundu, K. V. Le, H. Takezoe, and Surajit Dhara. Splay bend elasticity of a bent-core nematic liquid crystal. *Phys. Rev. E*, 81:010702, Jan 2010.
- [30] P. Sathyanarayana, V. S. R. Jampani, M. Skarabot, I. Musevic, K. V. Le, H. Takezoe, and S. Dhara. Viscoelasticity of ambient-temperature nematic binary mixtures of bent-core and rodlike molecules. *Phys. Rev. E*, 85:011702, Jan 2012.
- [31] J. F. Boettcher and P. Bordewijk. Theory of electric polarisation. *Elsevier, Amsterdam, Vol.II, 1978*.

4

Rheo-dielectric and electro-rheological properties of 8OCB liquid crystal

4.1 Introduction

In the previous chapter we have studied the rheological properties of three highly polar nematic liquid crystals, having a systematic variation in the molecular structure. In this chapter we discuss the simultaneous measurements of shear viscosity (η) and dielectric constant (ϵ) of octyloxy cyanobiphenyl (8OCB) liquid crystal as a function of temperature and electric field.

The structure property relation, phase transitions and electro-optic properties of low-molecular-weight thermotropic liquid crystals have always been the main area of research. Flow behavior of such materials has not been studied so rigorously as it is not directly related to the device properties. Nevertheless, some significant progress has been made in understanding the flow behavior of low-molecular-weight liquid crys-

tals both theoretically and experimentally [1–36]. Among them there are many reports on the measurement of Miesowicz viscosities or Leslie coefficients in the nematic phase as a function of temperature using various experimental techniques and the results are discussed on the basis of Leslie [1] and Ericksen [2] theories. However, the temperature-dependent shear viscosity is very different and complex in compounds exhibiting N -SmA phase transition. In a pioneering work Safinya *et al.* [14] have shown several steady-state structures that results from the interplay between the viscous frictional forces and flow-induced fluctuation forces by synchrotron X-ray radiation. They showed various shear-induced structural changes and precessional motions of nematic director in the octyl cyanobiphenyl (8CB) compound as the SmA phase is approached.

First, we briefly discuss the effect of shear on the N -SmA transition in 8CB compound [15]. In the nematic phase, under shear there are mainly three different director orientations namely a , b , c with respect to the flow (velocity) direction and the corresponding Miesowicz viscosities [4] are represented by $\eta_a = (\eta_3)$, $\eta_b = (\eta_2)$ and $\eta_c = (\eta_1)$ respectively which are shown in Fig. 4.1. Usually, for all nematic liquid crystals $\alpha_2 < 0$

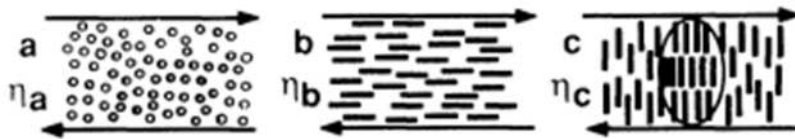


Figure 4.1: (a) Three fundamental director orientations under shear flow and SmA fluctuation is shown for the c orientation. Adapted from ref [15].

and the director orientation under flow depends on the sign of α_3 . Normally near nematic to isotropic transition (T_{NI}), $\alpha_3 < 0$ and the ratio of Leslie coefficients α_2/α_3 is positive and the director tends to align

along the flow direction with the orientation angle $\theta = \tan^{-1}(\sqrt{\alpha_2/\alpha_3})$ with respect to the velocity direction. Just below the I - N transition, the director is parallel to the shear plane in the b orientation, which is stable. This stable b orientation for \hat{n} is shown schematically in the right side of the Fig. 4.2(top). Below the I - N transition the director undergoes flip transition through a mixed state namely, a - b in Fig. 4.2 (bottom). On the otherhand, α_3 is renormalized ($\alpha_3^R > 0$) in compounds exhibiting N -SmA transition due to the pretransitional smectic fluctuations, those introduce an elastic distortion between the bulk and the wall layer. The flow alignment of the director is prohibited that leads to several structural distortions namely, $a_m, a_s, a(b)$ and a_c depending on the temperature and shear rate [14]. These structures arise because of precessional motion of the director at which $\dot{\gamma}\tau \rightarrow 1$ and the director oriented along the neutral direction (z-axis) that can be described by the equation of an ellipse: $n_x^2(t)/n_{x0}^2 + n_y^2(t)/n_{y0}^2 = 1$, where $n_x(t) = n_{x0}\cos(\omega_0 t)$ and $n_y(t) = n_{y0}\sin(\omega_0 t)$ are components of the director $\mathbf{n}(t) = (n_x(t), n_y(t), n_z(t))$. Thus the director precess with an angular frequency $\omega_0 = \sqrt{\dot{\gamma}^2(-\alpha_2\alpha_3^R)/\gamma_1^2}$ where α_3^R is the renormalized viscosity coefficient, $\dot{\gamma}$ is the shear rate and $\gamma_1 = \alpha_3 - \alpha_2$ [14]. The above mentioned structures are described as follows. In a_m structure: the precessional motion is anisotropic with a larger amplitude in the x direction than the y direction ($n_{x0} > n_{y0}$); a_s structure: isotropic precession with equal amplitude in both the directions ($n_{x0} = n_{y0}$); $a(b)$ structure: anisotropic precession with lesser amplitude in the x direction than the y direction ($n_{x0} < n_{y0}$) and in a_c structure: anisotropic precession with a very large amplitude in the y direction ($n_{x0} \ll n_{y0}$). The schematic representation of the distribution of \hat{n} for three structures are shown in Fig. 4.2 (top). In this chapter we discuss the electro-rheological and

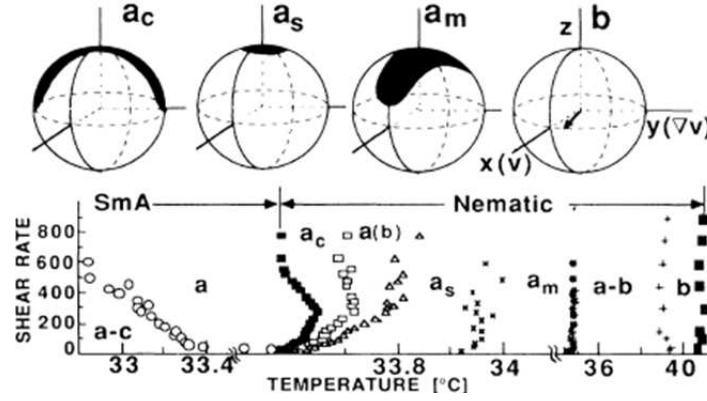


Figure 4.2: Bottom: The $\dot{\gamma} - T$ phase diagram for 8CB compound. Top: Schematics of the stable orientation of director in the b regime (right), and the distribution of director in three of the a regimes (left). Adapted from ref [15].

rheo-dielectric studies on octyloxy cyanobiphenyl (8OCB) liquid crystal.

4.2 Experimental

Compound octyloxy cyanobiphenyl (8OCB) was synthesized by our collaborators from Poland, and exhibits the following phase sequences as observed in polarising optical microscope on cooling: I 79.5°C N 66.6°C SmA 54.5°C Cr. The chemical structure and phase transition temperatures of 8OCB is shown in Fig. 4.3. Figure. 4.4 shows the schematic representation of the three fundamental director orientations in the N and SmA phase under shear. Rheological measurements were performed using a rheometer in the parallel plate geometry with a plate diameter of 50 mm. The parallel plate configuration was chosen for the simul-

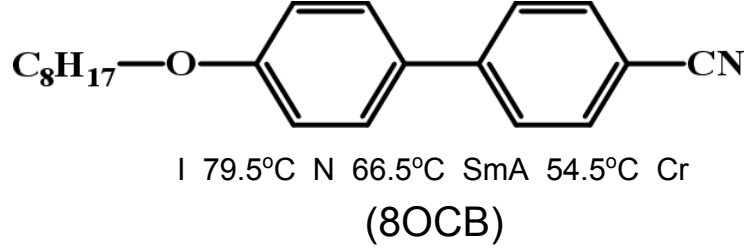


Figure 4.3: Chemical structure of 8OCB liquid crystal with phase transition temperatures.

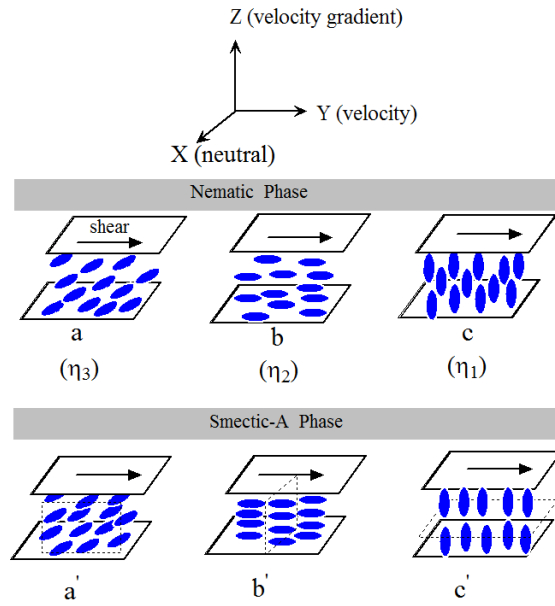


Figure 4.4: Schematic representation of the three fundamental director orientations in the N and SmA phase under shear. The director orientations are along the x (neutral), y (velocity) and z (velocity gradient) directions in a , b , c respectively. Layer orientations in the SmA phase that are parallel to the zy , xz , and xy planes in a' , b' , and c' respectively. Miesowicz viscosities corresponding to each orientations in the N phase are designated by η_3 , η_2 and η_1 respectively.

taneous measurements of rheological and dielectric properties. The cell gap was taken $75\ \mu\text{m}$ as we experimentally verified that the effect of surface anchoring is observed below $50\ \mu\text{m}$. In addition, we find that the zero field viscosity in the isotropic and nematic phases of the same compound agrees well with the values reported in the literature in which the measurements are made by using other geometries [19, 22]. A schematic setup and the experimental methods for measuring the rheological and rheo-dielectric properties are already discussed in the second chapter.

4.3 Results and discussion

4.3.1 Shear dependent effective viscosity (η) and dielectric constant (ϵ) measurements

The flow curve *i.e.*, the variation of shear viscosity (η) as a function of shear rate ($\dot{\gamma}$) at various applied electric fields in the nematic phase is shown in Fig. 4.5. The electric field is perpendicular (z-axis) to the flow field direction (y- axis in Fig. 4.4). At zero field the viscosity is low ($\simeq 10.5\ \text{mPa s}$) and is comparable to the shear viscosity η_3 [22]. It does not depend on the shear rate thus behaves like a Newtonian fluid. With increasing electric field the director tends to align along the field direction beyond a threshold field as the dielectric anisotropy is positive ($\Delta\epsilon = \epsilon_{\parallel} - \epsilon_{\perp} > 0$). Both η (Fig. 4.5(a)) and ϵ (Fig. 4.5(b)) increase with increasing field upto $\simeq 27 \times 10^4\ \text{V/m}$ in the low shear rate region. At higher shear rate the flow field is strong and forces the director to align parallel to the xy-plane (Fig. 4.4) as a result both the η and ϵ decreases. In the intermediate shear rate a Non-Newtonian flow behavior is observed where the director makes an angle with respect to the xy-

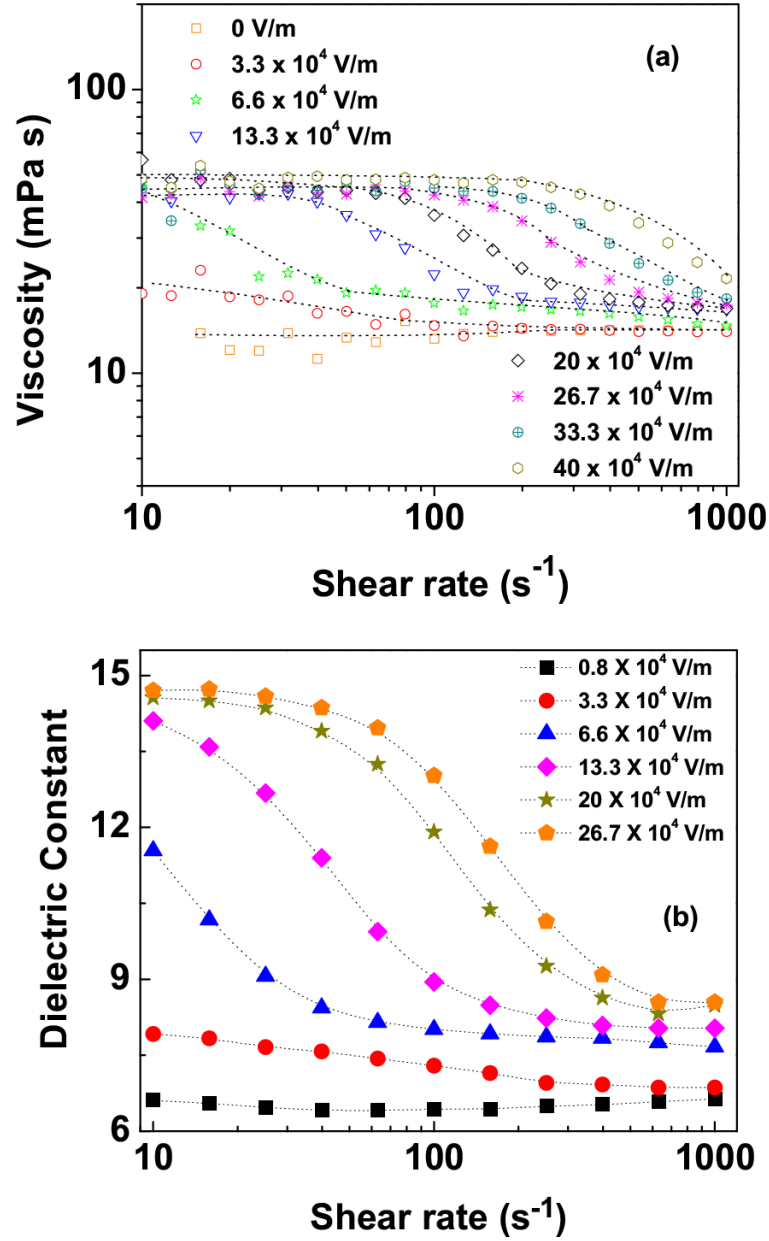


Figure 4.5: Variation of (a) shear viscosity (η) (which we represent as effective viscosity) and (b) dielectric constant (ϵ) (which we represent as effective dielectric constant) as a function of shear rate ($\dot{\gamma}$) at various applied a.c electric fields. Dotted lines are drawn as a guide to the eye.

plane due to the competition between the electric and the flow fields. Further beyond $\simeq 6.6 \times 10^4$ V/m viscosity shows two Newtonian regimes within the measured shear rate range. In the low shear rate region (upto $\dot{\gamma} \simeq 100 \text{ s}^{-1}$) there is no significant increase in η and ϵ beyond $\simeq 27 \times 10^4$ V/m, suggesting that the director orientation is almost parallel to the electric field (z-axis) direction. Furthermore, the shear rate at which the director orientation deviates from the electric field direction increases almost linearly with increasing field as seen in Fig. 4.4 demonstrating the opposite and competing orientational effect of the flow field and electric field.

4.3.2 Field dependent effective viscosity (η) and dielectric constant (ϵ) measurements

Variation of shear viscosity with the applied electric field at a few shear rates is shown in Fig. 4.6(a). At shear rate $\dot{\gamma} = 50 \text{ s}^{-1}$, the viscosity increases monotonically and saturates at higher field. No clear threshold is observed in the viscosity data as the director is already tilted by a finite angle with respect to the xy-plane. At higher shear rates ($\dot{\gamma} = 100$ and 199.5 s^{-1}) in the intermediate field region *i.e.*, from $\simeq 8 \times 10^4$ V/m to $\simeq 30 \times 10^4$ V/m (Fig. 4.6(a)), η is always low compared to the values at $\dot{\gamma} = 50 \text{ s}^{-1}$ suggests that the tilt angle is reduced with respect to the xy-plane at higher shear rates. Beyond $\simeq 30 \times 10^4$ V/m viscosity tends to saturate and merge together at higher field. There is a slight change in the slope of the viscosity at $\simeq 8 \times 10^4$ V/m (Fig. 4.6(a)) and can be explained as follows. The director gets partially aligned (homogeneously) due to the flow field and the slope change indicates a threshold field in homogeneously aligned sample at which the director starts tilting significantly.

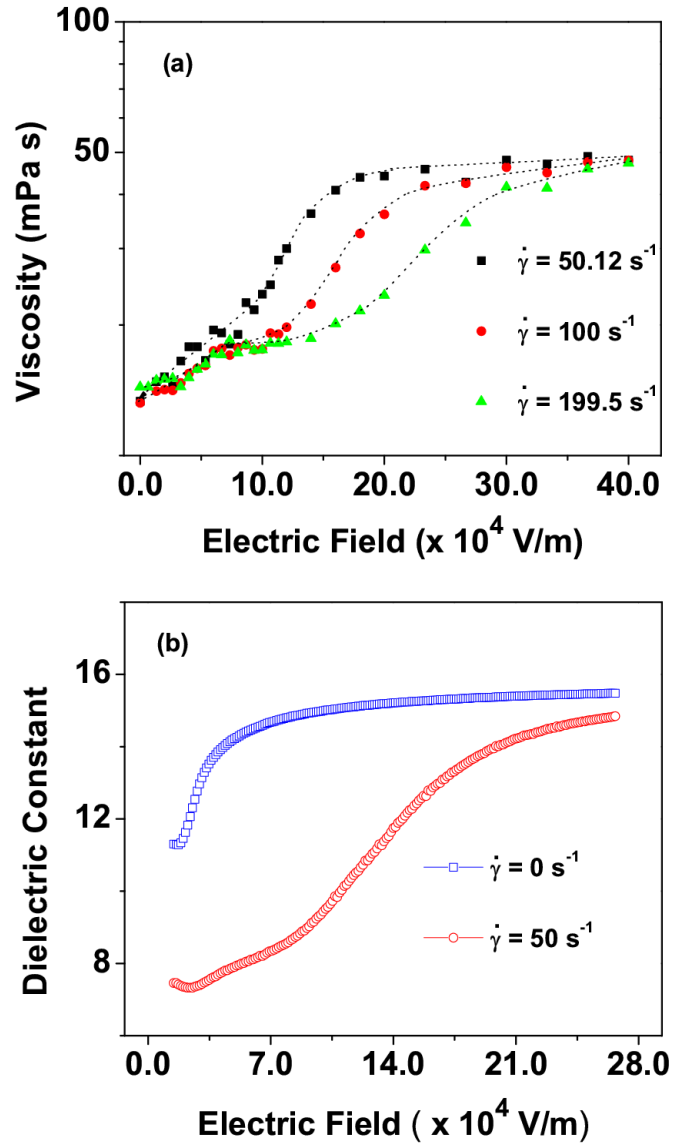


Figure 4.6: (a) Variation of shear viscosity (η) as a function of applied electric field at various shear rates ($\dot{\gamma}$) at 72 °C. (b) Variation of dielectric constant (ϵ) as a function of applied electric field at shear rates $\dot{\gamma} = 0$ and 50 s^{-1} at the same temperature. Dotted lines are drawn as a guide to the eye.

Simultaneous measurement of dielectric constant at the same temperature (72°C) and at shear rate $\dot{\gamma} = 50 \text{ s}^{-1}$ is shown in Fig. 4.6(b). In unsheared sample ($\dot{\gamma} = 0 \text{ s}^{-1}$) the dielectric constant remain constant upto the threshold electric field $\simeq 1.5 \times 10^4 \text{ V/m}$ and then increases rapidly to saturate beyond $\simeq 7 \times 10^4 \text{ V/m}$. The dielectric constant below threshold field is $\epsilon \simeq 11$ and comparatively larger than measured in aligned cell ($\epsilon_{\perp} \simeq 7.3$ [29]) suggesting that the director orientation is random in unsheared sample. The dielectric constant at high field ($\simeq 25 \times 10^4 \text{ V/m}$) is comparable to $\epsilon_{\parallel} \simeq 15.2$ [29] (measured in aligned cell) and suggests that the director is oriented almost parallel to the field direction at unsheared sample. At shear rate $\dot{\gamma} = 50 \text{ s}^{-1}$, the dielectric data is very different than unsheared sample (Fig. 4.6(b)). The dielectric constant is low ($\epsilon \simeq 7.6$) compared to the unsheared sample indicating that the director in some domains is oriented slightly out of xy-plane. Dielectric constant increases almost linearly upto $\simeq 8 \times 10^4 \text{ V/m}$ and saturates at higher field followed by a slope change at this field and is consistent with the viscosity data in Fig. 4.6(a).

4.3.3 Temperature dependent viscosity (η) and dielectric constant (ϵ) measurements

The variation of temperature dependent shear viscosity and simultaneous measurement of dielectric constant at various applied electric field is shown in Fig. 4.7. Viscosity does not depend on the electric field in the isotropic phase and comparable to the previously reported values [22]. The rheodielectric [19] and shear dependent X-ray measurements [15] of 8CB are suggestive for understanding the present temperature dependent electrorheological and rheodielectric data of 8OCB. In the nematic phase the zero field viscosity decreases initially upto $T - T_{NI} = -2^\circ\text{C}$ and

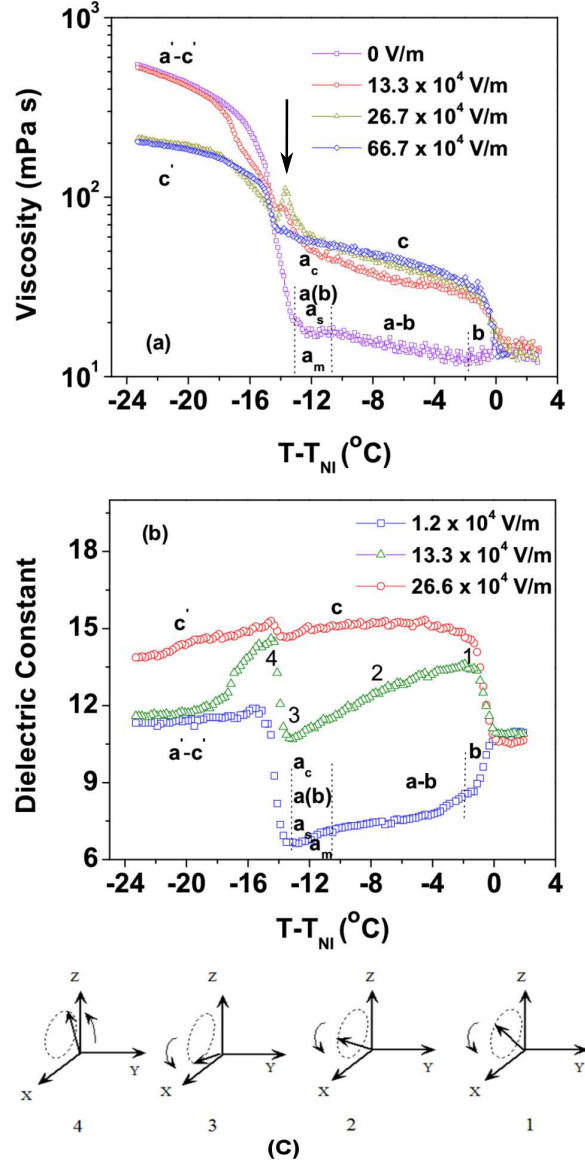


Figure 4.7: Variation of (a) shear viscosity (η) (which we represent as effective viscosity) and (b) dielectric constant (ϵ) (which we represent as effective dielectric constant) as a function of temperature and various applied electric fields. Vertical dotted lines are drawn considering the similarity of temperature dependent zero field viscosity with that of 8CB [19] and represent the approximate temperature regions with possible director orientations. The vertically down arrow indicates the peak position in the viscosity ($T - T_{NI} = -13.8^\circ\text{C}$). (c) Schematic representation of the precessional motion of the director at 13.3×10^4 V/m and at various temperatures.

Rheo-dielectric and electro-rheological properties of 8OCB liquid crystal

suggests flow induced alignment of director (similar to b orientation in Fig. 4.4). Below this temperature a mixed state namely a - b orientation occurs and the viscosity increases monotonically upto $T - T_{NI} = -11^\circ\text{C}$ (Fig. 4.7(a)). A slight slope change below this temperature followed by a rapid increase of the viscosity in the SmA phase is observed. The temperature dependent dielectric constant (Fig. 4.7(b)) together with the viscosity data between $T - T_{NI} = -11^\circ\text{C}$ to -13°C reflects the various precessional motion of the director along the neutral direction such as $a_c, a(b), a_s, a_m$ of the director that are seen in the x-ray measurements of similar compound 8CB. In the SmA phase the viscosity is high due to the occurrence of a' - c' orientation (Fig. 4.4). When the field is increased to 13.3×10^4 V/m, the viscosity increases in the nematic phase. The temperature dependent dielectric constant (Fig. 4.7(b)) at this field in the nematic phase is higher compared to the values measured at smaller field (1.2×10^4 V/m) and indicates that the director is tilted at lower field with respect to the field direction. However, in the SmA phase the viscosity at 13.3×10^4 V/m is comparable to the zero field viscosity suggesting that this field is not sufficient to change the director orientation compared to the zero field orientation. An anomalous increase in the viscosity is also observed across the N -SmA phase transition that will be discussed later. The dielectric constant (at 13.3×10^4 V/m) is rapidly increasing across the I - N transition and then decreases monotonically as the temperature is reduced to N -SmA transition. The temperature dependent viscosity and dielectric constant (Fig. 4.7(a) and 4.7(b)) at this field just above N -SmA transition does not show any signature of presence of several structures as seen in zero field. Further, comparatively smoother decrease of dielectric constant and increase of viscosity at 13.3×10^4 V/m with temperature in the nematic phase suggests about the *uniform* precessional motion of the director (below $T - T_{NI} = -2^\circ\text{C}$)

about an axis that is tilted with respect to the xy-plane. A schematic representation of the director orientation along a cone that is tilted with respect to the xy-plane is shown in Fig. 4.7(c). The dielectric constant at 26.7×10^4 V/m in the nematic phase agrees well with $\epsilon_{||}$ [29] at the same temperature and indicates that, at this temperature the director orients almost along the field direction and goes to $a'-c'$ orientation in the SmA phase. At the applied field 26.7×10^4 V/m, the temperature dependent viscosity is almost similar with the data measured at 13.3×10^4 V/m, except a slight increase in the viscosity in the nematic phase and a slight increase in the peak height of anomalous viscosity. In the SmA phase at 26.7×10^4 V/m, the viscosity is substantially low compared to the viscosity measured at zero field or 13.3×10^4 V/m. On the other hand the dielectric data in the SmA phase at 26.7×10^4 V/m is almost comparable to $\epsilon_{||}$ as measured in the aligned cell sample [29]. It indicates that at this particular field the SmA layers are parallel to the shear plane and acquire c' orientation (Fig. 4.4). Further, at higher field (66.7×10^4 V/m) there is no significant change in the viscosity in the nematic and SmA phases compared to the values at 26.7×10^4 V/m except the anomalous peak is suppressed completely. At least two possible explanations can be considered for the occurrence of anomalous peak across the N -SmA transition. The anomalous increase of shear viscosity can occur due to the effect of shear on the pretransitional fluctuating clusters as suggested by de Gennes [30] and Onuki [31]. When the SmA phase is approached from the nematic the relaxation time of the collective fluctuation of smectic clusters increases and the flow field can easily distort the clusters as suggested by Safinya *et al.* [15], as a result the viscosity can increase anomalously. However, the suppression of the viscosity peak at higher field can not be understood on this basis. Another possible explanation is based on the large contribution of Leslie coefficient α_1 to the measured

viscosity. When sufficient electric field is applied the director tends to align in the field direction (z-axis).

The orientational angle of the director is determined from a balance of the torque exerted on the director, it can be defined as [28].

$$I \frac{\partial^2 \theta}{\partial t^2} = \Gamma_v + \Gamma_e + \Gamma_{el} \quad (4.1)$$

here I is a moment of inertia, $\Gamma_v = (\alpha_3 \sin^2 \theta - \alpha_2 \cos^2 \theta) \dot{\gamma} - (\alpha_3 - \alpha_2) \frac{\partial \theta}{\partial t}$ is a viscous torque, $\Gamma_e = -(1/2) \Delta \epsilon E_o^2 \sin 2\theta$ is a torque due to the electric field ($\sqrt{2} E_o \cos \omega t$), $\Gamma_{el} = K \partial^2 \theta / \partial z^2$ is a torque originating from the elastic distortion and θ is the orientational angle of the director. If we consider that the moment of inertia term is negligibly small, and suppose that an flow alignment occurs and the contribution from the elastic distortion is small, then $I = 0$, $\partial \theta / \partial t = 0$ and $\partial^2 \theta / \partial z^2 = 0$, which reduces the torque balance equation as follows [16, 17].

$$(\alpha_3 \sin^2 \theta - \alpha_2 \cos^2 \theta) \dot{\gamma} - \Delta \epsilon E^2 \sin \theta \cos \theta = 0 \quad (4.2)$$

where $\Delta \epsilon$ is the dielectric anisotropy and E is the applied electric field. The viscosity in such condition can be calculated by using Leslie-Ericksen theory [1, 2], studied in the first chapter.

$$\begin{aligned} \eta(\theta) = & \alpha_1 \cos^2 \theta \sin^2 \theta + \frac{1}{2} (\alpha_3 + \alpha_6) \sin^2 \theta \\ & + \frac{1}{2} (\alpha_5 - \alpha_2) \cos^2 \theta + \frac{1}{2} \alpha_4 \end{aligned} \quad (4.3)$$

where α_1 to α_6 are the Leslie coefficients [16, 17]. In the isotropic phase, all of them vanish except α_4 , which becomes the isotropic shear viscosity coefficient. So effectively there are only five independent coefficients. Due to the smallness of α_1 it is neglected frequently in the nematic phase but this can contribute significantly to the measured viscosity near N -SmA phase transition as suggested by Negita *et al.* [27]. Under zero field there

are several precessional motions just above the T_{NA} which are suppressed at some finite field ($\simeq 13.3 \times 10^4$ V/m) and the director orientation changes gradually via precessional motion around a cone as shown in Fig. 4.7(c). In the nematic phase it starts from some finite angle on the cone (Fig. 4.7(c)-1) and rotates from some minimum angle (Fig. 4.7(c)-3) to maximum angle ($\simeq 90^\circ$, Fig. 4.7(c)-4) through 45° at which the first term in Eq. 4.3 has maximum contribution and can lead to the peak in the shear viscosity. Further, it is noticed from Fig. 4.7(b) that at 13.3×10^4 V/m the minimum (mark 3 in Fig. 4.7(b)) and the maximum (mark 4 in Fig. 4.7(b)) in the dielectric constant occurs at temperatures $T - T_{NI} \simeq -13.3^\circ\text{C}$ and $\simeq -14.3^\circ\text{C}$ respectively. Interestingly the anomalous peak in the viscosity data (Fig. 4.7(a)) at the same field appears at an intermediate temperature $T - T_{NI} \simeq -13.8^\circ\text{C}$ and indicate that the director orientation at the anomalous peak is nearly 45° . When the field is sufficiently high the director is aligned parallel to the field direction and the precessional motions are completely suppressed, consequently α_1 does not contribute to η and the peak is not observed.

4.4 Conclusions

In conclusion, we have measured shear viscosity of 8OCB in both the N and SmA phases as functions of temperature and applied electric field. The flow curve at various applied field shows the competing orientational effect of the flow field and electric field. The viscosity increases with increasing electric field in the nematic phase and saturates to η_1 . At sufficiently high field the SmA exhibits c' orientation and corresponding viscosity is significantly low compared to the viscosity of $a'-c'$ orientations. The shear viscosity and the dielectric data at zero or small electric

field suggests occurrence of several structures related to the precessional motion of the director as reported in 8CB. An anomalous peak is observed in the viscosity across the N -SmA transition (*i.e.*, from c to c' orientation). Two possible explanations are discussed for the anomalous increase in the viscosity namely the pretransitional smectic fluctuations and large contribution of α_1 to the shear viscosity near T_{NA} . We argue that the second explanation is more appropriate and explains our data satisfactorily.

References

- [1] F. M. Leslie. Some constitutive equations for anisotropic fluids. *The Quarterly Journal of Mechanics and Applied Mathematics*, 19(3):357–370, 1966.
- [2] J. L. Ericksen. Anisotropic fluids. *Arch. Rational Mech. Ana*, 4:231–237, 1960.
- [3] O. Parodi. Stress tensor for a nematic liquid crystal. *J. Phys. France*, 31(7):581–584, 1970.
- [4] M. Miesowicz. The three coefficients of viscosity of anisotropic liquids. *Nature (London)*, 158:27, 1946.
- [5] M. Miesowicz. Influence of a magnetic field on the viscosity of para-azoxyanisol. *Nature (London)*, 17:261, 1935.
- [6] M. Miesowicz. *Bull. Int. Acad. Pol. Sci. Lett., Cl. Sci. Math. Nat., Ser. A*, pages 228–230, 1936.
- [7] Ch. Gahwiller. The viscosity coefficients of a room temperature liquid crystals (mbba). *Phys. Lett. A*, 36:311, 1971.
- [8] Ch. Gahwiller. Direct determination of the five independent viscosity coefficients of nematic liquid crystals. *Mol. Cryst. Liq. Cryst*, 20:301–318, 1973.

-
- [9] Orsay Liquid Crystal Group. Viscosity measurements by quasi elastic light scattering in p-azoxyanisol. *Mol. Cryst. Liq. Cryst*, 13:187, 1971.
- [10] W. H. de Jeu. Physical properties of liquid crystal materials. *Gordon and Breach, New York*, 1980.
- [11] Joanna Janik, Jozef K. Moscicki, Krzysztof Czuprynski, and Roman Dabrowski. Miesowicz viscosities study of a two-component thermotropic mixture. *Phys. Rev. E*, 58:3251–3258, Sep 1998.
- [12] P. G. de Gennes. The physics of liquid crystals. *Oxford University Press, Oxford, 2nd ed., 1993*.
- [13] V. V. Belyaev. Viscosity of nematic liquid crystals. *Cambridge International Science Publishing Ltd, Cambridge, 1st Indian Ed., 2011*.
- [14] R. F. Bruinsma and C. R. Safinya. Landau theory of the nematic–smectic-a phase transition under shear flow. *Phys. Rev. A*, 43:5377–5404, May 1991.
- [15] C. R. Safinya, E. B. Sirota, and R. J. Plano. Nematic to smectic-a phase transition under shear flow: A nonequilibrium synchrotron x-ray study. *Phys. Rev. Lett*, 66:1986–1989, Apr 1991.
- [16] T. Carlsson and K. Skarp. The stabilizing effect of an electric field on the shear flow of nematic liquid crystals when $\alpha_3 > 0$: Flow alignment regained. *Molecular Crystals and Liquid Crystals*, 78(1):157–171, 1981.
- [17] T. Carlsson and K. Skarp. Theoretical investigation of the shear flow of nematic liquid crystals with the leslie viscosity $\alpha_3 > 0$: Hydrody-

- namic analogue of first order phase transitions. *Molecular Crystals and Liquid Crystals*, 104(3-4):307–334, 1984.
- [18] H. Knepppe, F. Schneider, and N. K. Sharma. Rotational viscosity γ_1 of nematic liquid crystals. *The Journal of Chemical Physics*, 77(6):3203–3208, 1982.
- [19] K. Negita, M. Inoue, and S. Kondo. Dielectric study on the shear-induced structural changes in the nematic and the smectic-a phase of 4-n-octyl-4'-cyanobiphenyl (8cb). *Phys. Rev. E*, 74:051708, Nov 2006.
- [20] K. Negita and H. Kaneko. Rheodielectric study on shear-induced structural change in the smectic-a phase of 4-n-octyl-4'-cyanobiphenyl (8cb). *Phys. Rev. E*, 80:011705, Jul 2009.
- [21] Jan Jadzyn and Grzegorz Czechowski. The shear viscosity minimum of freely flowing nematic liquid crystals. *Journal of Physics: Condensed Matter*, 13(12):L261, 2001.
- [22] A. G. Chmielewski. Viscosity coefficients of some nematic liquid crystals. *Molecular Crystals and Liquid Crystals*, 132(3-4):339–352, 1986.
- [23] Laurence Ramos, Martin Zapotocky, T. C. Lubensky, and D. A. Weitz. Rheology of defect networks in cholesteric liquid crystals. *Phys. Rev. E*, 66:031711, Sep 2002.
- [24] Keishi Negita. Electrorheological effect in the nematic phase of 4-n-pentyl-4'-cyanobiphenyl. *The Journal of Chemical Physics*, 105(17):7837–7841, 1996.
- [25] Jan Jadzyn and Grzegorz Czechowski. Shear viscosity of nematic

- liquid crystals in the vicinity of the smectic-a phase in alkyloxy-cyanobiphenyl mixtures. *Phys. Rev. E*, 64:052702, Oct 2001.
- [26] H. H. Graf, H. Knepe, and F. Schneider. Shear and rotational viscosity coefficients of two nematic liquid crystals. *Molecular Physics*, 77(3):521–538, 1992.
- [27] Keishi Negita. Effect of electric field on the rheology in the smectic and the nematic phases of octyl cyanobiphenyl. *Molecular Crystals and Liquid Crystals Science and Technology. Section A. Molecular Crystals and Liquid Crystals*, 300(1):163–178, 1997.
- [28] Keishi Negita. Electrorheological effect in the nematic and the smectic a phases of low molecular weight liquid crystal. *International Journal of Modern Physics B*, 13(14n16):2005–2010, 1999.
- [29] J. Jadzyn and G. Czechowski. Dielectric studies of nematic-smectic a-reentrant nematic transition in the 8ocb/6ocb mixtures. *Liquid Crystals*, 4(2):157–163, 1989.
- [30] P. G. De Gennes. Effect of shear flows on critical fluctuations in fluids. *Molecular Crystals and Liquid Crystals*, 34(4):91–95, 1976.
- [31] Akira Onuki and Kyozi Kawasaki. Nonequilibrium steady state of critical fluids under shear flow: A renormalization group approach. *Annals of Physics*, 121(1–2):456 – 528, 1979.
- [32] Joanna Janik, Agnieszka Krol-Otwinowska, Dagmara Sokolowska, and Jozef K Moscicki. pendulum viscometer: A new method for measurement of miesowicz nematic shear viscosity coefficients η_1 and η_2 . *Review of Scientific Instruments*, 77(12), 2006.
- [33] A. V. Zakharov and J. Thoen. Pretransitional anomalies in the shear

- flow near a second-order nematic-smectic-A phase change. *Phys. Rev. E*, 69:051709, May 2004.
- [34] Pawel Pieranski and Etienne Guyon. Two shear-flow regimes in nematic p-n-hexyloxybenziliden-p'-aminobenzonitrile. *Phys. Rev. Lett.*, 32:924–926, Apr 1974.
- [35] A. V. Zakharov, A. A. Vakulenko, and J. Thoen. Tumbling instability in a shearing nematic liquid crystal: Analysis of broadband dielectric results and theoretical treatment. *The Journal of Chemical Physics*, 118(9):4253–4260, 2003.
- [36] M. T. Cidade, C.R. Leal, and P. Patricio. An electro-rheological study of the nematic liquid crystal 4-n-heptyl-4'-cyanobiphenyl. *Liquid Crystals*, 37(10):1305–1311, 2010.

5

Rheology of a reentrant nematic liquid crystal

5.1 Introduction

In the previous chapter we have studied the shear viscosity and dielectric constant of octyloxy cyanobiphenyl (8OCB) in the nematic (N) and smectic-A (SmA) phases as functions of temperature and electric field. In this chapter we will discuss on the rheological measurements of a binary mixture of octyloxy cyanobiphenyl (8OCB) and hexyloxy cyanobiphenyl (6OCB) liquid crystals exhibiting reentrant nematic (N_R) phase.

LCs exhibit a variety of phase transitions owing to their molecular structures and shapes. The flow properties of these LCs are very interesting and there are many theoretical and experimental studies on the flow viscosities [1–18]. In previous chapter we showed that the viscosity increases and the director orientation changes under the application of an external electric field when the temperature is reduced in octyloxy cyanobiphenyl (8OCB) [19]. The rheodielectric measurements

mostly provide overall information on the director orientation during the flow. However, small angle light scattering (SALS) measurements have the potential to infer the effect of domain shape and size on the rheological properties and such studies are meager in these materials. In addition, the flow behavior and hence the rheological properties across the SmA -to- N_R transition are very rare and they are interesting from the phase transition point of view. In this chapter we discuss the small angle light scattering (SALS), rheo-dielectric, and electro-rheological studies on the binary mixture of hexyloxy cyanobiphenyl (6OCB) and octyloxy cyanobiphenyl (8OCB) and investigate the effect of an external a.c electric field on the effective visco-elastic properties. We emphasize that the flow behavior and effect of presmectic fluctuations are similar in both N and N_R phases. The viscoelasticity in the SmA phase is dominated by dislocations and shows an interesting variation on the application of an external field.

5.2 Experimental

The compounds octyloxy cyanobiphenyl (8OCB) and hexyloxy cyanobiphenyl (6OCB) were obtained from our collaborators in Poland. Chemical structures and the phase transition temperatures of these samples are shown in Fig. 5.1. 6OCB exhibits only N phase, while 8OCB exhibits both N and SmA phases. There have been several studies on the phase transitions in these mixtures [20, 21]. The phase diagram obtained from ref [22] is shown in Fig 5.2. We have chosen a mixture of 27 wt% of 6OCB and 73 wt% of 8OCB that exhibits a reasonably wide temperature range ($\simeq 10^\circ\text{C}$) of the SmA phase above the reentrant nematic phase. The mixture shows the following phase sequence as observed in polarizing

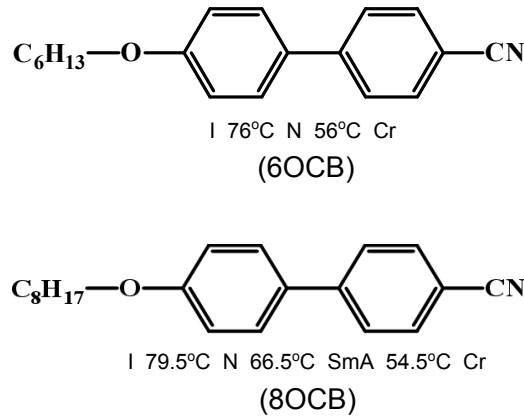


Figure 5.1: Chemical structures and phase transition temperatures of 6OCB and 8OCB liquid crystals.

optical microscope on cooling: N_R 32.4°C SmA 43.2°C N 77.5°C I. In the second chapter the experimental methods for both electro-rheology and small angle light scattering (SALS) have already been discussed. Samples were prepared physically by mixing without adding any solvent. It's done with the help of a glass rod by constant stirring for around 40 min in the isotropic phase. All the rheological measurements were made by cooling the sample from the isotropic phase.

5.3 Results and discussion

5.3.1 Shear dependent SALS and viscosity (η)

To understand the shear thinning behavior we measured simultaneously the effective shear viscosity (η_{eff}) in a quenched sample with shear rate, in both N and SmA phases along with the small angle light scattering

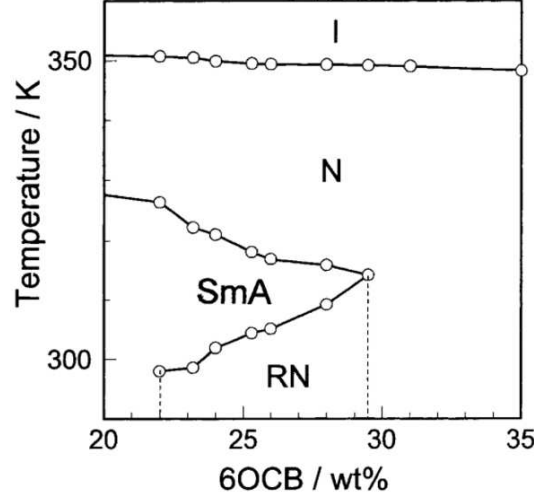


Figure 5.2: Phase diagram of the 6OCB-8OCB binary mixture: *I*-*N*-*SmA* and *RN* (which we represent as N_R) refer to the isotropic, ordinary nematic, smectic-A and reentrant nematic phase, respectively. The phase diagram was obtained from ref [22].

data (Fig. 5.3). In the *N* phase η_{eff} is very high ($\simeq 700$ mPa s) at shear rate ($\dot{\gamma}$) 0.1 s^{-1} and exhibits strong shear thinning behavior upto $\dot{\gamma} = 10 \text{ s}^{-1}$ ($\eta_{eff} \simeq 35$ mPa s). Beyond this shear rate η_{eff} is constant and hence the sample behaves like a Newtonian fluid. The shear rate dependent effective viscosity in the *N* phase can be described using the Sisco model [23].

$$\eta = \eta_{\infty} + a\dot{\gamma}^{-n} \quad (5.1)$$

where η_{∞} and n are the asymptotic value of the viscosity (at very high shear rate) and the power-law index, respectively. The best fit to the Sisco model is shown in Fig. 5.3. The index n is about 0.8 and comparable to the previously reported value [24]. In the *SmA* phase η_{eff} is about ten times higher than in the *N* phase and exhibits shear thinning

behavior upto $\dot{\gamma} = 50 \text{ s}^{-1}$. At higher shear rate η_{eff} does not saturate, indicating the presence of multiple shear thinning events.

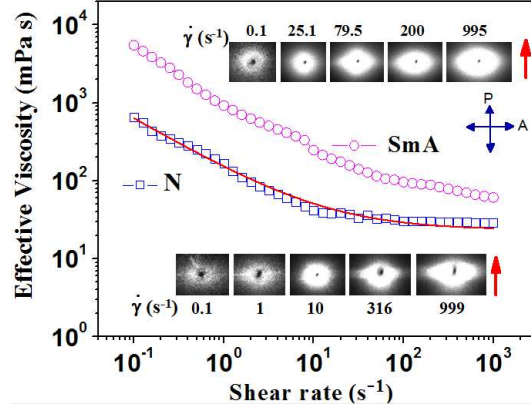


Figure 5.3: Shear rate dependent effective shear viscosity (η_{eff}) in the N ($T - T_{NI} = -30^\circ\text{C}$) and SmA phases ($T - T_{NI} = -43^\circ\text{C}$). The depolarized scattering patterns (HV) at some representative shear rates are shown in both the phases. The red arrow indicate the direction of shear. The upper and lower scattering patterns correspond to the SmA and N phases, respectively. The continuous line is a best fit to Eq. (5.1).

The depolarized light scattering (crossed polarisers) patterns obtained from the horizontal-vertical orientation of the polarizers (HV) at some representative shear rates are also shown in Fig. 5.3, and the shape remains symmetric (almost circular) upto $\dot{\gamma} = 10 \text{ s}^{-1}$ in the N phase. Beyond this shear rate the shape is elongated normal to the shear direction and tends to be elliptical. Nematic liquid crystals normally exhibit a polydomain texture, separated by spatially distributed disclination lines. Since SALS measures the image in the q space, it suggests that, below $\dot{\gamma} = 10 \text{ s}^{-1}$, the reorientation of the director takes place such that it tends to orient parallel to the shear plane without affecting the domain shape. At higher shear rate the polydomain texture is elongated along

the shear direction. In the SmA phase a non-Newtonian flow behavior is observed in the entire range of shear rate, and beyond $\dot{\gamma} = 50 \text{ s}^{-1}$ the onset of elongation of the scattering pattern is observed. Thus, this threshold shear rate is almost five times larger than that of the N phase. The SmA phase has focal conic domains with spatially distributed dislocations in the sample. The realignment of the director, and hence the SmA layers, take place within $\dot{\gamma} = 50 \text{ s}^{-1}$. The elongation of domains occurs beyond this shear rate. This was also observed previously in a polarizing optical microscope [25] but the shear rate dependent shape was not reported. It may be mentioned that the scattering intensity also increases with shear rate in both phases and similar behavior was also observed in other systems [26, 27]. Since HV scattering in the present sample arises preliminarily from orientational fluctuations, it suggests that these fluctuations are increasing with shear rate.

5.3.2 Temperature dependent SALS and viscosity (η)

We measured the temperature dependent effective viscosity (η_{eff}) at a steady shear rate ($\dot{\gamma} = 50 \text{ s}^{-1}$) and recorded the scattering patterns at some representative temperatures to investigate the domain structure. It was not possible to record SALS patterns above $T - T_{NI} \simeq 15^\circ\text{C}$ due to the limitation of the associated temperature controller. In Fig. 5.4 we present the variation of η_{eff} with temperature and a few SALS patterns. We find that η_{eff} decreases in the N phase just below the NI transition. This is due to the shear-induced alignment of the director along the shear direction as shown in Fig. 4.4(b) in previous chapter. Below $T - T_{NI} = -4^\circ\text{C}$, η_{eff} begins to increase, suggesting the onset of a mixed director orientation (*i.e.*, a - b structure). The viscosity increases almost linearly upto $T - T_{NI} \simeq 25^\circ\text{C}$. A small slope change below this

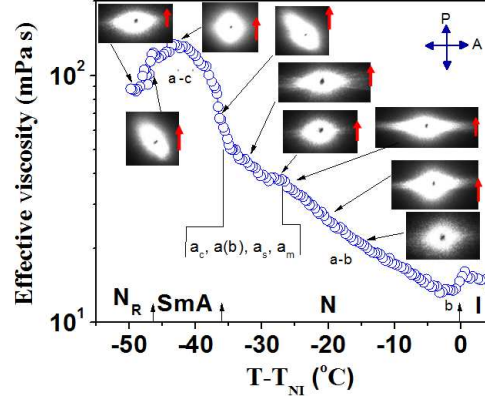


Figure 5.4: Temperature variation of effective shear viscosity (η_{eff}) at a steady shear rate ($\dot{\gamma} = 50 \text{ s}^{-1}$). HV scattering patterns at a few temperatures. The red arrows indicate the direction of shear. The possible director orientations at different temperatures are also indicated considering the similarity of temperature dependent zero-field viscosity of 8CB [18] and 8OCB [19].

temperature, followed by a rapid increase of the viscosity in the SmA phase, is observed. Similar behavior of η_{eff} was also observed above the N -SmA phase transition in pure 8CB and 8OCB liquid crystals [18, 19]. It was explained based on the occurrence of various structures, namely a_c , $a(b)$, a_s , and a_m , that arise because of precessional motion of the director, discussed earlier. The scattering patterns at this shear rate ($\dot{\gamma} = 50 \text{ s}^{-1}$) in the N phase (Fig. 5.4) are elongated perpendicular to the shear direction due to the deformation of domains, as explained previously. The orientations of the patterns at N -SmA and SmA- N_R transitions are noticeably different in the sense that the long axis of the ellipse is rotated by an angle $\simeq 45^\circ$ to the left side of the shear direction. This implies that the elongation directions of the domains are rotated by

the same angle on the right side of the shear direction. It seems that the precessional motion of the director (as described by Safinya *et al.* [14]) also induces significant change in the microtexture of the sample. In the SmA phase the domains have c' and a' director orientation (Fig. 4.4 in previous chapter), and the scattering pattern is almost circular (Fig. 5.4), suggesting that the shapes of the domains remain unaffected at this shear rate. This is also consistent with the observation in Fig. 5.3. In the N_R phase the viscosity decreases sharply and again the scattering pattern gets elongated perpendicular to the shear direction.

5.3.3 Rheodielectric and electrorheological measurements

To investigate the director orientation inside the domain we measured the effective dielectric constant (ϵ_{eff}) simultaneously with the viscosity as a function of temperature at various fields. First, we show the electric field-dependent effective viscosity (η_{eff}) as a function of temperature in Fig. 5.5(a). Its behavior at a low field (*i.e.*, 0.8×10^4 V/m) was already discussed in Fig. 5.4 and is presented here again for the purpose of comparison with the data at higher fields. At a fixed temperature in the N phase, η_{eff} increases with electric field and saturates beyond a threshold value (26.7×10^4 V/m). It exhibits two anomalous peaks [Fig. 5.5(a)] across N -SmA- N_R phase transitions beyond a particular field ($> 13.3 \times 10^4$ V/m). At much higher field the peaks become sharper and they tend to get suppressed beyond $\simeq 93.3 \times 10^4$ V/m [Fig. 5.5(a), inset]. The anomalous behavior of η_{eff} across the N -SmA transition was also observed in a few liquid crystals and it was attributed to the significant contribution of the Leslie coefficient α_1 near the N -SmA transition [10, 28]. Since the hydrodynamic theory of both the N and N_R phases is expected to be the same [17], the second peak across the

SmA- N_R transition could be due to the similar effect. Furthermore, it may be noted that both the peaks are asymmetric in shape with temperature and the second peak is relatively stronger than the first one. The origin of this asymmetry is not clear, however; the difference in the smectic short-range order in both N and N_R phases could be responsible.

The variation of ϵ_{eff} that was measured simultaneously with the viscosity measurement is shown in Fig. 5.5(b). At zero shear rate and low field (0.8×10^4 V/m) in the N phase, ϵ_{eff} is lower than in the I phase, suggesting that the parallel plate induces planar orientation of the director. Since the dielectric anisotropy ($\Delta\epsilon = \epsilon_{||} - \epsilon_{\perp}$) of the mixture is positive [22] we essentially measure the perpendicular component, *i.e.*, $\epsilon_{eff} \simeq \epsilon_{\perp}$. In the SmA phase, ϵ_{eff} is comparatively lower than both the N and the N_R phases, indicating a strong antiparallel correlation of the transverse component of the dipole moments in the SmA layers [29]. At the same field the temperature variation of ϵ_{eff} is significantly different when the sample is subjected to a steady shear rate ($\dot{\gamma} = 50$ s⁻¹), especially below $T - T_{NI} = -10^\circ\text{C}$. This is because of the orientational change of the director across the phase transitions. In the SmA phase ϵ_{eff} is slightly larger than the values in both N and N_R phases due to the a' - c' orientation of SmA layers as described in Fig. 5.4. At an intermediate field (*e.g.*, 13.3×10^4 V/m), ϵ_{eff} just below the NI transition is much larger than in the I phase and decreases gradually with decreasing temperature. Initially the director tends to orient along the field direction as $\Delta\epsilon > 0$. On the other hand, due to the effect of shear and presmectic fluctuations it tends to be parallel to the shear plane with decreasing temperature. Thus, at every temperature the direction of director orientation is determined by these two competing force fields. When the electric field is increased to 26.7×10^4 V/m, ϵ_{eff} is much higher and $\epsilon_{eff} \simeq \epsilon_{||}$ and

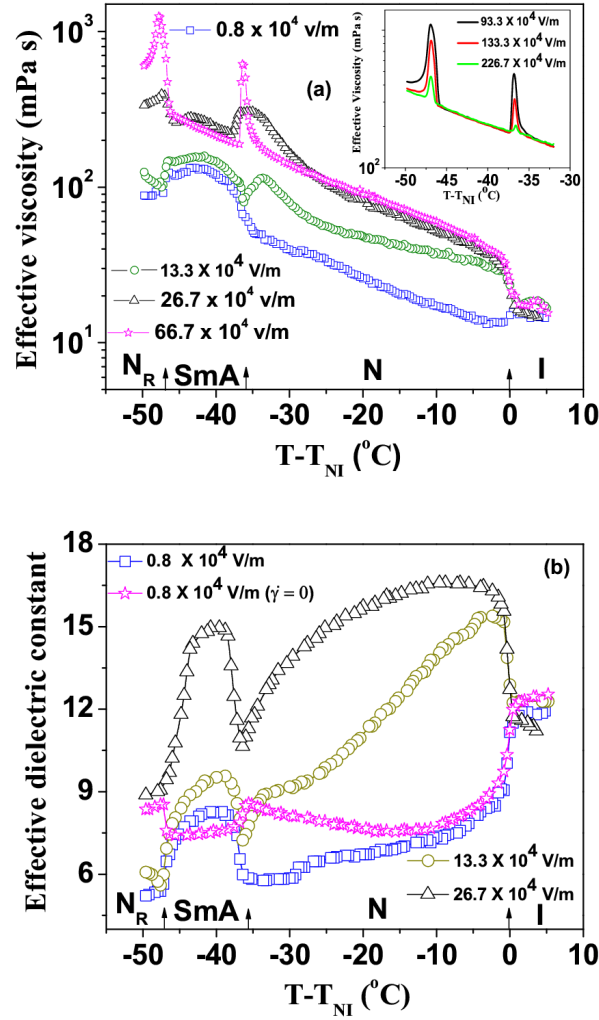


Figure 5.5: (a) Variation of effective shear viscosity (η_{eff}) with temperature at various a.c. electric fields. All the data were collected at a steady shear rate ($\dot{\gamma}=50 \text{ s}^{-1}$). Inset: Suppression of peaks under strong electric fields. (b) Static dielectric constant at same shear rates and same electric fields as in (a). The dielectric data represented by star were measured without shear and at a field $0.8 \times 10^4 \text{ V/m}$. The frequency of the applied field is 3.11 kHz.

decreases gradually as the N -SmA transition is approached. In the SmA phase ϵ_{eff} again increases and reaches a maximum value ($\epsilon_{eff} \simeq 15$) which is slightly less than that measured in the N phase (near the NI transition), suggesting that the layer orientation in this phase is almost c' type.

5.3.4 Field-dependent complex shear modulus measurements

The experimental results from the SALS measurement provided qualitative information about the microtexture, and the rheo-dielectric properties revealed the changes in the director orientation. In the phase diagram of this binary mixture the SmA phase is surrounded by the nematic phase [20] and has different types of defects (dislocations). We anticipated that the investigation on the shear modulus across the phase transitions could be interesting in the sense that the applied electric field can change the defect density. Hence we measured the storage and loss moduli (G' and G'') as a function of temperature. In Fig. 5.6(a) we show the variation of G' and G'' as a function of temperature at various applied electric fields. At a low field (0.8×10^4 V/m) G' and G'' are very small ($\simeq 0.5$ Pa) in both N and N_R phases compared to the SmA phase ($\simeq 20$ Pa). Both G' and G'' increase in the SmA phase when the field is increased to 13.3×10^4 V/m and decrease again at much higher field (66.6×10^4 V/m). For example, in the middle of the SmA phase (*i.e.*, $T - T_{NI} = -42^\circ\text{C}$) at a low field (0.8×10^4 V/m), $G' \simeq 20$ Pa and increases to $\simeq 32$ Pa at a field 13.3×10^4 V/m and then decreases to a small value $\simeq 4$ Pa beyond 226.7×10^4 V/m. Similar behavior with temperature and field is also observed in the case of G'' as shown in Fig. 5.6(b). To understand the temperature variation of G' and G'' at various fields we simultaneously measured the effective dielectric constant (ϵ_{eff}) as a function of temper-

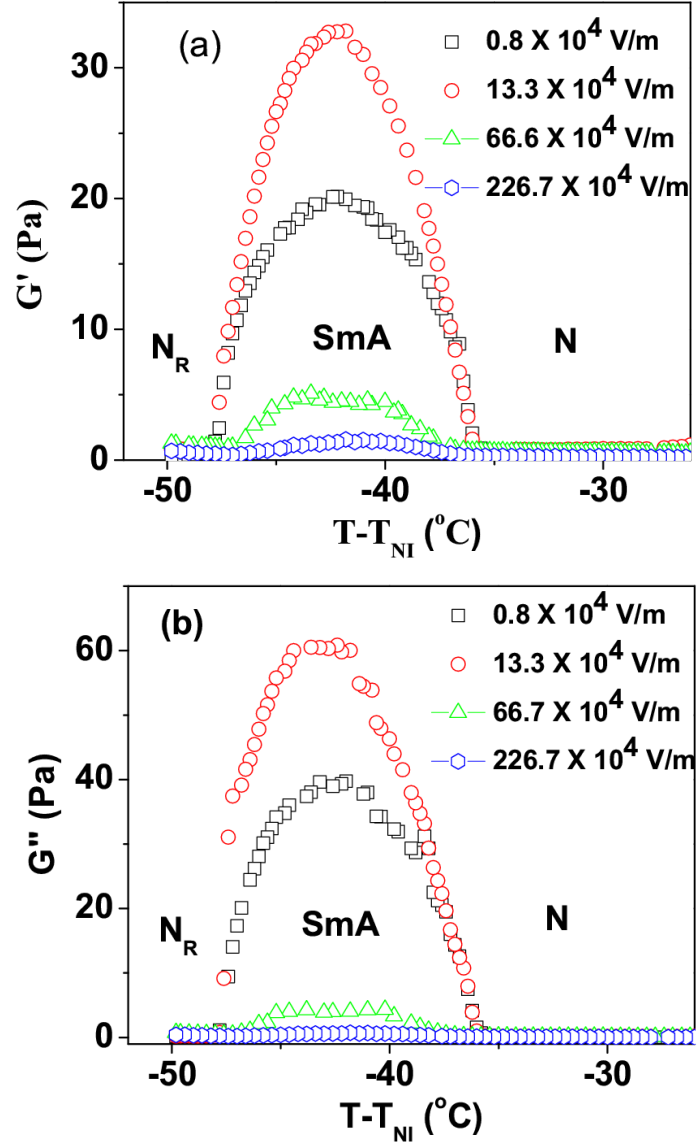


Figure 5.6: Variation of (a) storage modulus (G') and (b) loss modulus (G'') across N -SmA and N_R phase transitions at various a.c electric fields at angular frequency $\omega = 10$ rad/s and strain amplitude $\gamma = 0.05$.

ature as shown in Fig. 5.7. It is noticed that ϵ_{eff} at low field (0.8×10^4

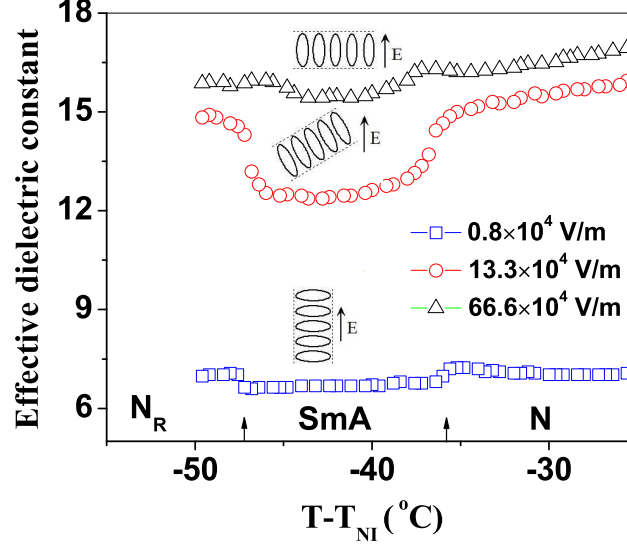


Figure 5.7: Variation of effective dielectric constant (ϵ_{eff}) across N -SmA and N_R phase transitions at various a.c electric fields at an angular frequency $\omega = 10$ rad/s and strain amplitude $\gamma = 0.05$. The frequency of the applied field is 3.11 kHz. Orientations of SmA layers with respect to field direction are shown schematically.

V/m) in N , SmA, and N_R phases are comparable to the perpendicular component of the dielectric constant (ϵ_{\perp}) measured in a surface aligned planar cell [33], suggesting that the SmA layers within the domains are oriented parallel to the field direction as shown in Fig. 5.7. When the field is increased to 13.3×10^4 V/m, ϵ_{eff} increases in all the phases due to the partial alignment of the director along the field direction. However, at the same field ϵ_{eff} is comparatively lower in the SmA phase than in both the N and N_R phases. For example, at the middle of the SmA temperature range (*i.e.*, $T - T_{NI} = -42^\circ\text{C}$) $\epsilon_{eff} \simeq 12.5$ whereas in both N and N_R phases it is $\simeq 15$. At much higher field (66.7×10^4 V/m) ϵ_{eff}

is almost comparable in all the phases, indicating that the director, and hence the layer normal in the SmA is almost parallel to the field direction. This suggests that in the intermediate field (13.3×10^4 V/m) SmA layers (within the domains) are oriented such that the layer normals in different domains are tilted in different directions with respect to the field direction. Such orientations of SmA layers are expected to create more dislocations, and as a result both the shear moduli can increase (in Fig. 5.6). At high field (66.7×10^4 V/m) the dislocation density decreases due to the almost complete orientation of the SmA layers (Fig. 5.7) and both the moduli decrease.

5.4 Conclusions

In conclusion, we have shown that strong shear thinning is due to both the elongation of domains and the realignment of a director within the domains in both *N* and SmA phases. The domain elongation starts beyond a threshold shear rate and in the case of SmA this shear rate is about five times higher than in the *N* phase. The director orientation changes under the application of electric field as the temperature is reduced across *N*-SmA-*N_R* phase transitions. We presented possible layer orientations at various electric fields and showed that the zero-field viscoelasticity in the SmA phase is aided by the presence of dislocations, which disappear on application of strong external field.

References

- [1] P. G. de Gennes. The physics of liquid crystals. *Oxford University Press, Oxford*, 2nd ed., 1993.
- [2] S. Chandrashekhhar. Liquid crystals. *Cambridge University Press, Cambridge*, 2nd ed., 1992.
- [3] V. V. Belyaev. Viscosity of nematic liquid crystals. *Cambridge International Science Publishing, Cambridge*, 1st Indian ed, 2011.
- [4] F. M. Leslie. Some constitutive equations for anisotropic fluids. *The Quarterly Journal of Mechanics and Applied Mathematics*, 19(3):357–370, 1966.
- [5] M. Miesowicz. Influence of a magnetic field on the viscosity of para-azoxyanisol. *Nature(London)*, 17:261, 1935.
- [6] M. Miesowicz. *Bull. Int. Acad. Pol. Sci. Lett., Cl. Sci. Math. Nat., Ser.A*, A 28:228–230, 1936.
- [7] Ch. Gahwiller. The viscosity coefficients of a room-temperature liquid crystal (mbba). *Physics Letters A*, 36(4):311 – 312, 1971.
- [8] Ch. Gahwiller. Direct determination of the five independent viscosity coefficients of nematic liquid crystals. *Molecular Crystals and Liquid Crystals*, 20(3-4):301–318, 1973.

-
- [9] H. Knepe, F. Schneider, and N. K. Sharma. Rotational viscosity γ_1 of nematic liquid crystals. *The Journal of Chemical Physics*, 77(6), 1982.
- [10] Keishi Negita. Electrorheological effect in the nematic and the smectic a phases of low molecular weight liquid crystal. *International Journal of Modern Physics B*, 13(14n16):2005–2010, 1999.
- [11] Keishi Negita. Electrorheological effect in the nematic phase of 4-n-pentyl-4'-cyanobiphenyl. *The Journal of Chemical Physics*, 105(17), 1996.
- [12] Orsay Liquid Crystal Group. Viscosity measurements by quasi elastic light scattering in p-azoxyanisol. *Molecular Crystals and Liquid Crystals*, 13(2):187–191, 1971.
- [13] R. F. Bruinsma and C. R. Safinya. Landau theory of the nematic–smectic-a phase transition under shear flow. *Phys. Rev. A*, 43:5377–5404, May 1991.
- [14] C. R. Safinya, E. B. Sirota, and R. J. Plano. Nematic to smectic-a phase transition under shear flow: A nonequilibrium synchrotron x-ray study. *Phys. Rev. Lett*, 66:1986–1989, Apr 1991.
- [15] Jan Jadzyn and Grzegorz Czechowski. The shear viscosity minimum of freely flowing nematic liquid crystals. *Journal of Physics: Condensed Matter*, 13(12):L261, 2001.
- [16] Jan Jadzyn and Grzegorz Czechowski. Shear viscosity of nematic liquid crystals in the vicinity of the smectic-a phase in alkyloxy-cyanobiphenyl mixtures. *Phys. Rev. E*, 64:052702, Oct 2001.
- [17] S. Bhattacharya and S. V. Letcher. Flow behavior of an oriented,

- reentrant, nematic liquid crystal. *Phys. Rev. Lett*, 44:414–417, Feb 1980.
- [18] K. Negita, M. Inoue, and S. Kondo. Dielectric study on the shear-induced structural changes in the nematic and the smectic-a phases of 4-n-octyl-4'-cyanobiphenyl (8cb). *Phys. Rev. E*, 74:051708, Nov 2006.
- [19] J. Ananthaiah, M. Rajeswari, V. S. S. Sastry, R. Dabrowski, and S. Dhara. Effect of electric field on the rheological and dielectric properties of a liquid crystal exhibiting nematic-to-smectic-a phase transition. *The European Physical Journal E*, 34(8):1–6, 2011.
- [20] P. E. Cladis, D. Guillon, F. R. Bouchet, and P. L. Finn. Reentrant nematic transitions in cyano-octyloxybiphenyl (8ocb). *Phys. Rev. A*, 23:2594–2601, May 1981.
- [21] A. R. Kortan, H. V. Känel, R. J. Birgeneau, and J. D. Litster. High-resolution x-ray-scattering study of the nematic-smectic a-reentrant nematic transitions in 8ocb/6ocb mixtures. *Phys. Rev. Lett*, 47:1206–1209, Oct 1981.
- [22] Atsushi Kubono, Kazuki Yoshino, Toshiro Ninomiya, Ryuichi Akiyama, and Katsufumi Tanaka. Visco-elastic properties of reentrant nematic liquid crystalline mixtures. *Liquid Crystals*, 29(8):1089–1095, 2002.
- [23] J. F. Hutton H. A. Barnes and K. Walters. An introduction to rheology. *Annals of Discrete Mathematics, Elsevier, Amsterdam*, 1989.
- [24] M. T. Cidade, G. Pereira, A. Bubnov, V. Hamplova, M. Kaspar, and J. P. Casquilho. Rheological characterisation of a liquid-crystalline

- diol and its dependence with an applied electric field. *Liquid Crystals*, 39(2):191–197, 2012.
- [25] S Fujii, S Komura, Y Ishii, and C-Y D Lu. Elasticity of smectic liquid crystals with focal conic domains. *Journal of Physics: Condensed Matter*, 23(23):235105, 2011.
- [26] Benjamin S. Hsiao, Richard S. Stein, Klaus Deutscher, and H. Henning Winter. Optical anisotropy of a thermotropic liquid-crystalline polymer in transient shear. *Journal of Polymer Science Part B: Polymer Physics*, 28(9):1571–1588, 1990.
- [27] Beth A. Schubert, Norman J. Wagner, Eric W. Kaler, and Srinivasa R. Raghavan. Shear-induced phase separation in solutions of wormlike micelles. *Langmuir*, 20(9):3564–3573, 2004. PMID: 15875385.
- [28] Keishi Negita. Effect of electric field on the rheology in the smectic and the nematic phases of octyl cyanobiphenyl. *Molecular Crystals and Liquid Crystals Science and Technology. Section A. Molecular Crystals and Liquid Crystals*, 300(1):163–178, 1997.
- [29] W. H. de Jeu. Physical properties of liquid crystal materials. *Gordon and Breach, New York*, 1980.

6

Rheology of a Bent-Core Nematic Liquid Crystal.

6.1 Introduction

We have previously discussed the small angle light scattering, rheo-dielectric and electro-rheological properties of a binary mixture of octyloxy cyanobiphenyl (8OCB) and hexyloxy cyanobiphenyl (6OCB) liquid crystals. In this chapter we will discuss on the measurement of viscosities of a bent-core nematic liquid crystal by using the rheometer as well as a micro-rheological technique.

The viscosity of liquid crystals strongly depends on the microscopic structure of the constituent molecules and the mesophases. There are several theoretical and experimental studies on the low molecular weight liquid crystals, where the molecules are mostly cylindrical symmetric [1–3]. Recently, liquid crystals consists of bent-core molecules have created immense interest [4, 5]. In 1996 Niori *et al.* [8] first observed the ferroelectric switching in a compound that are made of achiral bent-core molecules. In these bent-core molecules, the nematic phase is uncom-

mon due to their strong tendency to form smectic phases. However, a number of bent-core compounds exhibiting nematic phase have been reported [9]. Their physical properties are reported to be significantly different than conventional calamitic nematic liquid crystals [10–18]. In this context the measurement of flow or shear viscosity in the bent-core liquid crystals is very rare. The major problem in such measurements is the requirement of a large quantity of sample, which is in general not easy to get. In this chapter we report measurements of shear and micro-rheological viscosities of a bent-core nematic liquid crystal.

6.2 Experimental

The chemical structure and the phase transition temperatures of the bent-core nematic (BCN) liquid crystal are shown in Fig. 6.1, which

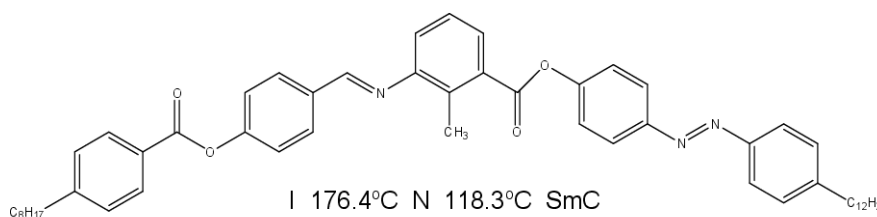


Figure 6.1: Chemical structure and the first two phase transition temperatures of the bent-core compound.

exhibits the following phase transitions (cooling): I 176.4°C N 118.3°C SmC 101.3°C SmX 90.4°C SmY 60.2°C Cr and was obtained from our collaborators in Poland. In Fig. 6.2 we present the typical textures of bent-core compound in the nematic phase. These textures are observed while cooling the sample at a rate 1°C/min from the isotropic phase under polarizing optical microscope. The shear (active) viscosity

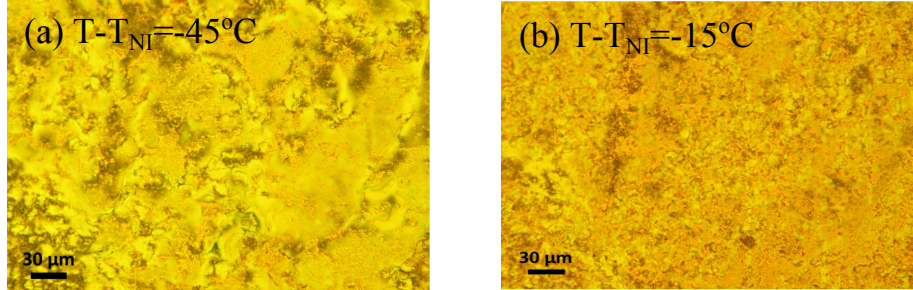


Figure 6.2: Photomicrographs of nematic phase of bent-core compound (a) $T - T_{NI} = -45^\circ\text{C}$ (b) $T - T_{NI} = -15^\circ\text{C}$ cooling from the isotropic phase.

measurements were made using a rheometer (Anton Paar MCR 501) in plate-cone geometry with plate diameter 50 mm and a cone angle of 1° . The plates were not treated for any specific orientation of the molecules. The temperature of the sample was controlled with a Peltier temperature controller within an accuracy of 0.1°C . We have used a videomicroscopy technique to measure the self-diffusion coefficients of a tiny silica microsphere (with a diameter = $0.98\ \mu\text{m}$) and hence the micro-rheological (passive) viscosities of the sample parallel and perpendicular to the director. To promote a specific molecular alignment on the surface of the silica microspheres were coated with octadecyldimethyl (3-trimethoxysilylpropyl) ammonium chloride (DMOAP) before mixing with the liquid crystal [20]. The Brownian motion of an isolated microsphere in a planar cell ($d = 23\ \mu\text{m}$) was recorded and the position was determined with the help of an appropriate computer program. The histogram of the microsphere displacements were fitted to Gaussian with a probability P that the particle would diffuse a certain distance δ in the time interval τ is $P(\delta|\tau) = P_0(\tau)\exp(-\delta^2/\Delta^2(\tau))$ [20], where $\Delta(\tau)$ is the width of the

distribution and $P_0(\tau)$ is the normalization constant. The self-diffusion coefficients of the microsphere parallel ($D_{||}$ and perpendicular D_{\perp}) to the director are obtained by using the relation $D_{||,\perp} = \Delta_{||,\perp}^2/4\tau$. The corresponding viscosities are estimated by using Stokes-Einstein relation $\eta_{||,\perp} = k_B T / (6\pi r D_{||,\perp})$, where r is the radius of the microsphere [20].

6.3 Results and discussion

6.3.1 Measurement of shear viscosity

We show the variation of shear stress with shear rate in Fig. 6.3 at various temperatures in the nematic phase. The sample was mounted on the rheometer in the nematic phase at a temperature 140°C. It is observed that the shear stress is proportional to the shear rate except at a low shear rate range ($\dot{\gamma} \leq 2 \text{ s}^{-1}$) where the stress is constant, suggesting a shear thinning behavior. This could be due to the shear induced realignment of the nematic director within the domains that are separated by disclination lines [21]. This effect is more prominent in the first measurement (140°C[1st]) *i.e.*, immediately after mounting the sample. Beyond $\dot{\gamma} \simeq 2 \text{ s}^{-1}$, the shear stress is proportional to the shear rate, hence BCN shows the behavior of a Newtonian fluid within the experimental limit ($\dot{\gamma} = 1000 \text{ s}^{-1}$). The shear-dependent viscosity of a bent-core nematic was also studied using a nanolitre rheometer by Bailey *et al.* [6] in the shear-rate range of 500-10000 s^{-1} . They reported Newtonian behavior below the shear rate range ($\leq 2000 \text{ s}^{-1}$) and non-Newtonian behavior above this range.

In Fig. 6.4 we show the variation of effective viscosity (η_{eff}) with shifted temperature (*i.e.*, $T - T_{NI}$) at a shear rate $\dot{\gamma} = 50 \text{ s}^{-1}$. The value

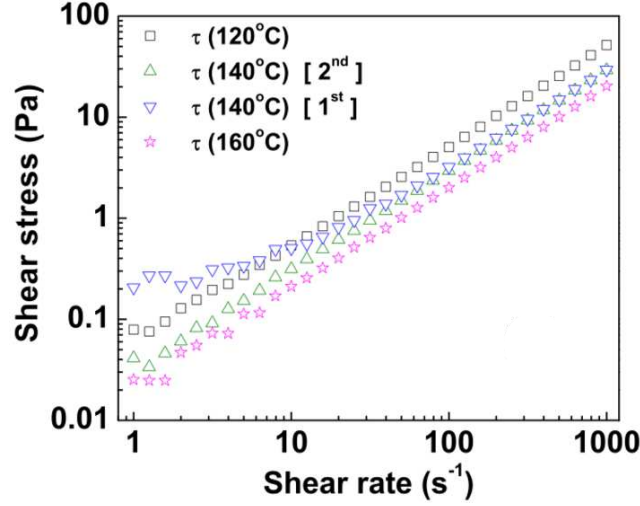


Figure 6.3: Variation of shear stress with shear rate at various temperatures. The sample was mounted at 140°C. 1st and 2nd indicates the two consecutive measurements at the same temperature.

of T_{NI} was determined from the temperature-dependent measurement of the viscosity. Here the effective viscosity means the bulk viscosity measured in the cone-plate arrangement. We notice that η_{eff} is reduced below the NI phase transition and increases with decreasing temperature. At $T - T_{NI} = -58^\circ\text{C}$, it sharply changes slope and increases very rapidly indicating a N - SmC phase transition. For the purpose of comparison we also measured η_{eff} for the 4'-octyloxy-4-cyanobiphenyl (8OCB) sample and present the results in Fig. 6.4. The behavior of η_{eff} has some common features in both compounds. It is reduced below the NI transition, increases with decreasing temperature, and diverges at the N to SmA or SmC transition. In addition there is a small slope change in the viscosity data near N to SmA or SmC transition in both samples. The data in the case of the BCN is shown in the inset of Fig.

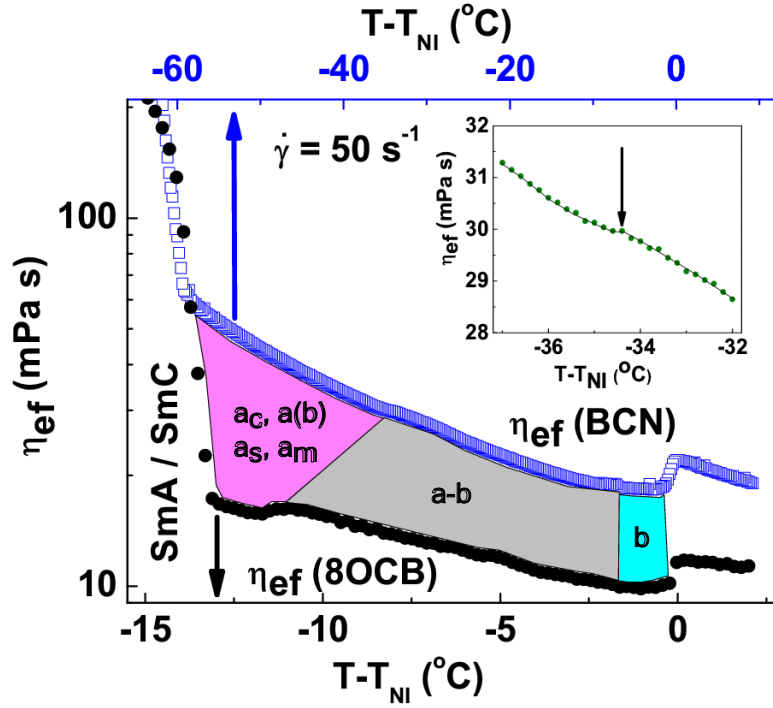


Figure 6.4: Temperature variation of η_{eff} in both 8OCB and BCN compounds at a shear rate $\dot{\gamma} = 50 \text{ s}^{-1}$. Upper and lower x-axes corresponds to the temperature scale of BCN (open squares) and 8OCB (filled circles) samples respectively. Common features indicating various steady state structures as described in the text are indicated in the shaded regions. The notation used in the shaded regions follow the notation that was used in the fourth chapter to describe the different dynamical response regimes of 8CB. (Inset) Arrow indicates a small slope change in the viscosity data of BCN liquid crystal.

6.4 for clarity. In contrast, η_{eff} behavior has at least two uncommon and distinct features. Firstly, η_{eff} in the BCN is significantly larger than 8OCB. For example at $T - T_{NI} = -2^\circ\text{C}$, $\eta_{eff}^{8OCB} = 10.2$ mPa s and $\eta_{eff}^{BCN} = 18.7$ mPa s for 8OCB and BCN liquid crystals, respectively. Assuming we are essentially measuring η_2 (since this temperature is close to NI), we assert that this viscosity is almost twice as high in the BCN than that of the 8OCB liquid crystal. Secondly, the small slope change in η_{eff} of the BCN (Fig. 6.4) appears at much higher temperature than that in the 8OCB liquid crystal. For example, it appears at 24.5°C above the N -Sm C phase transition for BCN and 2°C above the N -Sm A phase transition for 8OCB sample, respectively. A similar slope change in the viscosity data of 4'-octyl-4-cyanobiphenyl (8CB) in conjugation with X-ray [22] and rheodielectric data [23] was identified as the onset of precessional motion of the director at which $\dot{\gamma}\tau \rightarrow 1$ and several steady state structures appear as discussed in the fourth chapter. Considering the similarity to the previously measured viscosity data of 8CB and 8OCB, we conjecture that the precessional motion of the director in the present BCN sample begins far away *i.e.*, 24.5°C above the N -Sm C transition. Previously, some studies involving X-ray measurements indicated that this compound exhibits a uniaxial to biaxial nematic transition around $T - T_{NI} \simeq -30^\circ\text{C}$ [24, 25]. However, concurrently various experiments indicated that this is due to the onset of smectic fluctuations and no phase biaxiality was confirmed [26, 27]. Moreover, recently, in the same compound around a similar temperature we observed that the bend elastic constant as well as the rotational viscosity starts to increase more rapidly with the temperature [17, 19]. We believe that this small slope change (Fig. 6.4 (inset)) indicates the temperature at which $\dot{\gamma}\tau \rightarrow 1$.

6.3.2 Measurement of viscosity by using a micro-rheological technique

In the earlier chapters we have studied the temperature dependent Miesowicz viscosities (η_2 and η_1) of several samples by using rheometer. There, η_2 was measured in the partially aligned sample in which

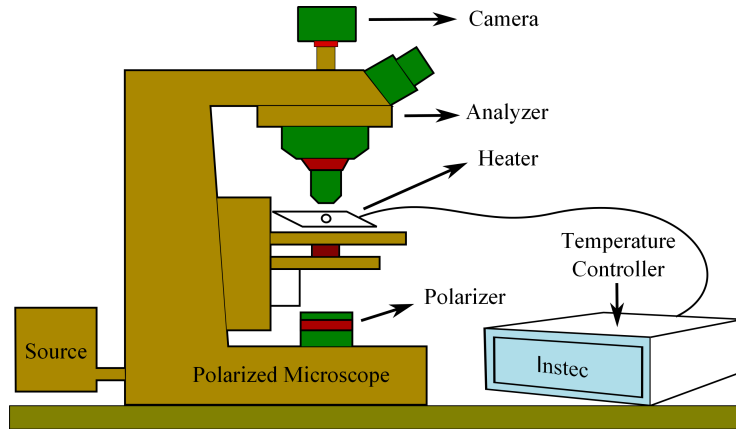


Figure 6.5: Schematic diagram for micro-rheology setup.

the alignment of the director parallel to the flow, was obtained by shearing the sample. In case of η_1 , the director was aligned perpendicular to the flow by applying a strong electric field. In case of the bent-core liquid crystal due to the large ionic conductivity of the sample, we could not measure η_1 following the same procedure. Hence, we adapted a micro-rheological technique to measure the anisotropic viscosities. The schematic setup for micro-rheology is shown in Fig. 6.5. Instec temperature controller is used to control the temperature of the sample; a polarized microscope to observe the Brownian fluctuations and a camera to record corresponding videos and images. The histograms of the particle displacement $\delta|\mathbf{r}(t + \tau) - \mathbf{r}(t)|$ in both x ($\parallel \mathbf{n}$) and y ($\perp \mathbf{n}$) and a microparticle with a dipole defect are shown in Fig. 6.6. It is evident that

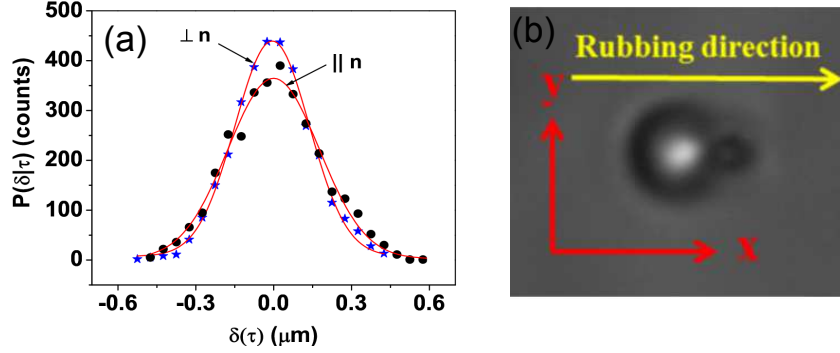


Figure 6.6: (a) Distribution of particle displacements along parallel (circles) and perpendicular (stars) to the director for $\tau = 1$ s. The solid lines are Gaussian fits. (b) A micro particle with a dipole defect.

$\Delta_{\parallel} > \Delta_{\perp}$, implying $D_{\parallel} > D_{\perp}$ as expected. The ratio D_{\parallel}/D_{\perp} varies with temperature and changes from 1.4 to 1.7, which is close to the number (1.6) reported in calamitic liquid crystal *e.g.*, 4'-pentyl-4-cyanobiphenyl (5CB) with dipole defects [28].

In Fig. 6.7 we show the temperature variation of η_{\parallel} and η_{\perp} of the BCN liquid crystal as determined from D_{\parallel} and D_{\perp} using the Stokes-Einstein relation. We note that in the isotropic phase, $\eta_{\parallel} = \eta_{\perp}$ and is comparable to η_{eff} measured by the rheometer. Just below the NI transition the director is aligned along the flow direction and η_{\parallel} is nearly equal to the Miesowicz viscosity *i.e.*, $\eta_{\parallel} \cong \eta_2 = (\alpha_3 + \alpha_4 + \alpha_6)/2$. In the nematic phase $\eta_{\parallel} < \eta_{\perp} (\cong \eta_3 = \alpha_4/2)$ and both increases as the temperature is reduced; η_{eff} also increases with temperature, but the relative rate of increase of the former two is larger. Two considerations can be made to understand their temperature dependence. Firstly, apart from the temperature effect, the viscosity can also increase as the smectic phase

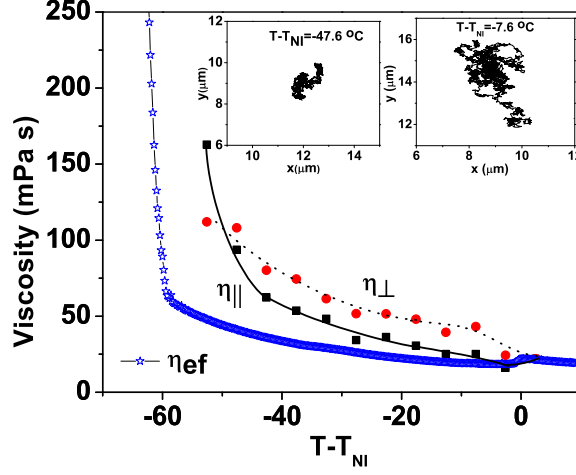


Figure 6.7: Variation of η_{eff} (stars), $\eta_{||}$ (squares) and η_{\perp} (circles) as a function of shifted temperature. (Inset) Two dimensional projection of trajectories of a microsphere closer to the NI transition ($T - T_{NI} = -7.6^{\circ}\text{C}$) and closer to the $N\text{-SmC}$ transition ($T - T_{NI} = -47.6^{\circ}\text{C}$).

is approached due to the occurrence of temporary smectic clusters in the bulk. Secondly, the colloids are coated with DMOAP, which promotes homeotropic alignment of the bent-core molecules. On the surface of the microsphere the free rotation of the molecules along the long axis is restricted due to steric hindrance; As a result, the hydrodynamic radius of the microsphere could be significantly larger than the actual radius due to the large cloud of the distorted nematic around the microsphere. Assuming $\eta_{||} = \eta_{eff} = 21.6 \text{ mPa s}$ near the NI transition ($T - T_{NI} = -18^{\circ}\text{C}$), the estimated hydrodynamic radius of the microsphere is $0.68 \mu\text{m}$, which is about $0.2 \mu\text{m}$ larger than the actual radius.

A schematic molecular orientation of bent-core molecules and some clusters around the microsphere with a dipolar defect is shown in Fig.

6.8. It is shown that both diffusion coefficients (D_{\parallel} and $D_{\perp} \propto 1/\eta$)

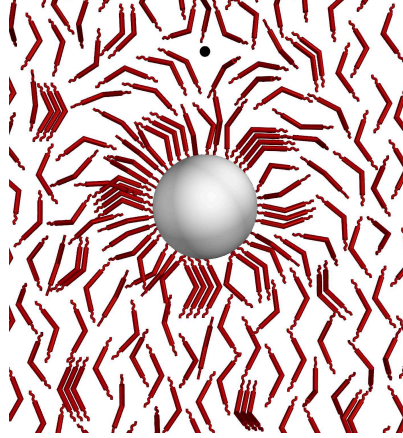


Figure 6.8: Schematic molecular orientation around the microsphere with dipolar defect configuration. It may be noted that the clusters attached to the microsphere are *permanent* whereas they are *temporal* in the bulk. A small dot on the upper side indicates a hyperbolic hedgehog.

decrease when the size of the microsphere is greater than $0.5 \mu\text{m}$. It is attributed to the effective size of the microsphere is bigger than the geometric size [20]. In addition, the smectic layering effect can increase with decreasing temperature due to a kind of condensation of the clusters around the microsphere effectively increasing the diameter of the microsphere with decreasing temperature. As the temperature is further reduced and we approach to the SmC phase, interestingly we notice that η_{\parallel} tends to diverge around 24°C above the N -SmC transition. To understand this we look at the Brownian trajectory of a microsphere. The two-dimensional projection of the trajectories of a microsphere near NI ($T - T_{NI} = -7.6^{\circ}\text{C}$) and N -SmC ($T - T_{NI} = -47.6^{\circ}\text{C}$) transitions are shown in the inset of Fig. 6.7. We notice that the fluctuations are highly restricted near the N -SmC transition compared to that observed near the NI transition. Since the cell is rubbed, it is expected that the smectic

layer planes in the temporarily fluctuating clusters are oriented perpendicular to the rubbing direction. In this case the fluctuating clusters are large enough and the self-diffusion of the microsphere in the direction perpendicular to the layer plane is expected to be lower than that in parallel direction and as a result $\eta_{||}$ can diverge.

6.4 Conclusions

In conclusion, the effective viscosity is larger and the effect of presmectic fluctuations are observed much higher than the N -SmC transition temperature than commonly seen in calamitic liquid crystals. The temperature dependence of micro-rheological viscosities are stronger than that of shear viscosity. The study of Brownian fluctuation is useful to understand the smectic fluctuations in bent-core nematic liquid crystals. This, however, needs to be substantiated by more experiments as well as simulations.

References

- [1] P. G. de Gennes. The physics of liquid crystals. *Oxford University Press, Oxford*, 2nd ed., 1993.
- [2] S. Chandrashekhhar. Liquid crystals. *Cambridge University Press, Cambridge*, 2nd ed., 1992.
- [3] V. V. Belyaev. Viscosity of nematic liquid crystals. *Cambridge International Science Publishing, Cambridge*, 1st Indian ed, 2011.
- [4] Hideo Takezoe and Yoichi Takanishi. Bent-core liquid crystals: Their mysterious and attractive world. *Japanese Journal of Applied Physics*, 45(2R):597, 2006.
- [5] R. Amaranatha Reddy and Carsten Tschierske. Bent-core liquid crystals: polar order, superstructural chirality and spontaneous desymmetrisation in soft matter systems. *J. Mater. Chem.*, 16:907–961, 2006.
- [6] C. Bailey, K. Fodor-Csorba, J. T. Gleeson, S. N. Sprunt, and A. Jakli. Rheological properties of bent-core liquid crystals. *Soft Matter*, 5:3618–3622, 2009.
- [7] D. Vorlander and A. Apel. *Ber. Dtsch. Chem. Ges*, 65:1101, Nov 1932.

- [8] T. Niori, T. Sekine, J. Watanabe, T. Furukawa, and H. Takezoe. Distinct ferroelectric smectic liquid crystals consisting of banana shaped achiral molecules. *J. Mater. Chem*, 6:1231–1233, 1996.
- [9] J. Matraszek, J. Mieczkowski, J. Szydłowska, and E. Gorecka. Nematic phase formed by banana-shaped molecules. *Liquid Crystals*, 27(3):429–436, 2000.
- [10] D. Wiant, J. T. Gleeson, N. Éber, K. Fodor-Csorba, A. Jákli, and T. Tóth-Katona. Nonstandard electroconvection in a bent-core nematic liquid crystal. *Phys. Rev. E*, 72:041712, Oct 2005.
- [11] D. Wiant, S. Stojadinovic, K. Neupane, S. Sharma, K. Fodor-Csorba, A. Jákli, J. T. Gleeson, and S. Sprunt. Critical behavior at the isotropic-to-nematic phase transition in a bent-core liquid crystal. *Phys. Rev. E*, 73:030703, Mar 2006.
- [12] Valentina Domenici, Carlo Alberto Veracini, and Bostjan Zalar. How do banana-shaped molecules get oriented (if they do) in the magnetic field ?. *Soft Matter*, 1:408–411, 2005.
- [13] Bharat R. Acharya, Andrew Primak, and Satyendra Kumar. Biaxial nematic phase in bent-core thermotropic mesogens. *Phys. Rev. Lett*, 92:145506, Apr 2004.
- [14] L. A. Madsen, T. J. Dingemans, M. Nakata, and E. T. Samulski. Thermotropic biaxial nematic liquid crystals. *Phys. Rev. Lett*, 92:145505, Apr 2004.
- [15] J. Harden, B. Mbanga, N. Éber, K. Fodor-Csorba, S. Sprunt, J. T. Gleeson, and A. Jákli. Giant flexoelectricity of bent-core nematic liquid crystals. *Phys. Rev. Lett*, 97:157802, Oct 2006.

- [16] S. Stojadinovic, A. Adorjan, S. Sprunt, H. Sawade, and A. Jakli. Dynamics of the nematic phase of a bent-core liquid crystal. *Phys. Rev. E*, 66:060701, Dec 2002.
- [17] P. Sathyanarayana, M. Mathew, Q. Li, V. S. S. Sastry, B. Kundu, K. V. Le, H. Takezoe, and Surajit Dhara. Splay bend elasticity of a bent-core nematic liquid crystal. *Phys. Rev. E*, 81:010702, Jan 2010.
- [18] Surajit Dhara, Fumito Araoka, Mongryong Lee, Khoa Van Le, Lingfen Guo, B. K. Sadashiva, Kigook Song, Ken Ishikawa, and Hideo Takezoe. Kerr constant and third-order nonlinear optic susceptibility measurements in a liquid crystal composed of bent-shaped molecules. *Phys. Rev. E*, 78:050701, Nov 2008.
- [19] Paladugu Sathyanarayana, Tatipamula Arun Kumar, Vanka Srinivasa Suryanarayana Sastry, Manoj Mathews, Quan Li, Hideo Takezoe, and Surajit Dhara. Rotational viscosity of a bent-core nematic liquid crystal. *Applied Physics Express*, 3(9):091702, 2010.
- [20] M. Skarabot and I. Musevic. Direct observation of interaction of nanoparticles in a nematic liquid crystal. *Soft Matter*, 6:5476–5481, 2010.
- [21] J. Ananthaiah, M. Rajeswari, V. S. S. Sastry, R. Dabrowski, and Surajit Dhara. Rheological properties of a reentrant nematic liquid crystal. *Phys. Rev. E*, 86:011710, Jul 2012.
- [22] C. R. Safinya, E. B. Sirota, and R. J. Plano. Nematic to smectic-a phase transition under shear flow: A nonequilibrium synchrotron x-ray study. *Phys. Rev. Lett*, 66:1986–1989, Apr 1991.
- [23] K. Negita and H. Kaneko. Rheodielectric study on shear-

- induced structural change in the smectic-*a* phase of 4-n-octyl-4'-cyanobiphenyl (8cb). *Phys. Rev. E*, 80:011705, Jul 2009.
- [24] Veena Prasad, Shin-Woong Kang, K. A. Suresh, Leela Joshi, Qingbing Wang, and Satyendra Kumar. Thermotropic uniaxial and biaxial nematic and smectic phases in bent-core mesogens. *Journal of the American Chemical Society*, 127(49):17224–17227, 2005.
- [25] Hyung Guen Yoon, Shin-Woong Kang, Ronald Y. Dong, Alberto Marini, Kattera A. Suresh, Mohan Srinivasarao, and Satyendra Kumar. Nematic biaxiality in a bent-core material. *Phys. Rev. E*, 81:051706, May 2010.
- [26] Khoa Van Le, Manoj Mathews, Martin Chambers, John Harden, Quan Li, Hideo Takezoe, and Antal Jákli. Electro-optic technique to study biaxiality of liquid crystals with positive dielectric anisotropy: The case of a bent-core material. *Phys. Rev. E*, 79:030701, Mar 2009.
- [27] B. Senyuk, H. Wonderly, M. Mathews, Q. Li, S. V. Shiyankovskii, and O. D. Lavrentovich. Surface alignment, anchoring transitions, optical properties, and topological defects in the nematic phase of thermotropic bent-core liquid crystal a131. *Phys. Rev. E*, 82:041711, Oct 2010.
- [28] J. C. Loudet. Colloidal inclusions in liquid crystals: Phase separation mechanisms and some dynamical aspects. *Liquid Crystals Today*, 14(1):1–14, 2005.

List of Publications

Publications

1. **J. Ananthaiah**, Rasmita Sahoo, M. V. Rasna and Surajit Dhara, *Rheology of nematic liquid crystals with highly polar molecules*, *Physical Review E* **89**, 022510 (2014).
2. S. Dhara, Y. Balaji, **J. Ananthaiah**, P. Sathyanarayana, V. Ashoka, A. Spadlo and R. Dabrowski, *Active and passive viscosities of a bent-core nematic liquid crystal*, *Physical Review E* **87**, 030501(R) (2013).
3. **J. Ananthaiah**, M. Rajeswari, V. S. S. Sastry, R. Dabrowski and Surajit Dhara, *Rheological properties of reentrant nematic liquid crystal*, *Physical Review E* **86**, 011710 (2012).
4. **J. Ananthaiah**, M. Rajeswari, V. S. S. Sastry, R. Dabrowski and Surajit Dhara, *Effect of electric field on the rheological and dielectric properties of a liquid crystal exhibiting nematic-to-smectic-A phase transition*, *Eur. Phys. J. E* (2011) **34**.
5. M. Rajeswari, **J. Ananthaiah**, R. Dabrowski, V. S. S. Sastry, S. Dhara and B. K. Sadashiva, *Rheological properties of a chiral liquid crystal exhibiting type-II character*, *Mol. Cryst. Liq. Cryst.*, Vol. **547**: pp. 39/[1729]-45[1735].

6. Mohd Qasim, **J. Ananthaiah**, S. Dhara, P. Paik and D. Das, **Synthesis and characterization of Ultra-Fine colloidal silica Nanoparticles**, *Advanced Science, Engineering and Medicine* **6.9** (2014): 965-973.

Poster presentation and conference attended

1. A poster entitled “Effect of molecular association on the Miesowicz viscosities of nematic liquid crystals with highly polar molecules” was presented at 25th International Liquid Crystal Conference (ILCC) 2014, Dublin, Ireland.
2. A poster entitled “Rheology of nematic liquid crystals with highly polar molecules” was presented at 20th National Conference on Liquid Crystals (NCLC) 2013, Manipal, India.
3. A poster entitled “Rheological properties of a reentrant nematic liquid crystal” was presented at Frontiers in Physics (FIP) 2013, UoH, Hyderabad.
4. A poster entitled “Rheological properties of a reentrant nematic liquid crystal” was presented at 19th national Conference on Liquid Crystals (NCLC) 2012, Patiala, India.
5. A poster entitled “Precessional motion of director under shear flow and electric field in liquid crystals exhibiting nematic to smectic-A and reentrant nematic phase transitions” was presented at soft matter chemistry workshop 2011, Bangalore, India.

Curriculum Vitae

Ananthaiah J

C/O Dr. Surajit Dhara
School of Physics
University of Hyderabad
P. O. Central University, Hyderabad
Telangana, India 500 046.
Phone: +91-99896 71220
Email: ananthjhcu@gmail.com
Skype: [ananth.j3](#)

Education:

- Pursuing Ph.D. in Physics on “Rheological Studies on Nematic and Smectic-A Thermotropic Liquid Crystals”, since 2009, School of Physics, University of Hyderabad, India.
- Master of Science (M.Sc.) in Physics, May 2008, Nizam College, Osmania University, India.
- Bachelor of Science (B.Sc.-MPC), Sree Anantha Padmanabha Arts, Science & Commerce College, Vikarabad, Osmania University, India.

Career Achievements:

- Selected for Senior Research Fellow (CSIR-SRF) conducted by Council of Scientific and Industrial Research and University Grant Commission (CSIR & UGC), Indian Government.
- Qualified State Eligibility Test (SET-2012) for Assistance Professor/Lectureship conducted by Osmania University, India.
- Qualified Graduate Aptitude Test in Engineering (GATE is an all India examination administered and conducted jointly by the Indian Institute of Science and seven Indian Institutes of Technology on behalf of the National Coordination Board-GATE, Department of Higher Education, Ministry of Human Resource Development (MHRD), Government of India.) in Physics, Feb 2009.
- Achieved Smt. Jogiraju Sree Rangamma Hanumanth Rao Memorial Gold Medal for having secured highest marks in Physics subject the examinations held in March 2006 from Sree Anantha Padmanabha Arts, Science & Commerce College, Vikarabad, Osmania University, India.
- Achieved Smt. M. Savithramma Channa Reddy Memorial Gold Medal for having secured highest marks in B.Sc. MPC in the examinations held in march 2006 from Sree Anantha Padmanabha Arts, Science & Commerce College, Vikarabad, Osmania University, India.
- Achieved Old Students Association Cash Award for having secured highest marks in Science Faculty in the examination held in March 2006 from Sree Anantha Padmanabha Arts, Science & Commerce

College, Vikarabad, Osmania University, India.

Experimental skills:

- Familiar with measurement of Electro-Rheology, Small Angle Light Scattering (SALS), Rheo-microscopy and Magneto-Rheology using MCR 501 Rheometer (Anton Paar).
- Hands on experience in using Polarizing Optical microscopes (Nikon and Olympus)

Personal details:

Date of Birth : 12th June, 1984

Sex : Male

Nationality : Indian

Marital status : Married

Languages known: English, Hindi and Telugu

Computer skills : Mathematica, LaTeX and LabView

References:

★ Dr. Surajit Dhara

School of Physics

University of Hyderabad

Telangana, India 500 046

Email: sdsp@uohyd.ernet.in

Phone No: 040-23134331

★ Prof. V. S. S. Sastry

School of Physics

University of Hyderabad

Telangana, India 500 046

Email: vssssp@uohyd.ernet.in

Phone No: 040-66798102